

INFORMATION TO USERS

This was produced from a copy of a document sent to us for microfilming. While the most advanced technological means to photograph and reproduce this document have been used, the quality is heavily dependent upon the quality of the material submitted.

The following explanation of techniques is provided to help you understand markings or notations which may appear on this reproduction.

1. The sign or "target" for pages apparently lacking from the document photographed is "Missing Page(s)". If it was possible to obtain the missing page(s) or section, they are spliced into the film along with adjacent pages. This may have necessitated cutting through an image and duplicating adjacent pages to assure you of complete continuity.
2. When an image on the film is obliterated with a round black mark it is an indication that the film inspector noticed either blurred copy because of movement during exposure, or duplicate copy. Unless we meant to delete copyrighted materials that should not have been filmed, you will find a good image of the page in the adjacent frame.
3. When a map, drawing or chart, etc., is part of the material being photographed the photographer has followed a definite method in "sectioning" the material. It is customary to begin filming at the upper left hand corner of a large sheet and to continue from left to right in equal sections with small overlaps. If necessary, sectioning is continued again—beginning below the first row and continuing on until complete.
4. For any illustrations that cannot be reproduced satisfactorily by xerography, photographic prints can be purchased at additional cost and tipped into your xerographic copy. Requests can be made to our Dissertations Customer Services Department.
5. Some pages in any document may have indistinct print. In all cases we have filmed the best available copy.

**University
Microfilms
International**

300 N. ZEEB ROAD, ANN ARBOR, MI 48106
18 BEDFORD ROW, LONDON WC1R 4EJ, ENGLAND

8018926

LEE, MOON KEY

MULTILAYERED PERIODIC REFLECTOR AND BRAGG WAVEGUIDE FOR
INTEGRATED OPTICS

The University of Oklahoma

PH.D.

1980

University
Microfilms
International

300 N. Zeeb Road, Ann Arbor, MI 48106

18 Bedford Row, London WC1R 4EJ, England

PLEASE NOTE:

In all cases this material has been filmed in the best possible way from the available copy. Problems encountered with this document have been identified here with a check mark .

1. Glossy photographs _____
2. Colored illustrations _____
3. Photographs with dark background _____
4. Illustrations are poor copy _____
5. Print shows through as there is text on both sides of page _____
6. Indistinct, broken or small print on several pages throughout _____
7. Tightly bound copy with print lost in spine _____
8. Computer printout pages with indistinct print _____
9. Page(s) _____ lacking when material received, and not available from school or author _____
10. Page(s) _____ seem to be missing in numbering only as text follows _____
11. Poor carbon copy _____
12. Not original copy, several pages with blurred type _____
13. Appendix pages are poor copy _____
14. Original copy with light type _____
15. Curling and wrinkled pages _____
16. Other _____

THE UNIVERSITY OF OKLAHOMA
GRADUATE COLLEGE

MULTILAYERED PERIODIC REFLECTOR AND
BRAGG WAVEGUIDE FOR INTEGRATED OPTICS

A DISSERTATION
SUBMITTED TO THE GRADUATE FACULTY
in partial fulfillment of the requirements for the
degree of
DOCTOR OF PHILOSOPHY

BY
MOON KEY LEE
Norman, Oklahoma
1980

MULTILAYERED PERIODIC REFLECTOR AND
BRAGG WAVEGUIDE FOR INTEGRATED OPTICS

APPROVED BY

Sam K. Kalup
Robert M. St. John
William L. Kurcio
Myrdal
Gerald Turner
DISSERTATION COMMITTEE

ACKNOWLEDGMENT

I would like to thank Professor M.Y. El-Ibiary, W.L. Kuriger, R.M. St. John and G. Tuma who reviewed my manuscript and provided many constructive suggestions. Particularly, it is my privilege to express my deep appreciation to Dr. Seun K. Kahng, Director of the School of Electrical Engineering and Computing Science, the University of Oklahoma, for his support and encouragement without which this research could have never been accomplished. Thanks are also due to Ms. Pat Ybarra for her beautiful typing.

I dedicate this manuscript to my parents Dr. and Mrs. Chan S. Lee for their love and encouragement.

I am also deeply grateful to my wife Sungsik and my children Sukkyoung and Jean who have lost their evenings and weekends.

TABLE OF CONTENTS

LIST OF TABLES.	v
LIST OF FIGURES	vi
Chapter	
I. INTRODUCTION.	1
II. THEORY OF DIELECTRIC WAVEGUIDE.	7
III. A CHARACTERIZATION OF A MULTILAYERED REFLECTOR.	25
IV. THE NUMERICAL RESULTS IN MULTILAYERED PERIODIC REFLECTOR.	49
V. TRIPLE LAYERED PERIODIC BRAGG WAVEGUIDE	76
VI. CONCLUSIONS	106
REFERENCES.	108
APPENDIX	113

LIST OF TABLES

Table

4-1.	Selectivity of Various Reflectors Consisted of Basic Period of More than 4 Layers.	70
4-2.	Reflectivity and Selectivity of the $(\frac{n_1}{8} \frac{n_2}{4} \frac{n_1}{8})$ Symmetric Structure	71
5-1.	Bragg Waveguide Parameters.	97
5-2.	Attenuation Constant and Selectivity for TE_1 Mode of the Bragg Waveguide I and II.	105

LIST OF FIGURES

Figure	Page
2.1. Reflection and Refraction of a Plane Wave at a Dielectric Interface.	9
2.2. Phase Shift of TE Mode as a Function of Incidence Angle.	12
2.3. Sketch of an Asymmetric Slab Waveguide (a) and the Zig-Zag Ray Path in Slab Waveguide (b)	13
2.4. Sketch of Propagation Constants, Electric Field Profiles and Zig-Zag Wave Picture of the Different Types of Wave Modes.	14
2.5. Typical ω - β Diagram for Dielectric Slab Waveguide	18
2.6. Dispersion Curves for the Confined Modes of $\text{Ga}_{1-x}\text{Al}_x\text{As}$ on GaAs Waveguide.	21
2.7. Amplitude of the Electric Field as a Function of Position for $\text{Ga}_{1-x}\text{Al}_x\text{As} - \text{GaAs} - \text{Ga}_{1-y}\text{Al}_y\text{As}$ Waveguide with $d/\lambda_0 = 0.2$ and $\lambda_0 = 1.15 \mu\text{m}$	22
2.8. The Confinement Factor Γ for the Fundamental Mode of Asymmetric Waveguide	24
3.1. Schematic Representation of a Multilayer	28
3.2. Chebyshev Polynomial $C_n(x)$	38
3.3. Chebyshev Polynomial $S_n(x)$	39
3.4. Equivalent Optical Admittance for the Structure $(\frac{n_1}{8} \frac{n_2}{4} \frac{n_1}{8})$ with $n_1 = 3.45$ and $n_2 = 3.24$ at 80° Incidence Angle.	46
3.5. Equivalent Optical Thickness of the Structure Described in Figure 5.4.	47
4.1. TE Waves (a) and TM Waves (b) Reflectivity vs. Relative Wavelength at Various Angles of Incidence of a Typical 28 Periods Bragg Reflector.	51

Figure	Page
4.2. Reflectivity for Double $\lambda_0/4$ Layer Periodic Bragg Reflector as a Function of λ_0/λ . $n_1 = 3.62$, $n_2 = 3.44$, $n_s = 3.62$, $n_g = 3.34$, $\theta = 80^\circ$	52
4.3. Reflectivity for Tuned $\lambda_0/4$ Triple (a), Quadruple (b), and Quintuple (c) with $n_1 = 3.45$, $n_2 = 3.24$, $N = 10$ and $\theta = 60^\circ$	54
4.4. Reflective Spectral for Triple Layered Bragg Reflector with $N = 30$, $n_1 = 3.45$, $n_2 = 3.42$ and $\theta = 80^\circ$. (a) $(\frac{n_2}{8} \frac{n_1}{4} \frac{n_2}{8})$, (b) $(\frac{n_1}{8} \frac{n_2}{4} \frac{n_1}{8})$	55
4.5. Reflectivity vs. Relative Wavelength for Several Value of Guiding Layer's Refractive Index n_g with $\theta = 80^\circ$	57
4.6. Reflectivity as a Function of Period N for a Quarter Wave Double Structure	58
4.7. Reflectivity as a Function of Period N for Reflector with Basic Period of $(\frac{n_1}{6} \frac{n_2}{6} \frac{n_1}{6})$ and $(\frac{n_1}{8} \frac{n_2}{4} \frac{n_1}{8})$	59
4.8. Reflectivity at the Center of Stopzone vs. Periods N for Quadruple and Quintuple Basic Period Reflector	60
4.9. The Effect of Index Ratio n_1/n_2 on Reflectivity for $(\frac{n_1}{4} \frac{n_2}{4})$ Double Structure at Several Different Incident Angles	61
4.10. The Effect of Index Ratio n_1/n_2 on Reflectivity for Triple Structure at Incident Angles 40° , 60° , 80°	62
4.11. The Effect of Incidence Angle on Reflectivity of TE Waves (a) and TM Waves (b)	63
4.12. Stopband Width of Double Layer Bragg Reflector Against Refractive Index Ratio at Several Incidence Angles. Dotted Curves; Exact Calculation, Solid Curves; Using Equation (3.47).	66
4.13. Selectivity of Double Layer Bragg Reflector as a Function of N. Reflector Parameters; $n_1/n_2 = 1.065, 1.052, 1.030$, $\lambda_0 = 1.15$ (μm), $n_g = 3.24$, $n_s = 3.45$	67
4.14. Selectivity of Untuned Triple Structure Bragg Reflector. Solid Curves: $(\frac{n_1}{4} \frac{n_2}{8} \frac{n_3}{8})$	68

Figure	Page
4.15. Center Wavelength Shift $(\lambda_0/\lambda_\theta)$ of a Double $\frac{\lambda_0}{4}$ Layer Periodic Bragg Reflector.	72
4.16. Center Wavelength Shift of a Typical Bragg Reflector with 20 Number of Triple, Quadruple, Quintuple Basic Period.	74
4.17. Selectivity Variation Against Incident Angle (a) $(\frac{3.45}{4}, \frac{3.35}{4})$, (b) $(\frac{3.45}{4}, \frac{3.40}{8}, \frac{3.24}{8})$ (c) $(\frac{3.45}{4}, \frac{3.45}{4}, \frac{3.45}{4}, \frac{3.40}{4})$	75
5.1. Triple Layered Dielectric Periodic Bragg Waveguide Structure with Semi-infinite Outer Media.	79
5.2. Dispersion Relation for Bragg Waveguide II of Table 5.1. Solid Curves: d/λ_0 vs. n_e , Broken Curves: $\exp(-K_i\Lambda)$ vs. n_e	95
5.3. Dispersion Relation for Bragg Waveguide I for Table 5.1. Solid Curves: d/λ_0 vs. n_e , Broken Curves: $\exp(-K_i\Lambda)$ vs. n_e	96
5.4. Bloch Wave Constant vs. Normalized Propagation Constant . . .	99
5.5. Electric Field Distribution of Bragg Waveguide I. a) TE_0 Mode for $d = 0.73 \mu\text{m}$ b) TE_1 , c) TE_2 , d) TE_3 with $d = 2.35 \mu\text{m}$	100
5.6. Confinement Factor for the Fundamental, first, second, and third-order TE mode as a Function of Guiding Layer Thickness	101
5.7. The Attenuation Constant vs. Number of Period for TE Mode in Bragg Waveguide with $n_1 = 3.45$ and $n_2 = 3.24$. Solid Graph: $\Lambda = 0.42 \mu\text{m}$, Broken Graph: $\Lambda = 0.73 \mu\text{m}$	103
5.8. The Attenuation Constant α as a Function of Guiding Layer Thickness d for three different number of Period N . . .	104

MULTI-LAYERED PERIODIC REFLECTOR AND BRAGG
WAVEGUIDE FOR INTEGRATED OPTICS

CHAPTER I

INTRODUCTION

The advent of integrated optics has given an enormous stimulus to the entire field of optical communication. Integrated optics is a diverse field which can be characterized in the broad sense by considering a device which combines optical components, such as light sources, modulators, switches, lenses, detectors, filters, couplers, and other components into a common substrate. Traditional optical apparatuses must be aligned with extreme accuracy and are thus susceptible to a minute amount of vibration and temperature change. Integrated optical devices allow concentrated light beam in thin film waveguides that are constructed on the surface or inside of a substrate. Because of the short wavelength of light, a dielectric optical light guide can be made extremely small in physical dimensions. Primary advantages of the small size and rugged construction of integrated optical devices are their insensitivity to vibration and temperature change in their environment. And also it is possible to package a higher density of components compared to conventional optical devices.

Of many optical devices that are being studied, one of key elements of integrated optical devices is a waveguide which can transport information onto the other optical device. The integrated optical waveguides

are a dielectric type, usually in a form of a planar film or strip with a refractive index higher than that of substrate.

In a recent review paper, Kogelnik ⁽¹⁾ offered a good bibliography and also discussed the current development in integrated optics.

An optical dielectric waveguide with a slab configuration is capable of supporting lossless confined modes when the index of refraction of the guide layer exceeds the indices of the two bounding media. This condition is necessary to obtain an imaginary transverse propagation constant which corresponds to an evanescent decay of the mode field in the bounding media. However, for some application, it may be desirable to guide optical power in a layer with a lower index than those of two bounding media. A typical example is the hollow core waveguide laser where power is flowing in the air ⁽²⁻⁴⁾.

It was suggested that confined guiding with arbitrary low loss is possible using Bragg reflection in waveguide ⁽⁵⁾. In a Bragg waveguide the conventionally used substrate is replaced by a periodic layered medium. The propagation may be considered formally as that of a plane wave zigzagging inside the guiding layer and undergoing total internal reflection at the interface between the guide and guide cover and Bragg reflection at the interface between the guide layer and the periodic layer. Total Bragg reflection happens only when the incidence angle satisfies the Bragg condition, that is, the propagation condition inside the periodic layered medium fall within one of the optical forbidden gaps ⁽⁶⁾.

The introduction of the Bragg waveguide opens a new dimension for light propagation in integrated optics.

Optical waveguides based on the Bragg reflection principle are free

from some of the fundamental constraints imposed on conventional waveguides and are expected to play an important role in applications where a high degree of selectivity is important or in case where use of conventional waveguides provide inadequate performance. For instance in case of an x-ray laser, the oscillation wavelength is so small, 100\AA , that the use of an external resonator structure is highly unlikely. A great deal of work was done on the theory of anti-reflectivity and high reflecting multi-layer systems as well as for interference filter in the first half of the century ⁽⁷⁻⁹⁾. However, the first general treatment of stratified media in terms of electromagnetic theory of light was not available until Abeles ⁽¹⁰⁾ introduced the matrix method to treat the propagation of light in layered media. Electromagnetic propagation in a periodically layered dielectric media was considered in detail with the direction of propagation normal to the layers by many workers ⁽¹¹⁾. Dispersion equations and mode functions for a periodic structure were previously discussed by Brillouin ⁽¹²⁾, and Allen ⁽¹³⁾ in connection with crystal band structure for a square well potential and more recently for electromagnetic case ⁽¹⁴⁾. Kossel ⁽¹⁵⁾ showed that the analogies between the thin film optics and electron band theory. The propagation characteristics of periodic array of dielectric slab was also studied by Lewis and Hessel ⁽¹⁶⁾.

The historical interest in optical properties of multi-layer thin film was largely confined to the use of high reflectance coatings in high resolution interferometry or anti-reflection coatings. Little attention, however, was given to the guided wave in the parallel direction to the layer until 1974 when Arnaud ⁽¹⁷⁾ derived approximate

dispersion expression of a semi-infinite sequence of periodic layers on the basis of transmission line representation for special case of loosely bound waves.

The use of Bragg reflection in waveguide was first suggested by Ash (18) and Fox (5) in 1970 and 1974, respectively. In recent research of electromagnetic wave propagation in the periodic dielectric layer is facilitated with the help of the Floquet's theorem which reduces the considerations to a single unit period (6).

First confined propagation at $1.15 \mu\text{m}$ has been observed by Cho and Yariv (19) in $\text{Ga}_{1-x}\text{Al}_x\text{As} - \text{GaAs}$ Bragg waveguide grown by molecular beam epitaxy. This asymmetric Bragg waveguide has eight period of double layer $\text{Ga}_{0.8}\text{Al}_{0.2}\text{As} - \text{GaAs}$ reflector with each layer thickness of $0.26 \mu\text{m}$ and an excessively high attenuation coefficient of $\alpha = 14.49 \text{ cm}^{-1}$, neglecting the loss due to the bulk absorption in this structure. It would be necessary to have 32 layers to provide a low attenuation coefficient such as $\alpha = 0.355 \text{ cm}^{-1}$.

The application of such Bragg reflectors has also been reported in the operation of injection laser (20). Recently Dupuis and Parkus (20,21) reported a symmetric Bragg waveguide grown by metal organic chemical vapor deposition technique and it consists of 56 layers of alternating $\text{Ga}_{0.73}\text{Al}_{0.27}\text{As} - \text{GaAs}$.

All the Bragg waveguides reported to date have double layered structures, symmetric and asymmetric, and require a large number of periodic layers to process, and thus have inherent disadvantages in cost effective production and limitations in device performance.

Although the most basic principle of operation remains the same for

the waveguide, certain aspects of a multi-layered periodic Bragg waveguide device have not been discussed in any literature up to this date. For instance, various layer parameter, such as refractive index and thickness of each layer, play an important role in reflectivity of a Bragg reflector. But in most of the previously published papers, no detailed explanation about the relationship between refractive index and thickness of each layer was given.

During the design of a periodic layered Bragg waveguide for integrated optics, the dependence of the reflectivity of the various layer parameters can guide the scientist to an optimal configuration. It would be useful to include them in a discussion of the Bragg waveguide.

The main purpose of this paper is to deal directly with the closed form expression for reflectivity, dispersion relation and related wave functions with improved confinement of the wave in the guide with the least number of periodic layers. Also intended is to seek the complete characterization of triple layered periodic Bragg waveguide.

Three chapters will be presented that characterize the properties of the multi-layered periodic Bragg waveguide. These chapters are arranged in a modular format that will allow early chapters to be used as a reference to support some points in the later chapters. New and old information is interwoven throughout the discussion to create continuity in the total picture of the Bragg waveguide and to supply useful comparison between double, triple, quadruple, and quintuple layered periodic structure.

A brief statement of the content and purpose of each chapter will now be made.

Chapter 2 is basically a review of the conventional slab waveguide to characterize the propagation of optical waves in this dielectric layer.

The chapter also establishes a basic picture for optical waveguide theory. While the information is not totally new, the intention is to bring certain points into focus for a clearer understanding of optical waveguide model discussed in later chapters.

Chapter 3 contains a closed form expression of reflectivity which is valid to any polarization, layer thickness, wavelength and incident angle for a Bragg reflector composed of a multi-layered periodic dielectric medium. This has not been discussed previously in connection with Bragg waveguide including the effect of guiding layer and substrate.

Chapter 4 is primarily a numerical comparison and discussion material related to double, triple, quadruple, and quintuple layered periodic structure.

Specific interest is directed toward the magnitude of reflectivity and selectivity. More importantly, the comparison between the various structures and the condition for optimum layer thickness are essentially new and necessary for estimating the number of periods of a Bragg reflector.

Chapter 5 is a discussion of the triple layered periodic structure with regard to dispersion relation, field profile and optical power confinement. The information in this chapter is new and important for the final estimation of a triple layered periodic Bragg waveguide. In Chapter 6, conclusions and recommendations are described. Finally, it is felt that, the specific insight and numerical data presented in this study will provide a useful reference for further application of Bragg waveguide in various area of integrated optics.

CHAPTER II

THEORY OF DIELECTRIC WAVEGUIDE

2.1. Introduction

Dielectric waveguides are the structures that are used to confine and guide the light in the guided-wave devices and circuits of integrated optics.

The purpose of this chapter is to review the important theory of these waveguides and to give both an introduction to the subject as well as a collection of important results sufficiently detailed to be of use to later chapters.

I also aim to provide a compact theoretical framework of sufficient generality to be used as the basis for later chapters, which deal with the Bragg waveguide. The properties of dielectric waveguides are discussed in great detail in references (22-25).

Dielectric slabs are the simplest optical waveguides. Because of their simple geometry, guided and radiation modes of slab waveguides can be described by simple mathematical expressions. The study of slab waveguides and their properties is thus often useful in gaining an understanding of the waveguiding properties of more complicated dielectric waveguides. However, slab waveguides are not only useful as models for more general types of optical waveguides, but they are actually employed for light guidance in integrated optics (26,27).

In integrated optical applications, slab waveguides are formed by various means, the simplest of which use the deposition of glass or plastic films on glass or crystal substrates. These films can be deposited by evaporations, sputtering, or by epitaxial growth techniques. The latest method is such as molecular beam epitaxial restricted to the deposition of thin single crystalline films on crystal substrates. Another method of forming dielectric optical waveguides for integrated optics applications employs ion implantation techniques. By bombarding the substrate material with suitable ions it is possible to alter the refractive index of the substrate so that a dielectric slab waveguide results. More detailed fabrication can be found elsewhere (28). The general treatise in this chapter is based on the formulation presented by Marcuse (29). In section 2.1 we discuss the ray optics picture of light propagation in slab waveguides. This is meant to provide both a first physical understanding as well as an introduction to the concepts and the terminology of dielectric waveguides in general. Section 2.2 is a discussion of the general fundamental of the electromagnetic theory of dielectric waveguides and their modes of propagation. Section 2.3 gives details of the guided modes and the fields of the slab waveguides, both for TE and TM modes.

2.2 Geometrical Optics of the Slab Waveguide

Consider an interface separating two lossless, isotropic, homogeneous dielectric media of refractive index n_1 and n_2 as shown in Figure 2.1, and a coherent light wave incident at an angle θ_1 between the wave normal and the normal to the interface. With the definition of

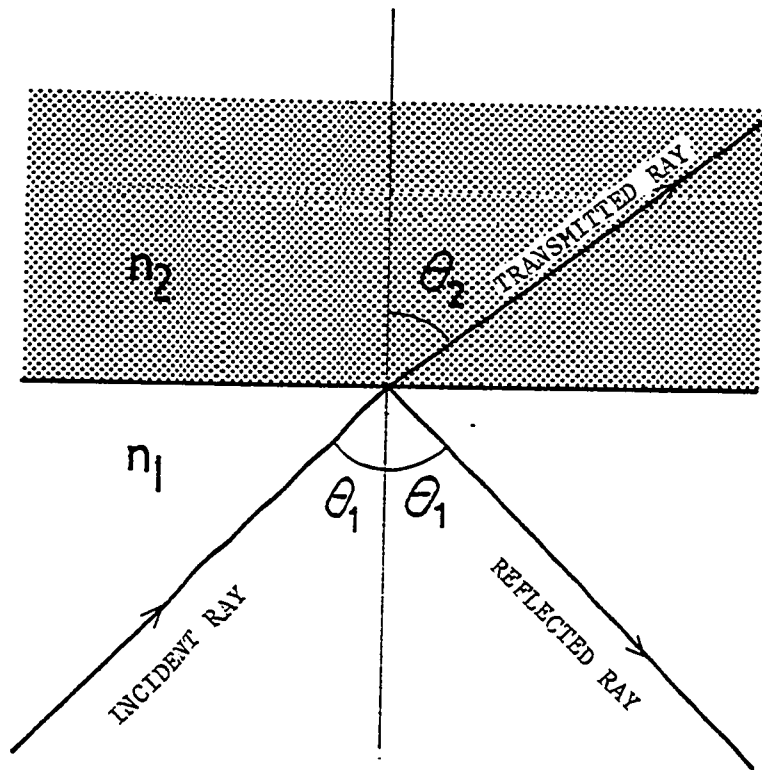


Figure 2.1. Reflection and Refraction of a Plane Wave at a Dielectric Interface.

the angles shown in Figure 2.1 Snell's law can be expressed in the form

$$n_1 \sin \theta_1 = n_2 \sin \theta_2 \quad (2.1)$$

The reflection coefficient of a plane wave at a dielectric interface, which is polarized so that its electric vector is parallel to the interface (i.e. TE polarization), follows from the Fresnel formula,

$$R = (n_1 \cos \theta_1 - \sqrt{n_2^2 - n_1^2 \sin^2 \theta_1}) / (n_1 \cos \theta_1 + \sqrt{n_2^2 - n_1^2 \sin^2 \theta_1}). \quad (2.2)$$

The critical angle for total internal reflection is defined by

$$\sin \theta_c = n_2 / n_1$$

For $\theta_1 < \theta_c$, the reflection coefficient R , given by Equation (2.2), is real and positive, and the incident wave is partially reflected. As the critical angle is exceeded ($\theta_1 > \theta_c$), total internal reflection occurs at the dielectric interface. In this case, R is complex because the inside of square root in numerator and denominator of Equation (2.2) is negative value. The negative sign is necessary since a decaying instead of a growing wave must result in medium 2. Under conditions of total internal reflection, a phase shift is imposed on the reflected light. The phase shifts ϕ_{TE} and ϕ_{TM} corresponding to the TE polarization and TM polarization (i.e. a wave polarized so that its magnetic vector is parallel to the interface) are respectively,

$$-2 \arctan (\sqrt{n_1^2 \sin^2 \theta_1 - n_2^2} / n_1 \cos \theta_1), \quad \text{for TE} \quad (2.3)$$

$$-2 \arctan [(n_1^2 / n_2^2) \sqrt{n_1^2 \sin^2 \theta_1 - n_2^2} / n_1 \cos \theta_1] \quad \text{for TM} \quad (2.4)$$

Figure 2.2 shows the dependence of phase shift of TE on the angle of incidence θ_1 for a selection of index ratio n_2/n_1 where the values 0.29, 0.47, 0.68, 0.90 and 0.99 correspond to interfaces between air - GaAs, air - LiNbO_3 , air - SiO_2 , GaAs - $\text{Ga}_{0.57}\text{Al}_{0.43}\text{As}$ and GaAs - $\text{Ga}_{0.9}\text{Al}_{0.1}\text{As}$, respectively. It is noted that the phase shift increases from 0° at the critical angle to 180° at $\theta_1 = 90^\circ$. It increases with infinite slope at $\theta_1 = \theta_c$ and a slope of $(1 - n_2^2/n_1^2)^{-1/2}$ at grazing incidence.

Having collected these few facts from ray optics and the theory of plane wave reflection at interfaces, mode guidance in the slab waveguide shown schematically in Figure 2.3 will be presented. The core region of the waveguide is assumed to have refractive index n_1 and is deposited on a substrate with index n_2 . The refractive index of the medium above the core is indicated as n_3 . If $n_2 = n_3$, slab waveguide is symmetric and in case of $n_2 \neq n_3$, the slab waveguide is asymmetric. In general, we assume that

$$n_1 > n_2 \geq n_3, \quad (2.5)$$

and there are two critical angles, θ_{2c} and θ_{3c} for total internal reflection from the $(n_1 - n_2)$ and $(n_1 - n_3)$ interfaces, respectively. For small angles $\theta < \theta_{2c}, \theta_{3c}$ light incident from the substrate side escapes through the structure, this situation is depicted in Figure 2.4(a) and called as a radiation mode.

The case of $\theta_{3c} < \theta < \theta_{2c}$, is shown in Figure 2-4(c). The light incident from the substrate is refracted at the $(n_1 - n_2)$ interface and then totally reflected at the $(n_1 - n_3)$ interface, refracted back into the

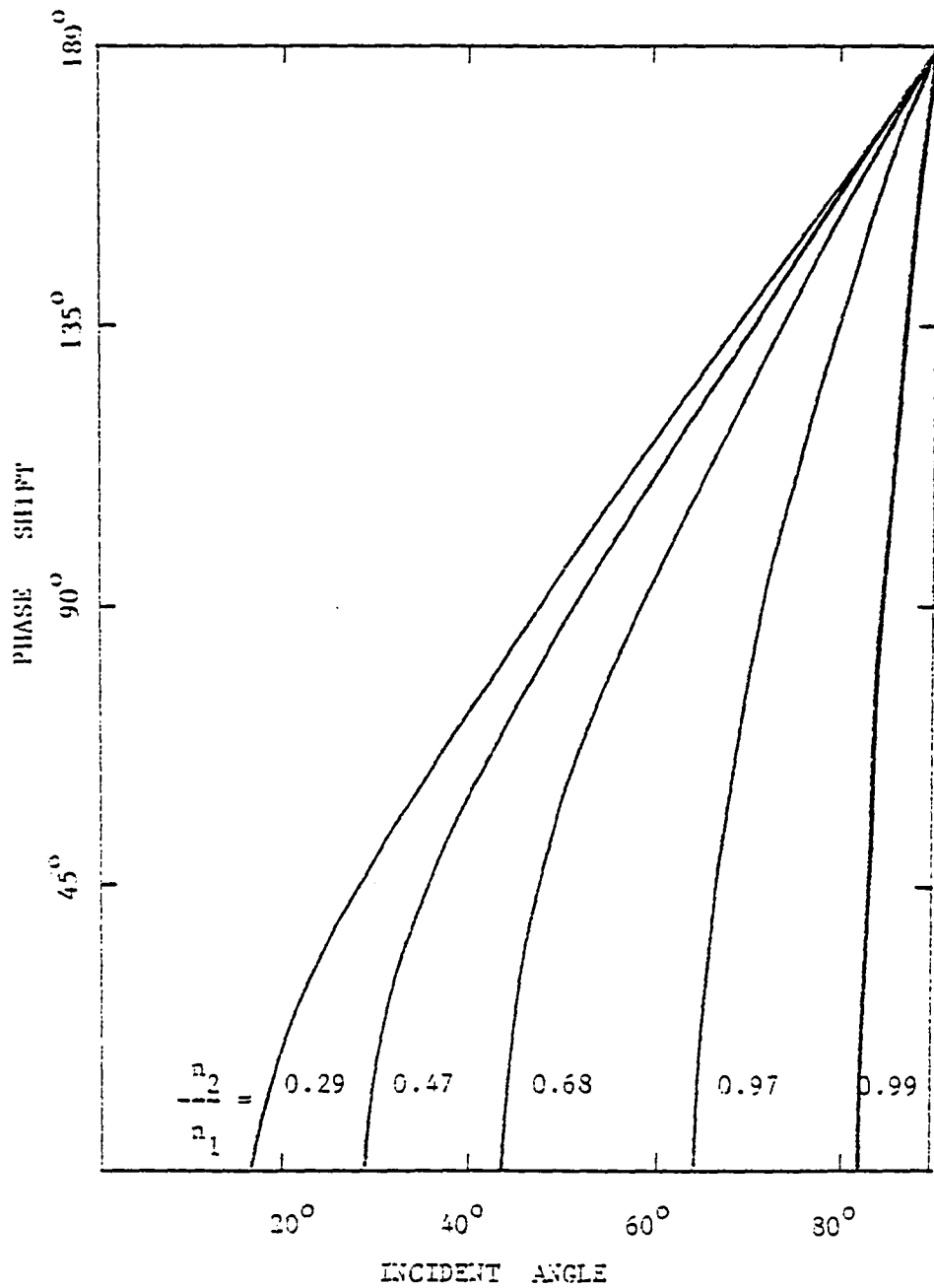
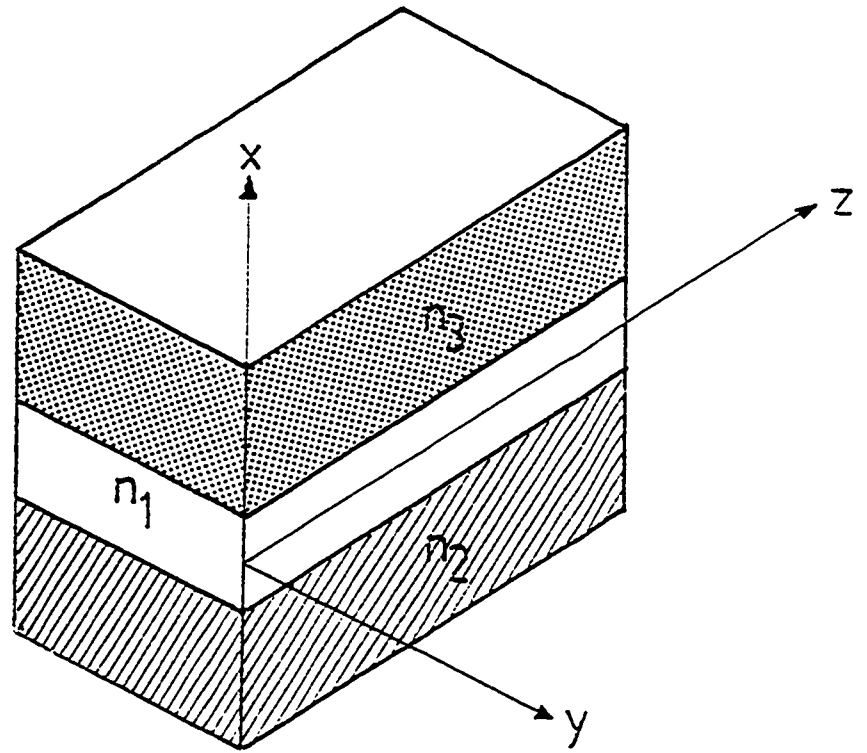
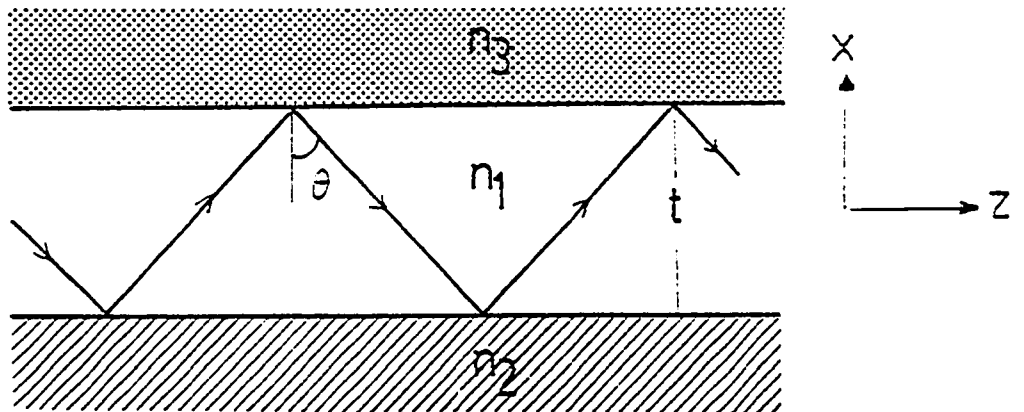


Figure 2.2. Phase Shift of TE Mode as a Function of Incidence Angle θ_1 .



(a)



(b)

Figure 2.3. Sketch of an Asymmetric Slab Waveguide (a) and the Zig Zag Ray Path in Slab Waveguide (b)

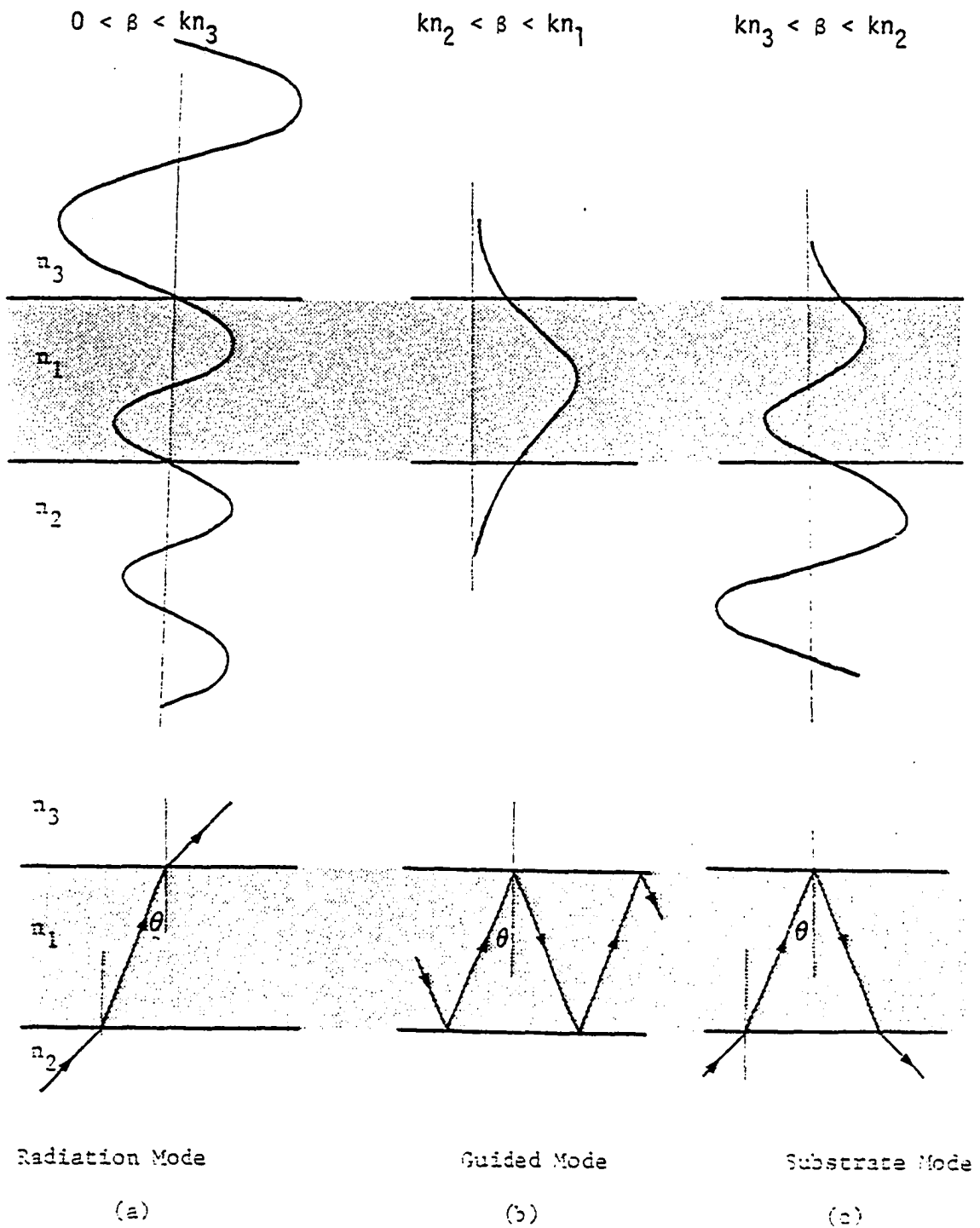


Figure 2.4. Sketch of Propagation Constants, Electric Field Profiles and Zig-Zag Wave Picture of the Different Type of Wave Modes.

substrate through which the light escapes from structure. Again, there is no light confinement and it is called a substrate mode. In Figure 2-4(b) the angle is large enough, total internal reflection at both interfaces are occurred. The light is trapped and confined in n_2 and propagates in a zig zag path which corresponds to a guided mode. For a guided mode of the slab guide, the zig zag model is represented by plane wave with propagation constant β .

$$\beta = \omega/v_p = kn_1 \sin\theta, \quad (2.6)$$

where $k = 2\pi/\lambda_0 = \frac{\omega}{c}$, λ_0 is the free space wavelength, ω the angular frequency of the light, and c the velocity of light. For an n_1 layer of thickness t , there is a phase shift for transverse passage through an n_1 layer and for reflection on interface, thus the sum of all these phase shifts must be a multiple of 2π . Thus the transverse resonance condition of TE modes yields

$$2kn_1 t \cos\theta - 2 \arctan \left[\frac{\sqrt{n_e^2 - n_2^2}}{n_1 \cos\theta} \right] - 2 \arctan \left[\frac{\sqrt{n_e^2 - n_3^2}}{n_1 \cos\theta} \right] = 2m\pi \quad (2.7)$$

where m is an integer (0,1,2,...) which identifies the mode number and n_e is known as an effective guide index or normalized propagation constant defined by

$$n_e = \beta/k = n_1 \sin\theta. \quad (2.8)$$

Equation (2.7) is essentially the dispersion equation of a waveguide yielding the propagation constant as a function of wavelength and guiding layer thickness for TE case. Equation (2.7) is developed

in the section 2.4 by starting from Maxwell's equations and using the boundary conditions at the dielectric interfaces.

2.3 General Discussion of the Electromagnetic Theory of Dielectric Waveguide

In order to obtain a complete description of the modes of a dielectric waveguide, Maxwell's equations must be solved. A mode of a dielectric waveguide at a radian frequency ω is a solution of Maxwell's propagation equation

$$\nabla \times \mathbf{E} = -j\omega\mu_0 \mathbf{H} \quad (2.9)$$

$$\nabla \times \mathbf{H} = j\omega\epsilon_0 n^2 \mathbf{E}, \quad (2.10)$$

subject to the continuity of the tangential components of \mathbf{E} and \mathbf{H} at the dielectric interface. Here ϵ_0 and μ_0 are the dielectric permittivity and magnetic permeability of vacuum. It is assumed that the media in consideration are dielectric material so that the use of the vacuum constant μ_0 is sufficient. The index of refraction of the medium is designated by n and the time dependence term has been suppressed. A simple description of the dielectric waveguide by limiting discussions to the slab waveguide is shown in Figure 2.3, in which no variation of field in y direction is assumed. And assuming that wave front is normal to the waveguide axis z , the wave equation is

$$\frac{\partial^2}{\partial x^2} E(x,y) + (k^2 n^2 - \beta^2) E(x,y) = 0 \quad (2.11)$$

Before embarking on a formal solution of Equation (2.11) in each layer we may learn a great deal about the physical nature of the

solutions as a function of the propagation constant β at some fixed frequency ω . The simple physical conceptual treatments in conjunction with a slab waveguide have been explored and used by Taylor and Yariv⁽²⁸⁾.

Assuming the index of refraction in each layer satisfies Equation (2.5), for $\beta > kn_1$, it follows directly from Equation (2.11) that

$\frac{1}{E} \frac{\partial^2 E}{\partial x^2} > 0$ everywhere. The field increases without bound away from the waveguide so that the solution is not physically realizable.

For $kn_2 < \beta < kn_1$, as in Figure 2.4(b) it follows that the solution is sinusoidal in n_1 layer, but is exponential in n_3 and n_2 layers. The energy carried by these modes is confined to n_1 layer and its vicinity. From the ray optics and above discussion, it follows that a necessary condition for confined modes is that $n_1 > n_2, n_3$.

Solutions of Equation (2.11) for $kn_3 < \beta < kn_2$ correspond to exponential behavior in n_3 layer and to sinusoidal behavior in n_1 and n_2 layers. We refer to these modes as substrate radiation modes. For $0 < \beta < kn_3$, as in Figure 2.4(a), the solution for $E(x)$ becomes sinusoidal in all three layers. These are so called radiation modes of waveguide. Figure 2.5 shows a sketch of an ω - β diagram which are typical for a dielectric slab waveguide. At the cut off frequency, the propagation constants assume the value of lower bound kn_2 , and as ω (or the thickness t) increases, β approaches its upper bound kn_1 and more and more guided modes exist. In addition to the discrete values of allowed β of the guided modes, the diagram also shows the continuous value of β of the radiation modes.

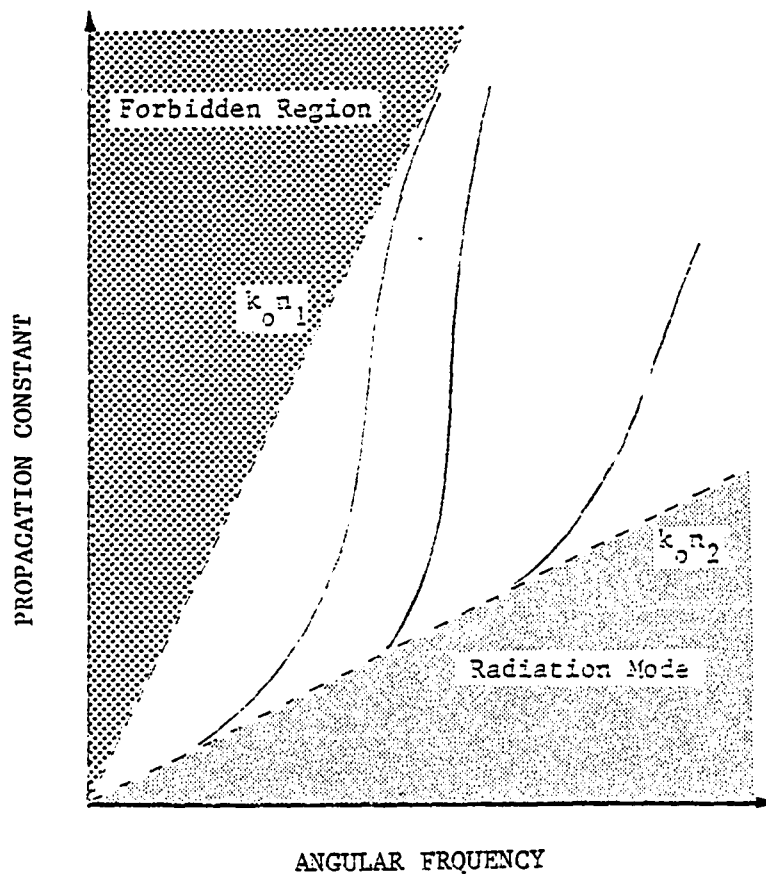


Figure 2.5. Typical ω - β Diagram for Dielectric Slab Waveguide. Three Discrete Guided Modes are Shown.

2.4 Guided Modes and Confinement Factor of an Asymmetric Waveguide

The modal field can be derived from the wave equation in section 2.3 and the corresponding solutions have been discussed by Marcuse (29), Nelson (30), and McKenna (31). In this section, the relationships for the fields of the mode of a planar waveguide shown in Figure 2.3 and the confinement factor are presented. We limit the derivation to the guided modes which according to Figure 2.4 have propagation constants β ,

$$kn_2 < \beta < kn_1 \quad (2.12)$$

where

$$n_2 > n_3$$

The field component E_y of the TE modes satisfies the wave equation (2.11). For guided propagation wave along z direction,

$$E_y = \begin{cases} E_0 \cos\left(\frac{ht}{2} - \phi\right) \exp[q\left(\frac{t}{2} - x\right)], & x \geq \frac{t}{2} \\ E_0 \cos(hx - \phi), & -\frac{t}{2} \leq x \leq \frac{t}{2} \\ E_0 \cos\left(\frac{ht}{2} + \phi\right) \exp[p\left(\frac{t}{2} + x\right)], & x \leq -\frac{t}{2} \end{cases} \quad (2.13)$$

$$E_y = \begin{cases} E_0 \cos(hx - \phi), & -\frac{t}{2} \leq x \leq \frac{t}{2} \end{cases} \quad (2.14)$$

$$E_y = \begin{cases} E_0 \cos\left(\frac{ht}{2} + \phi\right) \exp[p\left(\frac{t}{2} + x\right)], & x \leq -\frac{t}{2} \end{cases} \quad (2.15)$$

where h , p , q and ϕ are given by

$$h = \sqrt{n_1^2 k^2 - \beta^2}, \quad (2.16)$$

$$p = \sqrt{\beta^2 - n_2^2 k^2}, \quad q = \sqrt{\beta^2 - n_3^2 k^2} \quad (2.17)$$

$$2\phi = \arctan\left[\frac{(p - q)h}{pq + h^2}\right] \quad (2.18)$$

By imposing the continuity condition, the dispersion relation for TE modes can be written as

$$ht - \arctan\left(\frac{p}{h}\right) - \arctan\left(\frac{q}{h}\right) = m\pi \quad (2.19)$$

where

the modal label m is an integer. This is in agreement with the dispersion relation obtained previously. The dispersion equation for TM mode is same as Equation (2.19) with $\left(\frac{n_1}{n_2}\right)^2 p$ and $\left(\frac{n_1}{n_3}\right)q$ for p and q , respectively.

The constant, E_0 , appearing in Equations (2.12)~(2.14) is arbitrary. Yet for many applications especially those in which propagation and exchange of power involve more than one mode, it is advantageous to define E_0 in such a way that the constant E_0 is related to total power in the mode.

The general properties of TE and TM mode solutions are illustrated in Figure 2.6. In general a mode becomes confined above a certain value of t/λ_0 . At the cut off value of $p = 0$, the mode extends to $x = \infty$. For an increasing value of t/λ_0 with $p > 0$, the mode becomes increasingly confined to layer 1. This is reflected in the effective guide index n_e (or normalized propagation constant) which, at cut off, equals to n_2 . And for a large value of t/λ_0 , n_e approaches to n_1 . In a symmetric waveguide the lowest order modes TM_0 and TE_0 have no cut off and are confined for all values of t/λ_0 .

Figure 2.7 shows that E_y can have considerable magnitude outside the guiding layer of the three layer slab waveguide. For some applications of waveguide such as double heterojunction lasers, the stimulated emission and gain coefficient are related to the photon flux. It is important to consider the field distribution in order to determine

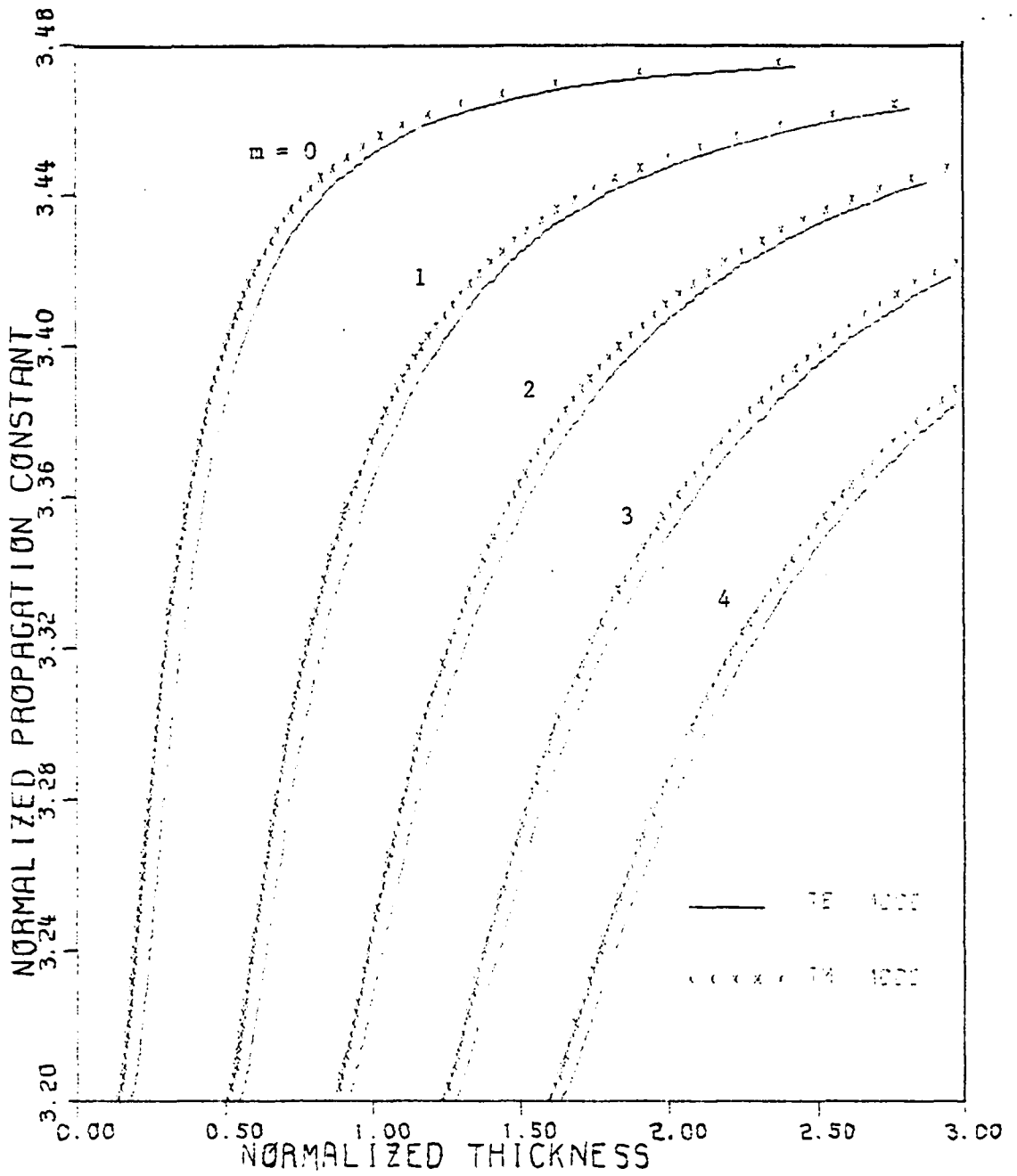


Figure 2.6. Dispersion Curves for the Confined Modes of $\text{Ga}_{1-x}\text{Al}_x\text{As}$ on GaAs Waveguide.

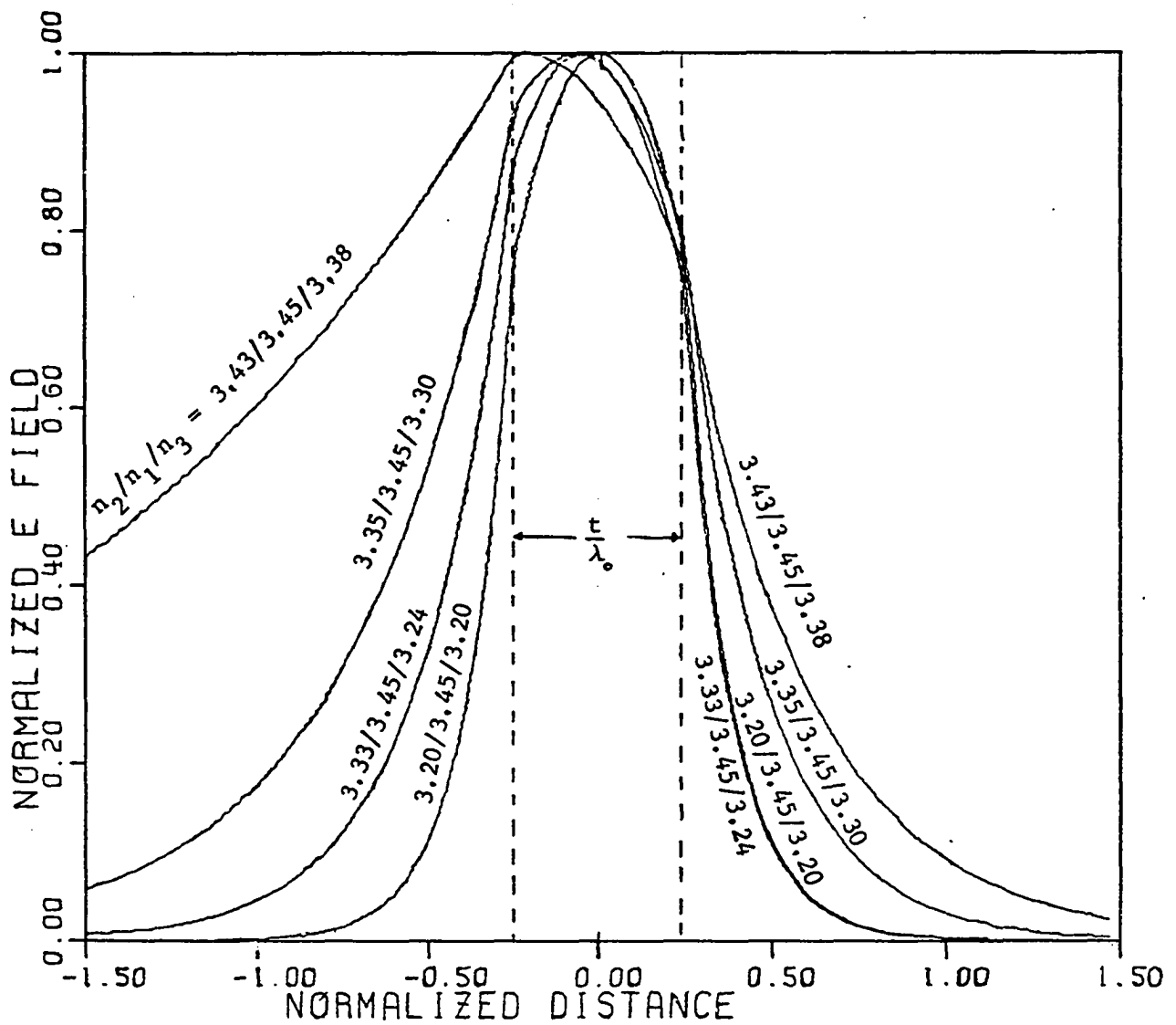


Figure 2.7. Amplitude of the Electric Field as a Function of Position for $\text{Ga}_x\text{Al}_{1-x}\text{As} - \text{GaAs} - \text{Ga}_y\text{Al}_{1-y}\text{As}$ Waveguide With $t/\lambda_0 = 0.5$ and $\lambda_0 = 1.15 \text{ } (\mu\text{m})$.

the fraction of the optical mode within the guiding layer. The optical flux is given by the Poynting vector and is proportional to $|E_y|^2$.

The confinement factor is defined as the ratio of the light intensity within the guiding layer to the sum of light intensity within and outside the guiding layer.

The confinement factor Γ for the symmetric three layer slab waveguide is given by

$$\Gamma = \frac{\int_{-t/2}^{t/2} \cos^2(hx - \phi) dx}{\left\{ \int_{-\infty}^{-t/2} \frac{t}{2} \cos^2\left(\frac{ht}{2} + \phi\right) \exp[2p\left(\frac{t}{2} + x\right)] dx + \int_{-t/2}^{t/2} \cos^2(hx - \phi) dx + \int_{t/2}^{\infty} \cos^2\left(\frac{ht}{2} - \phi\right) \exp[2q\left(\frac{t}{2} - x\right)] dx \right\}} \quad (2.20)$$

which gives

$$\Gamma = \left[1 + \frac{\frac{1}{p} \cos^2\left(\frac{ht}{2} + \phi\right) + \frac{1}{q} \cos^2\left(\frac{ht}{2} - \phi\right)}{t + \frac{1}{h} \cos 2\phi \sin ht} \right]^{-1} \quad (2.21)$$

for the TE modes. The confinement factor is frequently used because it represents the energy of the propagating mode within the guiding layer. Figure 2.8 shows the confinement factor as a function of the guiding layer thickness t for various TE modes.

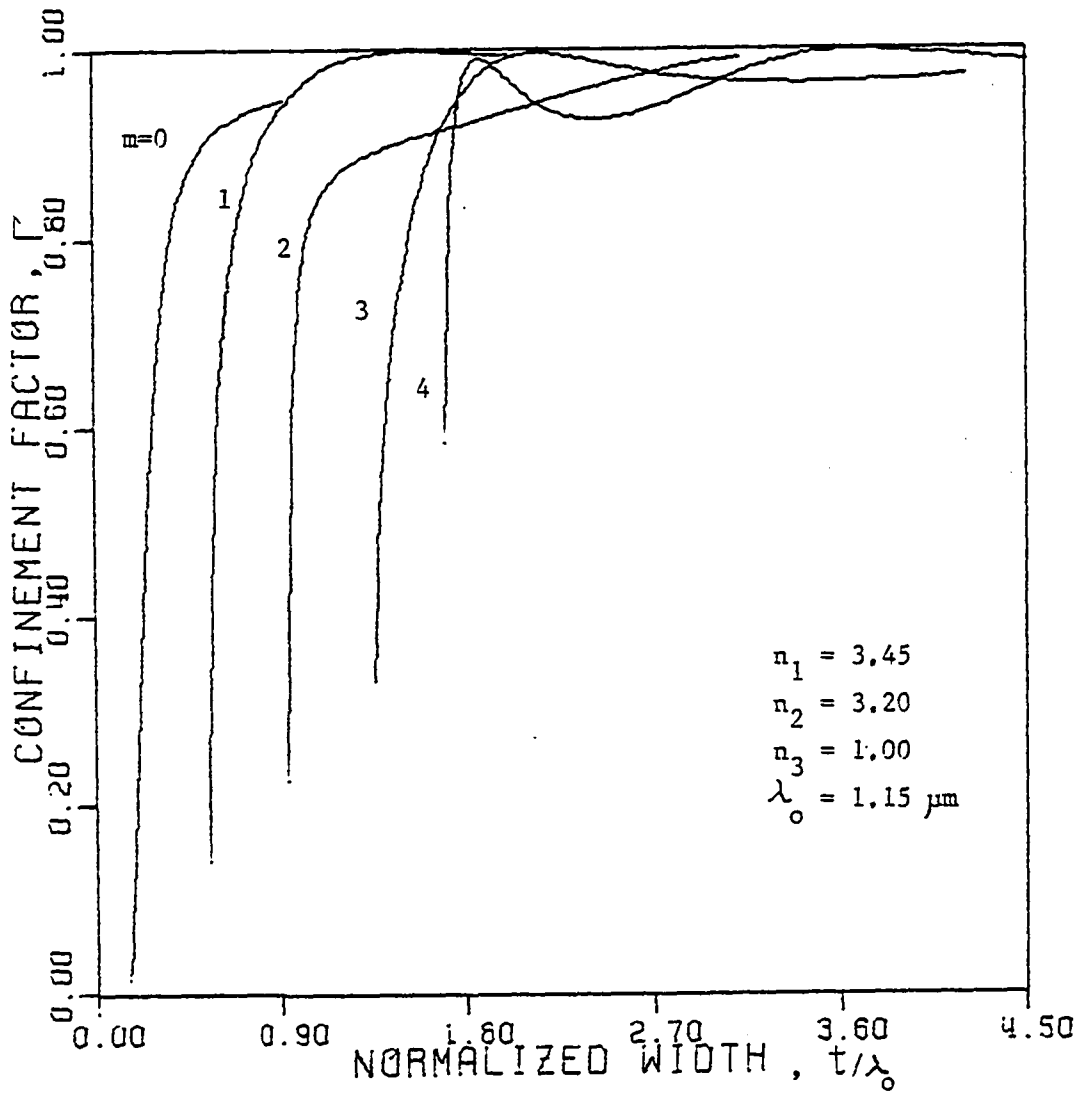


Figure 2.8. The Confinement Factor Γ for the TE Mode of Asymmetric Waveguide.

CHAPTER III

A CHARACTERIZATION OF A MULTILAYERED REFLECTOR

3.1. Introduction

Multilayered media play an important role in a number of applications. These include narrow band optical filter, anti-reflective coating, highly reflective mirror, and polarizers. The design and the characteristic of these devices are strongly dependent upon the understanding of electromagnetic propagation in multilayered media. Propagation of waves in stratified media is of great interest in areas other than thin film optics, also. And much work has been done in seismic waves, elastic waves, acoustic waves and also electromagnetic waves, especially in connection with reflection of radio waves in earth's atmosphere. Reviews of these works have been made by Brillouin (32), Wait (33) and Brekhouskikh (34).

The propagation of light through stratified medium has been considered by various authors (35-37), mainly with the thin film optical filter. Historically the earliest approach of dealing with the interference effect in thin film, and still perhaps the simplest and most intuitive is the classical approach of Airy (38) on summing multiple reflections. It becomes readily apparent, of course, that any numerical work will be a time consuming affair especially in an absorbing film. Moreover, the complete recursion process has to be

repeated for each change of parameter in a layer and the result is of little use for numerical work when there are more than four layers. Some of the other approaches, such as the one based on Stoke's relations and the principle of superposition ⁽³⁹⁾, are interesting in general, but again they are insufficient for numerical computation. Another approach to thin film computation is the form of graphical method ⁽⁴⁰⁾, certain of which have considerable value either in offering a degree of visualization or as a spot check calculation where only a few layers are involved.

In this chapter, the closed form expression for the reflectivity of periodic multilayer reflector making use of the so called Abele's method is derived. Yeh, et. al., ⁽⁶⁾ recently published reflectivity of a Bragg reflector. However this result is for the special Bragg reflector whose two outer most media have the same indices as one of the refractive indices of periodic layers.

In application of a Bragg reflector in waveguiding structure, various layer parameter, such as refractive index and thickness of each layer play an important role in reflectivity and selectivity of a Bragg waveguide. But in most of the previously published papers, no detailed explanation about the relationship between various layer parameters can be found.

It is the purpose of this chapter to provide the necessary relationship together with the description of some important characteristics of multilayered reflectors.

3.2 Recurrence Relations in Multilayer

A multilayer shown schematically in Figure 3-1, consists of ℓ number of layers surrounded on the two sides by semifinite media. The cartesian coordinate system is chosen such that the x axis is normal to the interfaces. The layers are numbered in order from the left to right. The interface between the layers are numbered from 0 to ℓ . n_1 will stand for the refractive index of guiding layer and $n_{\ell+1}$ for that of substrate. But n_g and n_s will be used instead of n_0 and $n_{\ell+1}$, respectively. The refraction angles will be denoted by $\theta_0, \theta_1, \dots, \theta_\ell$.

It is assumed that the incident light is monochromatic plane polarized and the individual layers are homogeneous, isotropic, non-magnetic and lossless.

The index of refraction of each layer is given by

$$n(x) = \begin{cases} n_g & x < x_0 \\ n_1 & x_0 < x < x_1 \\ \cdot & \\ \cdot & \\ n_i & x_{i-1} < x < x_i \\ \cdot & \\ \cdot & \\ \cdot & \\ n_\ell & x_{\ell-1} < x < x_\ell \\ n_s & x_\ell < x \end{cases} \quad (3.1)$$

The electric and magnetic fields can be obtained as solutions of Maxwell's equations subject to the certain boundary conditions at interfaces. Interference effects within the multilayer give rise, in general, to a reflected as well as transmitted wave in each layer except

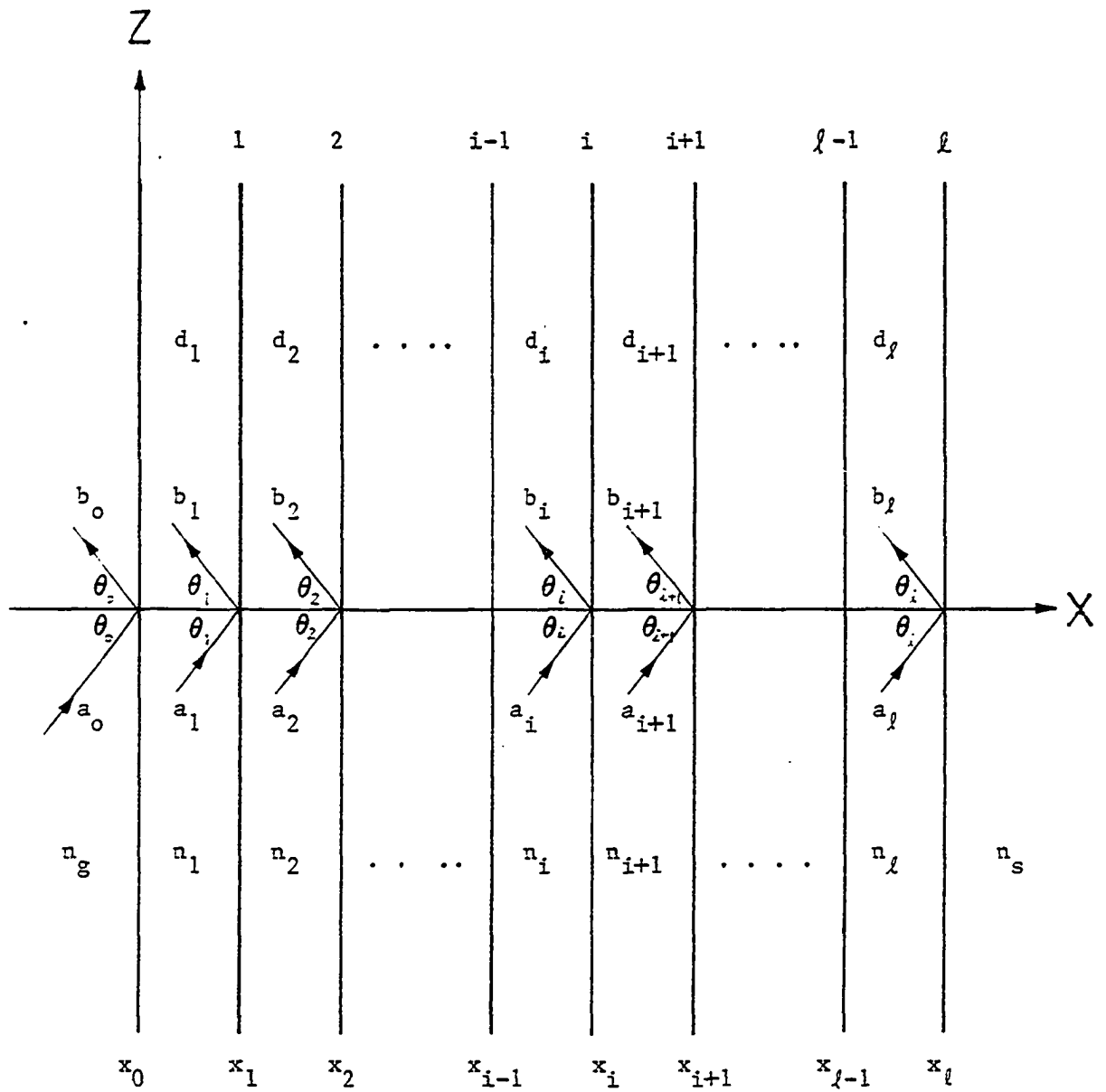


Figure 3.1. Schematic Representation of a Multilayer.

in the emergent semifinite medium where only a transmitted wave exists. Within the i^{th} layer the general form of the solution for the electric field distribution can be expressed as a sum of a transmitted and reflected waves. The complex amplitude of these two waves constitute the components of a column vector. The electric and magnetic field is described in matrix form,

$$\begin{bmatrix} E(x, z, t) \\ H(x, z, t) \end{bmatrix} = \begin{bmatrix} \exp\{jk_i(x-x_i)\} & \exp\{-jk_i(x-x_i)\} \\ n_i \exp\{jk_i(x-x_i)\} & -n_i \exp\{-jk_i(x-x_i)\} \end{bmatrix} \begin{bmatrix} a_i \\ b_i \end{bmatrix} \exp\{j(\beta z - \omega t)\} \quad (3.2)$$

where

β : propagation constant

a_i : incident complex amplitude at i^{th} interface

b_i : reflected complex amplitude at i^{th} interface

n_i : optical admittance of i^{th} layer

$$k_i = \frac{2\pi}{\lambda_0} n_i \cos \theta_i, \quad i = 0, 1, 2, \dots, \ell \quad (3.3)$$

λ_0 : wavelength in vacuum

The amplitude column vector in equation (3.2) is related to that of the adjunct layers. They are related through the continuity condition at the interfaces. Imposing the continuity condition at i^{th} interface (i.e. $x = x_i$) leads to

$$\begin{bmatrix} 1 & 1 \\ n_i & -n_i \end{bmatrix} \begin{bmatrix} a_i \\ b_i \end{bmatrix} = \begin{bmatrix} \exp(-jk_{i+1}d_{i+1}) & \exp(jk_{i+1}d_{i+1}) \\ n_{i+1} \exp(-jk_{i+1}d_{i+1}) & -n_{i+1} \exp(jk_{i+1}d_{i+1}) \end{bmatrix} \begin{bmatrix} a_{i+1} \\ b_{i+1} \end{bmatrix} \quad (3.4)$$

Here d_{i+1} is thickness of the $(i+1)^{\text{th}}$ layer and given as $d_{i+1} = x_{i+1} - x_i$.

Equation (3.4) can be put into a more useful form as shown.

$$\begin{bmatrix} a_i \\ b_i \end{bmatrix} = \frac{1}{2} \begin{bmatrix} 1 & 1/\eta_i \\ 1 & -1/\eta_i \end{bmatrix} \begin{bmatrix} 1 & 1 \\ \eta_{i+1} & -\eta_{i+1} \end{bmatrix} \begin{bmatrix} a_{i+1} \exp(-jk_{i+1}d_{i+1}) \\ b_{i+1} \exp(jk_{i+1}d_{i+1}) \end{bmatrix} \quad (3.5)$$

The above equation (3.5) may be written as the following simple matrix equation.

$$\begin{bmatrix} a_i \\ b_i \end{bmatrix} = \frac{1}{t_{i+1}} \begin{bmatrix} 1 & r_{i+1} \\ r_{i+1} & 1 \end{bmatrix} \begin{bmatrix} a_{i+1} \exp(-jk_{i+1}d_{i+1}) \\ b_{i+1} \exp(jk_{i+1}d_{i+1}) \end{bmatrix}, \quad (3.6)$$

where t_{i+1} , r_{i+1} are Fresnel transmission and reflection coefficient, respectively and defined as

$$t_{i+1} = c_{i,i+1} \frac{2 \eta_i}{\eta_i + \eta_{i+1}}, \quad (3.7)$$

$$r_{i+1} = \frac{\eta_i - \eta_{i+1}}{\eta_i + \eta_{i+1}}. \quad (3.8)$$

And in Equation (3.7) $c_{i,i+1}$ denotes

$$c_{i,i+1} = \begin{cases} \cos \theta_i / \cos \theta_{i+1}, & \text{for TM} \\ 1, & \text{for TE} \end{cases} \quad (3.9)$$

here i is integer $0, 1, 2, \dots, l$. Equation (3.6) describes the transformation of column vector from right side of interface to the left side.

There can be several alternate notations that can be used in multilayer calculations, which are related to one another but modify the computational format substantially. Matrix notation has considerable practical importance in one or another aspect of numerical or design

work and will be discussed in detail.

3.3 Matrix Method to Calculate Reflectivity

We are now ready to introduce the matrix method for analyzing the propagation of plane waves in multilayer media. The recursion relation (3.5) has the form of a linear transformation of variables, and they can conveniently be written as a matrix equation,

$$\begin{bmatrix} a_i \\ b_i \end{bmatrix} = V_i^{-1} V_{i+1} U_{i+1} \begin{bmatrix} a_{i+1} \\ b_{i+1} \end{bmatrix}, \quad (3.10)$$

where

$$V_i = \begin{bmatrix} 1 & 1 \\ \eta_i & -\eta_i \end{bmatrix} \quad (3.11)$$

$$V_i^{-1} = \frac{1}{2} \begin{bmatrix} 1 & 1/\eta_i \\ 1 & -1/\eta_i \end{bmatrix} \quad (3.12)$$

and

$$U_i = \begin{bmatrix} \exp(-jk_i d_i) & 0 \\ 0 & \exp(jk_i d_i) \end{bmatrix} \quad (3.13)$$

The matrix V_i is called the optical admittance matrix, and depends only on the direction of polarization of waves. The matrix U_i is called phase matrix and depend only on the phase excursion of two oppositely traveling partial waves.

Equation (3.10) forms a basic defining relation of the reflected and incident complex amplitude between the adjunct layers.

The introduction of matrix notation is to be an important

development in multilayer media, especially in its use with an alternate set of variables, namely the resultant field complex amplitude. One of the conveniences of using the matrix method can be seen in the ease and compactness of the expression involved in combining this equation for a multilayer.

By successive repetition of the Equation (3.10), it is clear that the reflected and transmitted amplitude on the side of incidence wave can be written in the following form

$$\begin{bmatrix} a_0 \\ b_0 \end{bmatrix} = S \begin{bmatrix} a_{\ell+1} \\ b_{\ell+1} \end{bmatrix} \quad (3.14a)$$

here S will be called the system transfer matrix and is given as

$$S = V_0^{-1} V_1 U_1 V_1^{-1} V_2 U_2 \dots V_i^{-1} V_{i+1} U_{i+1} \dots V_{\ell-1}^{-1} V_{\ell} U_{\ell} V_{\ell}^{-1} V_{\ell+1} \quad (3.15)$$

Let the transfer matrix Equation (3.15) be rewritten in following form,

$$S = V_0^{-1} \left(\prod_{q=1}^{\ell} M_q \right) V_{\ell+1} \quad (3.16)$$

where M_q is called interference or characteristic matrix of q^{th} layer and denoted as

$$M_q = V_q U_q V_q^{-1} \quad (3.17)$$

Some of the more significant advantages of using the characteristic matrix become apparent at this point. For example, a change in the optical thickness or effective index of the q^{th} layer affects only q^{th} matrix, while the partial products of the matrices except the q^{th} layer are not affected. Let s_{ij} , with $i, j = 1, 2$, denotes the elements

of matrix S

$$S = \frac{1}{2}[s_{ij}] \quad (3.18)$$

Now we can compute the amplitude reflection coefficient and transmission coefficient using Equation (3.14). When light is incident from the left side only, the transmission coefficient t and reflection coefficient r are described by

$$r = \frac{b_0}{a_0} = \frac{s_{21}}{s_{11}} \quad (3.19)$$

$$t = \frac{a_{2+1}}{a_0} = \frac{c_{0,2+1}}{s_{11}} \quad (3.20)$$

The characteristic matrix assumes an even more important role if electric and magnetic field are introduced as the explicit variables.

Let the Equation (3.2) be written in the following form,

$$E_i(x, z, t) = E_i(x) \exp\{j(\beta z - \omega t)\} \quad (3.21)$$

$$H_i(x, z, t) = H_i(x) \exp\{j(\beta z - \omega t)\}$$

thus the electric and magnetic field in i^{th} layer is described as

$$\begin{bmatrix} \bar{E}_i(x) \\ \bar{H}_i(x) \end{bmatrix} = \begin{bmatrix} \exp\{jk_i(x-x_i)\} & \exp\{-jk_i(x-x_i)\} \\ \eta_i \exp\{jk_i(x-x_i)\} - \eta_i \exp\{-jk_i(x-x_i)\} \end{bmatrix} \begin{bmatrix} \bar{a}_i \\ \bar{b}_i \end{bmatrix} \quad (3.22)$$

Equation 3.10 at i^{th} interface can be rewritten as

$$\begin{bmatrix} \bar{a}_i \\ \bar{b}_i \end{bmatrix} = V_i^{-1} \begin{bmatrix} \bar{E}_i(x_i) \\ \bar{H}_i(x_i) \end{bmatrix} \quad (3.23)$$

Again evaluating Equation (3.10) at $(i-1)^{\text{th}}$ interface and combining with Equation (3.10) and Equation (3.23), the recursion relation for

$H(x)$ and $E(x)$ in matrix form is obtained as follows,

$$\begin{bmatrix} E_{i-1}(x_{i-1}) \\ H_{i-1}(x_{i-1}) \end{bmatrix} = M_i \begin{bmatrix} E_i(x_i) \\ H_i(x_i) \end{bmatrix} \quad (3.24)$$

Obviously the characteristic matrix transforms the electric and magnetic field at interface x_i into those at x_{i-1} . Thus $E_0(x_0)$ and $H_0(x_0)$ are related to $E_\ell(x_\ell)$ and $H_\ell(x_\ell)$ by an equation similar to Equation (3.14).

By inserting Equations (3.11)~(3.13) into the Equation (3.17), M_q is given as,

$$M_q = \begin{bmatrix} \cos \delta_q & -j/\eta_q \sin \delta_q \\ -jn_q \sin \delta_q & \cos \delta_q \end{bmatrix} \quad (3.25)$$

where

$$\delta_q = (2\pi/\lambda_0)n_q \cos \theta_q, \quad \eta_q = \begin{cases} n_q \cos \theta_q, & \text{for TE,} \\ n_q/\cos \theta_q, & \text{for TM} \end{cases}$$

And q denotes integer $1, 2, \dots, \ell$. It is important to note that the determinant of Equation (3.25) is equal to unity.

The characteristic matrices, Equation (3.25) completely describes the characteristics of individual layers in multilayer media. Writing

$$\prod_{q=1}^{\ell} M_q = \begin{bmatrix} m_{11} & jm_{12} \\ jm_{21} & m_{22} \end{bmatrix}, \text{ the system transfer matrix element } s_{ij} \text{ is given}$$

by

$$s_{11} = m_{11} + j \frac{m_{21}}{\eta_g} + jm_{12}\eta_s + \frac{\eta_s}{\eta_0} m_{22}$$

$$\begin{aligned}
s_{12} &= m_{11} + j \frac{m_{21}}{n_g} - jm_{12}n_s - \frac{n_s}{n_o} m_{22} \\
s_{21} &= m_{11} - j \frac{m_{21}}{n_g} + jm_{12}n_s - \frac{n_s}{n_g} m_{22} \\
s_{22} &= m_{11} - j \frac{m_{21}}{n_g} - jm_{12}n_s + \frac{n_s}{n_g} m_{22}
\end{aligned} \tag{3.26}$$

The reflection and transmission coefficient are obtained, by inserting Equation (3.26) into Equation (3.19) and (3.20),

$$r = \frac{(n_g m_{11} - m_{22} n_s) + j(m_{12} n_s n_g - m_{21})}{(n_g m_{11} + m_{22} n_s) + j(m_{12} n_s n_g + m_{21})} \tag{3.27}$$

$$t = \frac{2C_{o,z} n_g}{(n_g m_{11} + m_{22} n_s) + j(m_{12} n_s n_g + m_{21})} \tag{3.28}$$

where

$$C_{o,z} = \begin{cases} \cos\theta_o / \cos\theta_z & \text{for TM} \\ 1 & \text{for TE} \end{cases} \tag{3.29}$$

Equation (3.24) is similar in form to the recursion relation equation (3.14) for the reflected and transmitted electric field amplitude, but the important difference is that the i^{th} matrix depends exclusively on the elements of the i^{th} layer. Accordingly, the advantages mentioned before for the use of matrix notation become even greater when $E(x)$ and $H(x)$ are used as the explicit variables, since a change in optical parameter such as thickness or index affects only one matrix.

3.4 Multilayer with Periodic Structure

The properties of a multilayer with periodic structure can be computed by the methods described in section 3.2. In particular, if the matrix method is used, the matrix for the fundamental period can be computed and raised to the appropriate power numerically. A closed expression for the n th power of a matrix is known and this enables a number of useful general properties of periodic structure to be predicted: it was first applied by Abeles and extended in detail by Mielenz ⁽⁴¹⁾. This section deals with some properties of multilayer reflector built up from a multilayer fundamental period repeated N times. The fundamental period of each layer is presented by a matrix which is a product of the characteristic matrix of its individual layer

$$M = \prod_{q=1}^L M_q \quad (3.30)$$

where matrices M_q are given by Eq. 3.25. Then the reflector which consists of N member of fundamental period is represented by the matrix whose element are obtained by N^{th} power of matrix m .

$$M = M^N = \begin{bmatrix} M_{11} & jM_{12} \\ jM_{21} & M_{22} \end{bmatrix} \quad (3.31)$$

where

$$M_{11} = C_N(x) + \left(\frac{m_{11} - m_{22}}{2} \right) S_{N-1}(x)$$

$$M_{12} = m_{12} S_{N-1}(x)$$

$$M_{21} = m_{21} S_{N-1}(x) \quad (3.32)$$

$$M_{22} = C_N(x) - \left(\frac{m_{11} - m_{22}}{2} \right) S_{N-1}(x)$$

The $C_n(x)$ and $S_n(x)$ used in Equation (3.32) are called Chebyshev polynomial of the first and second kind, respectively. In Equation (3.32), x denotes

$$x = \frac{m_{11} + m_{22}}{2} \quad (3.33)$$

and discriminates the stop zone. This will be examined in detail in later part of this chapter.

$C_n(x)$ and $S_n(x)$ are given by ⁽⁴²⁾

$$C_n(x) = \begin{cases} \cos(n \cos \theta) & , \quad |x| \leq 1 \\ \cosh(n \cosh \phi) & , \quad |x| \geq 1 \end{cases} \quad (3.34a)$$

$$S_n(x) = \begin{cases} \sin(n+1)\theta / \sin\theta & , \quad |x| \leq 1 \\ \sinh(n+1)\phi / \sinh\phi & , \quad |x| \geq 1 \end{cases} \quad (3.34b)$$

with $\theta = \cos^{-1}x$ and $\phi = \cosh^{-1}x$, and shown in Figure 3.2 and 3.3.

The reflection and transmission coefficients of multilayer periodic are immediately obtained by replacing $[m_{ij}]$ with $[M_{ij}]$ in Equation (3.27).

$$r_N = \frac{(\eta_g M_{11} - \eta_s M_{22}) + j(\eta_g \eta_s M_{12} - M_{21})}{(\eta_g M_{11} + \eta_s M_{22}) + j(\eta_g \eta_s M_{12} + M_{21})} \quad (3.35)$$

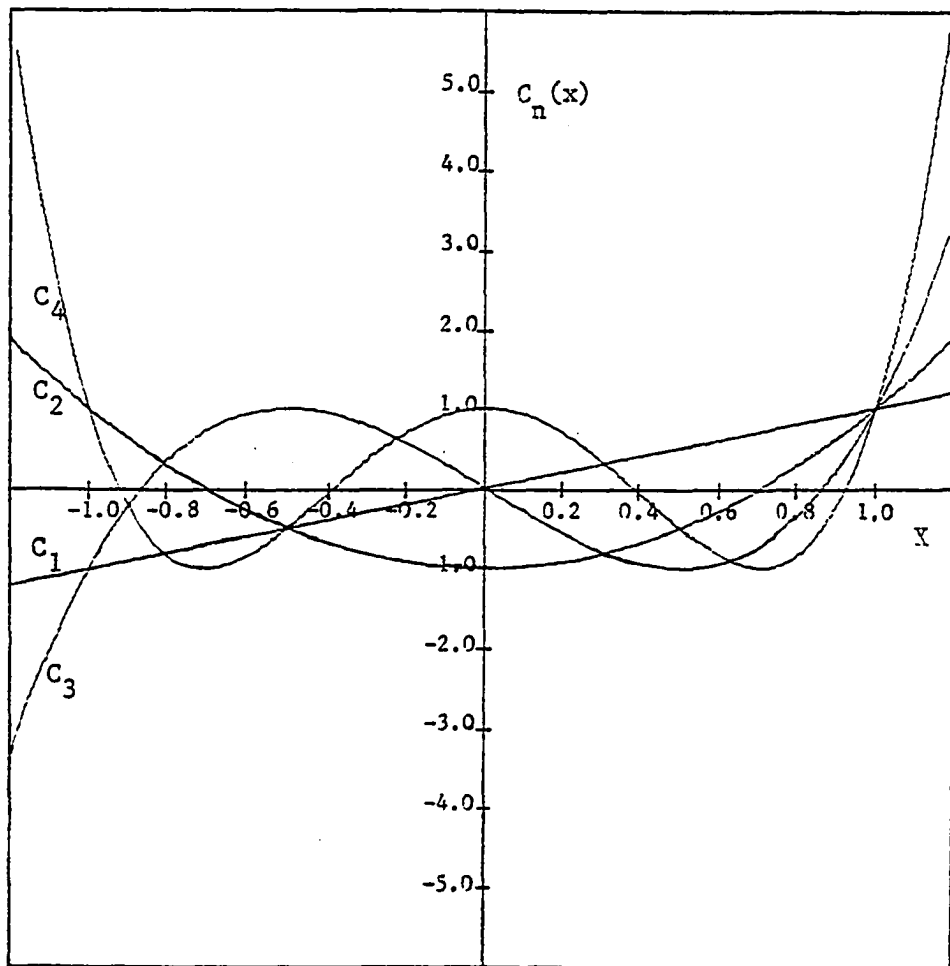


Figure 3.2. Chebyshev Polynomial $C_n(x)$.

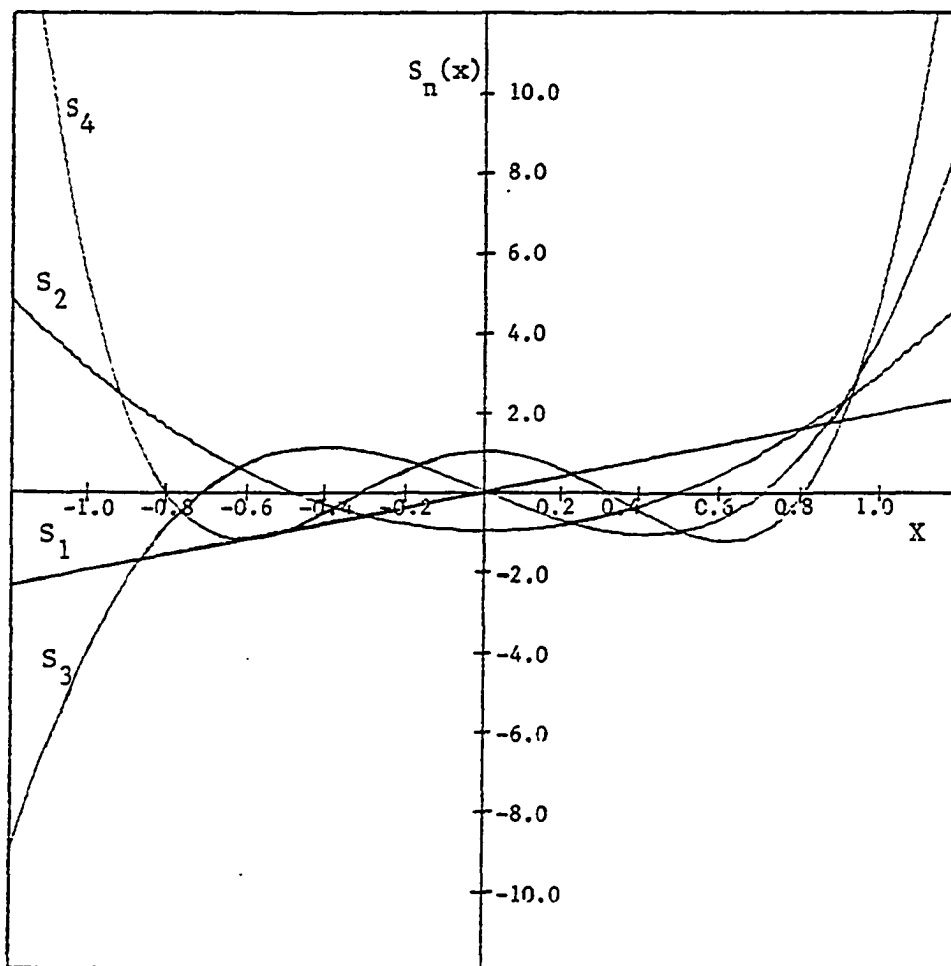


Figure 3.3. Chebyshev Polynomial $S_n(x)$.

$$t_N = \frac{2C_{o, \epsilon} n_g}{(n_g M_{11} + n_s M_{22}) + j(n_g n_s M_{12} + M_{21})} \quad (3.36)$$

The reflectivity and transmittivity can be written as, by substituting Equation (3.32) into Equation (3.35) and (3.36) and then taking absolute square,

$$R_N = \frac{\{(n_g - n_s)C_N(x) + (n_g + n_s)\left(\frac{m_{11} - m_{22}}{2}\right)S_{N-1}(x)\}^2 + \{(n_g n_s m_{12} - m_{21})S_{N-1}(x)\}^2}{\{(n_g + n_s)C_N(x) + (n_g - n_s)\left(\frac{m_{11} - m_{22}}{2}\right)S_{N-1}(x)\}^2 + \{(n_g n_s m_{12} + m_{21})S_{N-1}(x)\}^2} \quad (3.37)$$

$$T_N = \frac{4 C_{o, \epsilon}^2 n_g^2}{\{(n_g + n_s)C_N(x) + (n_g - n_s)\left(\frac{m_{11} - m_{22}}{2}\right)S_{N-1}(x)\}^2 + \{(n_g n_s m_{12} + m_{21})S_{N-1}(x)\}^2} \quad (3.38)$$

If the index of the medium in both sides of the multilayer is n_g , the reflectivity can be written as

$$R_N = \frac{D_N}{D_N + 4} \quad (3.39)$$

where

$$D_N = S_{N-1}^2(x) \left\{ (m_{11} - m_{22})^2 + (m_{12} n_g - \frac{m_{21}}{n_g})^2 \right\} \quad (3.40)$$

And also D_N is related to D_1 by

$$D_N = S_{N-1}^2 D_1 \quad (3.41)$$

For the single fundamental period, we have

$$R_1 = \frac{D_1}{D_1 + 4} \quad (3.42)$$

The R_1 for a typical multilayer Bragg reflector is much less than one. Substituting Equation (3.41) into Equation (3.39), we have,

$$R_N = \frac{D_1}{D_1 + \left(\frac{2}{S_{N-1}(x)}\right)^2} \quad (3.43)$$

According to Equation (3.43), unit reflectivity can be obtained when $S_{N-1}(x)$ approaches to infinity. It is shown in Figure 3.3 that $S_{N-1}(x)$ increase rapidly if the absolute value of x is greater than one.

In Equation (3.33) we mentioned the stop zone briefly. At a wavelength such that $|x| > 1$ the reflectivity increases steadily with the number of periods and tends to unity as N approaches to infinity. Such a zone, if it exists, is called a stop zone or stop band. (7-9) Yeh, et. al., (6) called it as forbidden gap which is widely used terminology of solid state physics. We will use the former terminology because of its familiarity.

For commonest case of fundamental period composed of two $\lambda_0/4$ layer of refractive index n_1 and n_2 , the discriminant is written as

$$\frac{m_{11} + m_{22}}{2} = \cos^2 \delta - \frac{1}{2} \left(\frac{n_1}{n_2} + \frac{n_2}{n_1} \right) \sin^2 \delta \quad (3.44)$$

Equation (3.44) is obtained using Equation (3.25). In Equation (3.44), δ denotes

$$\delta = \frac{2\pi}{\lambda_0} n_1 d_1 \cos \theta_1 = \frac{2\pi}{\lambda_0} n_2 d_2 \cos \theta_2 \quad (3.45)$$

The right hand side of Equation (3.44) can not be greater than 1, and so to find the edge of stop zone we must set

$$-1 = \cos^2 \delta_e - \frac{1}{2} \left(\frac{n_1}{n_2} + \frac{n_2}{n_1} \right) \sin^2 \delta_e \quad (3.46)$$

Then the width of zones defined as $\lambda_0/\Delta\lambda$ is given by

$$\Delta g = \frac{4}{\pi} \sin^{-1} \left(\frac{n_1 - n_2}{n_2 + n_1} \right) \quad (3.47)$$

This shows that the width of the zone is a function of the indices of the two media used in the construction of multilayer. The greater the width of the zone is obtained for the higher ratio of refractive indices.

3.5 Symmetrical Multilayer

Any dielectric layer combination is known as symmetric if each half is a mirror image of the other. The simplest example of this is a triple layer combination in which a central layer is sandwiched between two identical outer layers. According to Herpin's theorem ⁽⁴³⁾, any multilayer is equivalent, to a two layer combination at a given wavelength. In the particular case where the given multilayer combination is symmetrical, the Herpin equivalent is a single layer regardless of wavelength ⁽⁴⁴⁾. This property of a symmetrical multilayer was pointed out by Epstein ⁽⁴⁵⁾ who used it in designing filter. Consider the symmetric triple layered basic period such as $n_1 n_2 n_1$ structure, made up of dielectric layers of refractive indices n_1, n_2 , and phase angle δ_1, δ_2 , respectively. The element of the characteristic matrix is given by

$$m_{11} = \cos 2\delta_1 \cos \delta_2 - \frac{1}{2} \left(\frac{n_2}{n_1} + \frac{n_1}{n_2} \right) \sin 2\delta_1 \sin \delta_2 \quad (3.48a)$$

$$m_{12} = \frac{-1}{\eta_1} \left[\sin 2\delta_1 \cos \delta_2 + \frac{1}{2} \left(\frac{\eta_2}{\eta_1} + \frac{\eta_1}{\eta_2} \right) \cos 2\delta_1 \sin \delta_2 + \frac{1}{2} \left(\frac{\eta_1}{\eta_2} - \frac{\eta_2}{\eta_1} \right) \sin \delta_2 \right] \quad (3.48b)$$

$$m_{21} = -\eta_1 \left[\sin 2\delta_1 \cos \delta_2 + \frac{1}{2} \left(\frac{\eta_2}{\eta_1} \right) \cos 2\delta_1 \sin \delta_2 - \frac{1}{2} \left(\frac{\eta_1}{\eta_2} - \frac{\eta_2}{\eta_1} \right) \sin \delta_2 \right] \quad (3.48c)$$

and $m_{22} = m_{11}$

This relationship, together with the unimodularity of the characteristic matrix, permits the following definition of an equivalent layer to be made, .

$$\begin{aligned} \cos \delta_{eq} &= m_{11} = m_{22} \\ - \frac{\sin \delta_{eq}}{\eta_{eq}} &= m_{12} \\ - \eta_{eq} \sin \delta_{eq} &= m_{21} \end{aligned} \quad (3.49)$$

These quantities have exactly the same form as a single layer of phase thickness δ_{eq} and admittance η_{eq} .

$$\delta_{eq} = \cos^{-1} m_{11} \quad (3.50)$$

$$\eta_{eq} = \sqrt{\frac{m_{21}}{m_{12}}} \quad (3.51)$$

The equivalence is purely mathematical rather than a case of true physical equivalence, but the result is of considerable in giving an

insight into the physical properties, particularly for a periodic structure.

If a Bragg reflector is made up of N identical symmetrical periods, each of which has an equivalent phase thickness δ_{eq} and equivalent admittance η_{eq} , then physical considerations show that Bragg layer will be equivalent to single layer to thickness $N \delta_{eq}$ and admittance η_{eq} . This result also follows,

$$\begin{bmatrix} \cos \delta_{eq} & -j \sin \delta_{eq} / \eta_{eq} \\ -j \eta_{eq} \sin \delta_{eq} & \cos \delta_{eq} \end{bmatrix}^N = \begin{bmatrix} \cos N \delta_{eq} & -j \sin N \delta_{eq} / \eta_{eq} \\ -j \eta_{eq} \sin N \delta_{eq} & \cos N \delta_{eq} \end{bmatrix} \quad (3.52)$$

In the present symmetrical case, the stop zone is given as

$$|M_{11}| = |M_{22}| = |\cos N \delta_{eq}| > 1. \quad (3.53)$$

Inside the stop zone, the equivalent phase thickness and the equivalent admittance are both imaginary. Outside the stop zone the phase thickness and admittance are real and these zones are known as pass zones or pass bands. For the symmetric basic period such as $(\frac{n_1}{8} \frac{n_2}{4} \frac{n_1}{8})$, where $\frac{n_1}{8}$ and $\frac{n_2}{4}$ represent eighth wavelength layer of refractive index n_1 and quarter wavelength layer of refractive index n_2 , stop zone width is expressed exactly same as Equation (3.47) which was obtained for the double quarter wave layer. This equation also valid for $(\frac{n_2}{8} \frac{n_1}{4} \frac{n_2}{8})$ structure.

Figure 3.4 and 3.5 represent the equivalent optical admittance and optical thickness for a symmetric triple layer at 80° incidence

with typical value of ratio of refractive index. In passband, the symmetric multilayer can be replaced by a single layer of n_{eq} and δ_{eq} . Thus the reflectivity will oscillate between two values, the reflectivity of bare substrate

$$\left(\frac{n_g - n_s}{n_g + n_s} \right)^2 \quad (3.54)$$

and that given by

$$\left(\frac{n_g n_s - n_{eq}^2}{n_g n_s + n_{eq}^2} \right)^2 \quad (3.55)$$

The actual position of maximum and minimum of ripple in pass band is given by

$$\delta_{eq} = \begin{cases} \left(\frac{S}{N} \right) \left(\frac{\pi}{2} \right) & \text{for maximum} \\ \left(\frac{r}{N} \right) \pi & \text{for minimum} \end{cases} \quad (3.56)$$

here

$$S = 1, 3, 5, 7, \dots$$

$$r = 1, 2, 3, 4, \dots$$

N : number of period

It was shown in Equation (3.33) and (3.43) that the reflectivity of a reflector depends on the stop zone x . And also optical confinement and loss of a Bragg waveguide, which will be discussed in Chapter V are related to the value of the stop zone. In order to get maximum reflectivity, it is desirable to find a reflector with layer thickness such that x has its maximum possible value. In other words, the optimum thickness of the reflector is such that

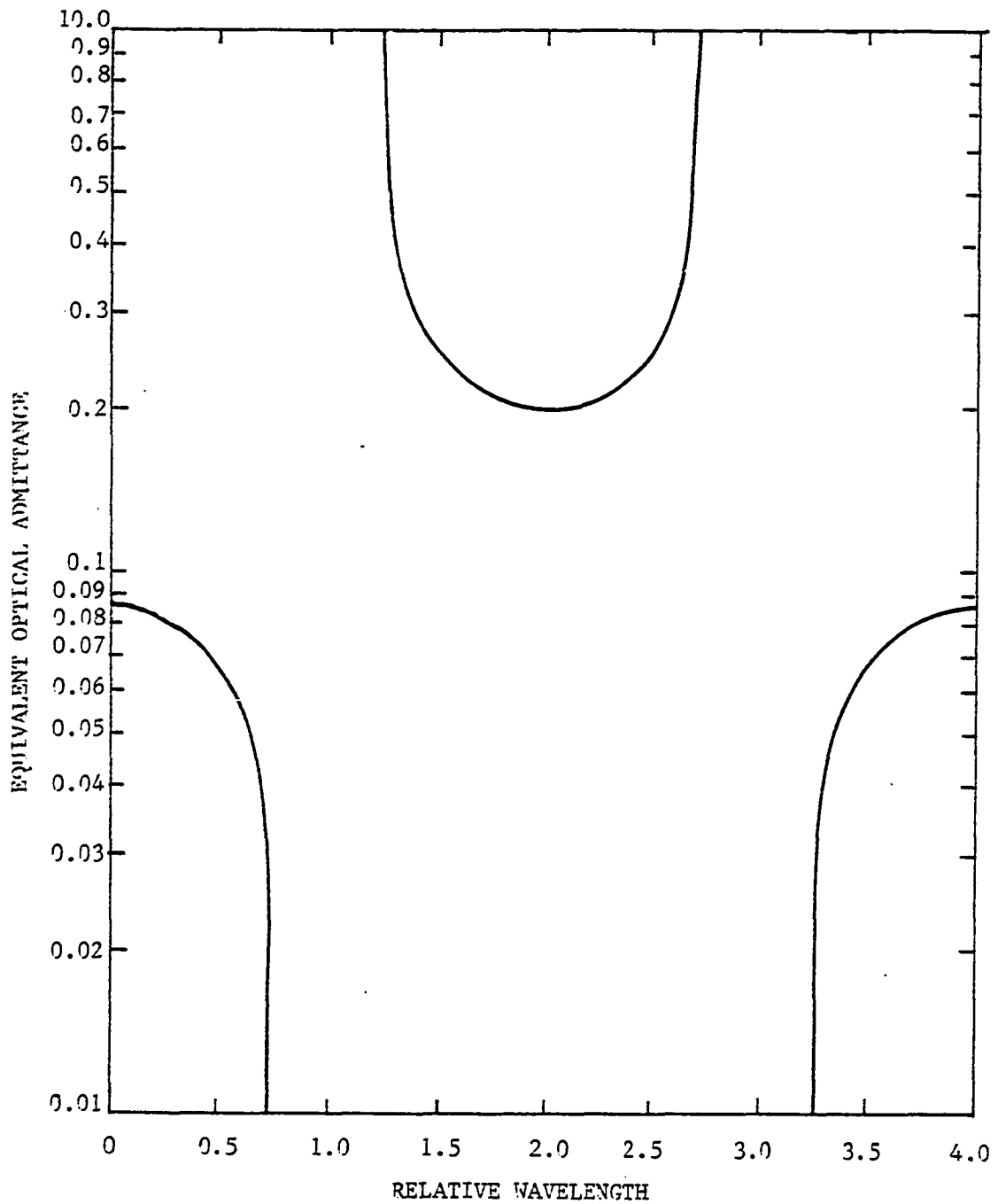


Figure 3.4. Equivalent Optical Admittance for the Structure $\left(\frac{n_1}{8} \frac{n_2}{4} \frac{n_1}{8}\right)$ with $n_1 = 3.45$ and $n_2 = 3.24$ at 80° Incidence Angle.

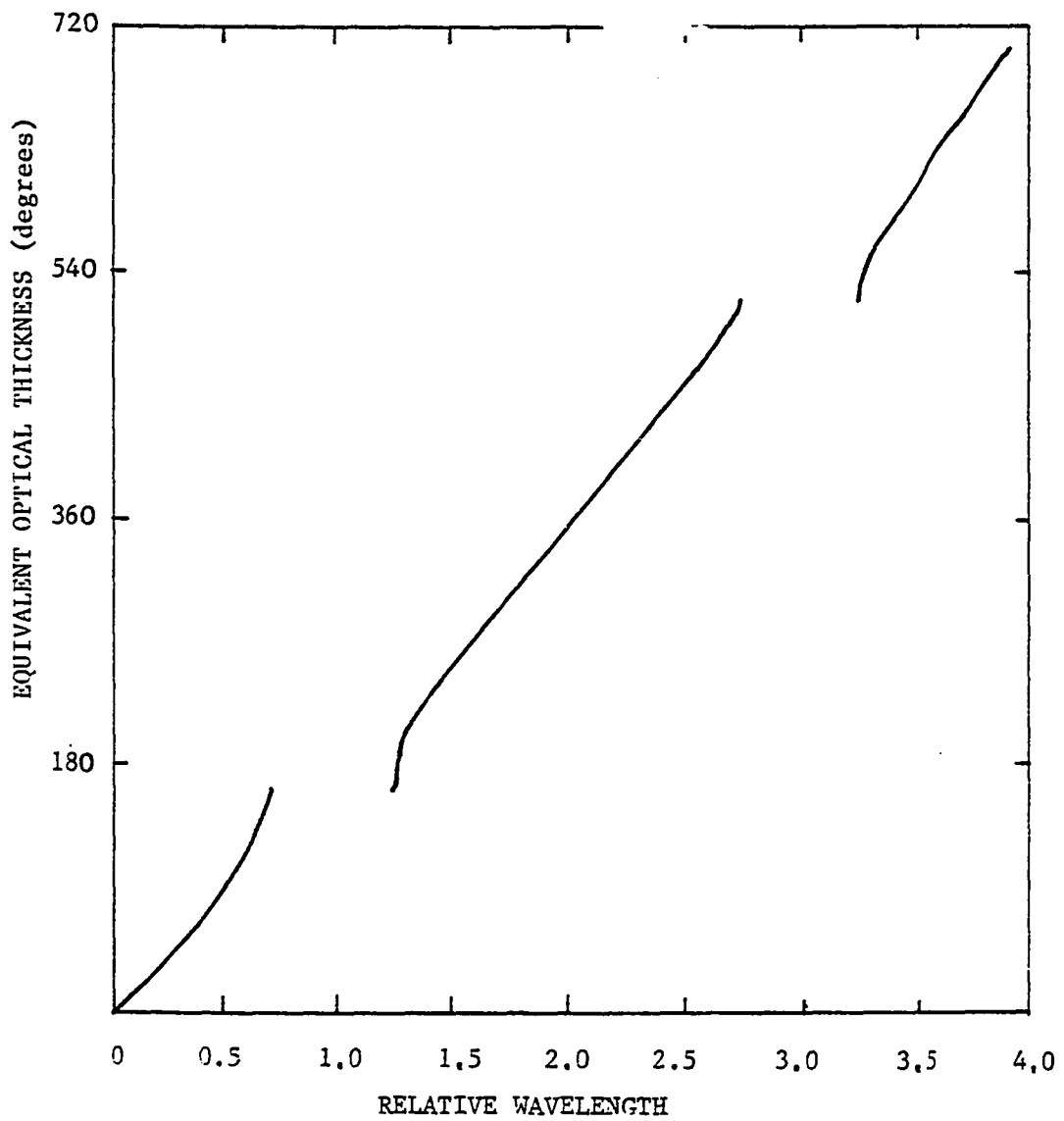


Figure 3.5. Equivalent Optical Thickness of the Structure Described in Figure 3.4.

$$\frac{\partial x}{\partial d_i} = 0, \quad i = 1, 2, \dots, q \quad (3.57)$$

Applying Equation (3.57) to Equation (3.33), the optimum thicknesses of each layer for symmetric triple structure are obtained by

$$\begin{aligned} k_1 d_1 &= \frac{\pi}{4} \\ k_2 d_2 &= \frac{\pi}{2} \\ k_3 d_3 &= \frac{\pi}{4} \end{aligned} \quad (3.58)$$

Equation (3.58) represent that $(\frac{n_1}{8} \frac{n_2}{4} \frac{n_1}{8})$ triple symmetric structure has its maximum value of a stop zone for a given incidence condition. At this optimum condition the stop zone is given by

$$x = -\frac{1}{2} \left(\frac{n_2}{n_1} + \frac{n_1}{n_2} \right) \quad (3.59)$$

CHAPTER IV

THE NUMERICAL RESULTS IN MULTILAYERED PERIODIC REFLECTOR

4.1. Introduction

The introduction of Bragg reflection principle opens a new dimension for light propagation in Integrated Optics.^(46 - 48) The application of such Bragg reflection has been recently reported in optical guiding structure and injection lasers. In both cases, various layer parameter such as refractive index and thickness of each layer, play an important role in reflectivity and selectivity of a Bragg waveguide. But in most of the previously published papers, no detail explanation about the relationship between refractive index and thickness to each layer can be found. All the Bragg reflector reported up to date have a double layered structure and have a large number of periodic layers. It is the purpose of this chapter to provide the necessary data together with the description of some important characteristic of reflectivity and selectivity.

In this chapter, we deal with a double, triple, quadruple and quintuple layered periodic reflector, and compare the characteristics of each structure.

Throughout this chapter, all numerically calculated data for multilayered reflectors is for $\text{Ga}_{1-x}\text{Al}_x\text{As}$ and GaAs layers. It is extremely difficult to get a systematic method, in general, to the design of a periodic Bragg reflector which satisfy the given specifications such as reflectivity,

stop band width, and others. This is due to the fact that the closed form equation for reflectivity given by Equation (3.38) is a transcendental function. Even though we try the analytical solution in design problem, it has a practical limit to meet naturally available range of refractive index, for GaAs case, $3.20 \leq \text{index} \leq 3.45$ at $1.15 \mu\text{m}$. (49-51)

4.2. Reflectivity Spectrum

To investigate the reflectivity for a typical reflector, it is necessary to evaluate Equation (3.37). The reflectivities for a double layered Bragg reflector as a function of relative wavelength which is defined as λ_0/λ , and angle of incidence are displayed in Figure 4.1. The TM waves incident at Brewster angle has zero reflectivity. The Brewster angle for the double layered structure is (52)

$$\theta_B = \sin^{-1} \left[\frac{n_1 n_2}{n_g \sqrt{n_1^2 + n_2^2}} \right], \quad (4.1)$$

and can be observed in Figure 4.1(b). It is observed that change in incidence angle remarkably affects the reflective spectrum. The behavior of a typical quarter wave period is shown in Figure 4.2. The high reflection zone became smaller with an increasing N. On either side of a plateau, the reflectance falls abruptly to a low oscillatory value. The oscillation of reflectivity outside the stopband are called secondary or subsidiary maximum. The additional period not only affect the width of zone of high reflectance but also increase the reflectance within the zone and the number of subsidiary maxima. The values of subsidiary maxima also increase with the number of periods and have a tendency to be smaller towards the outsides. Their envelope, as well as the value of

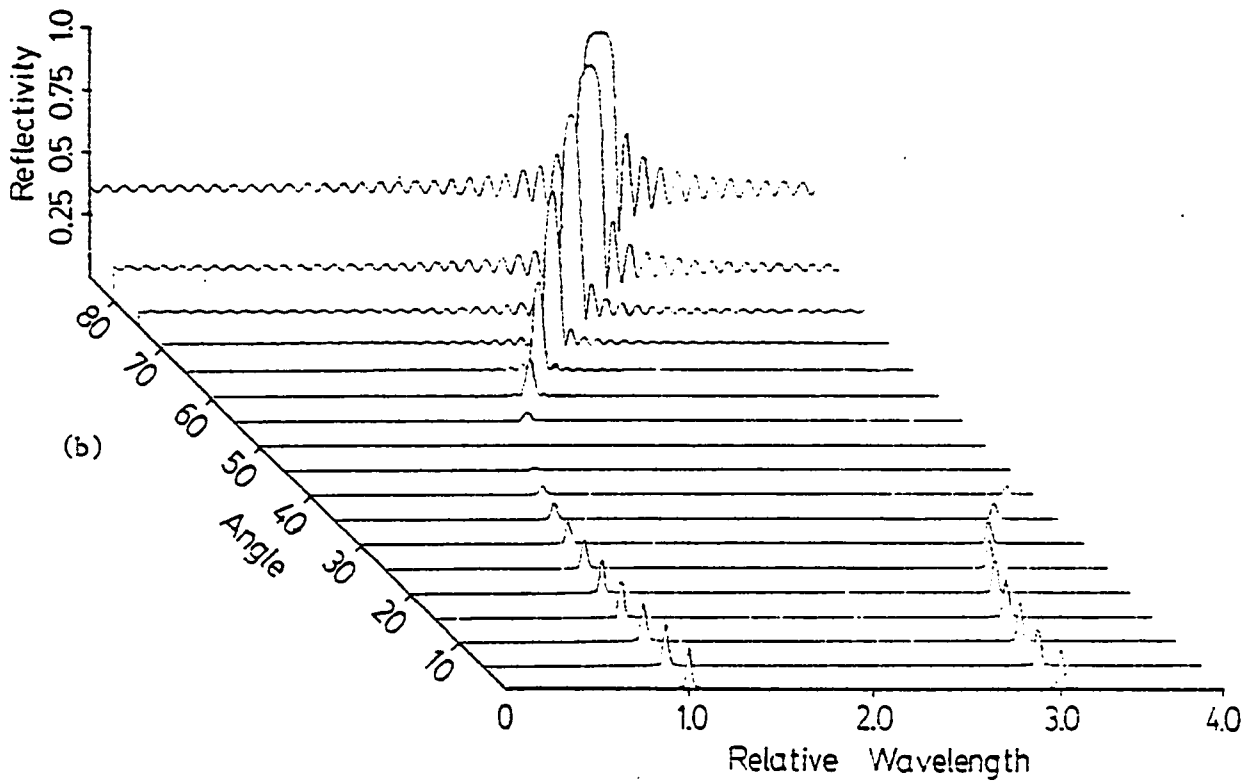
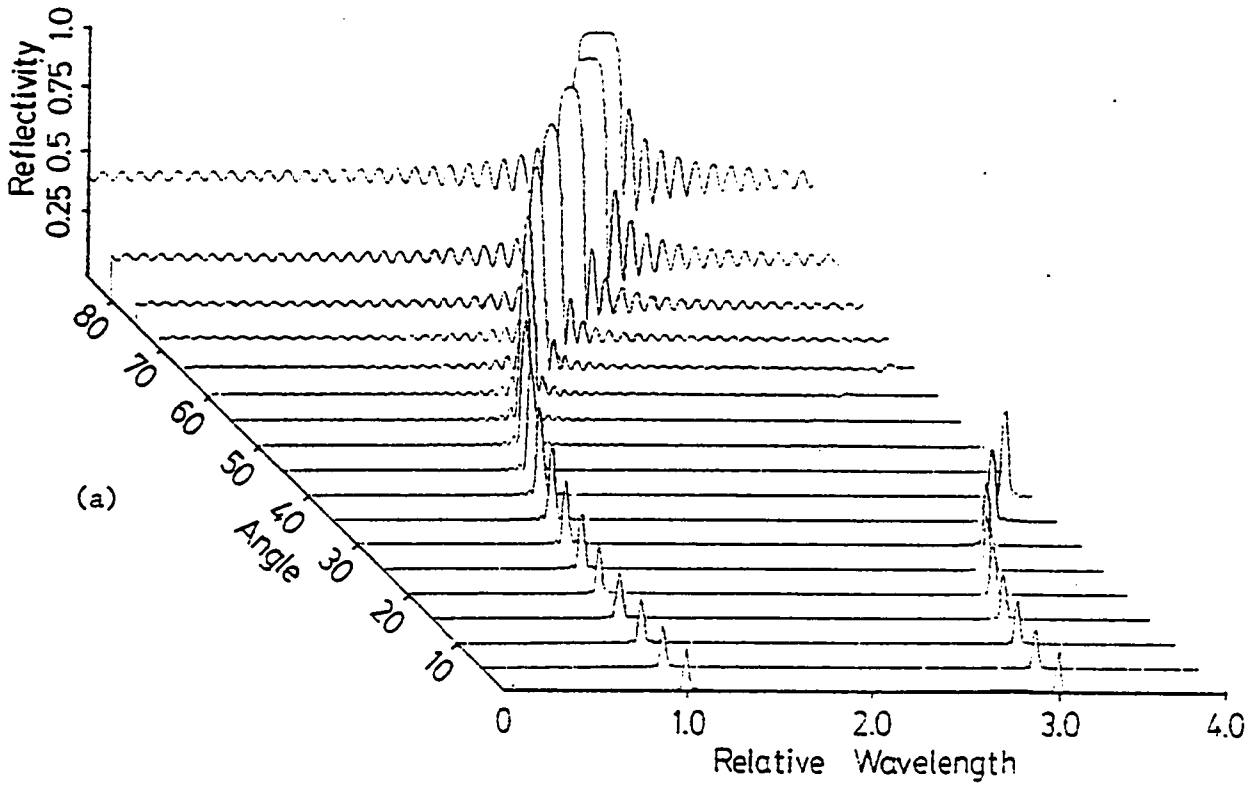


Figure 4.1. TE Waves (a) and TM Waves (b) Reflectivities vs. Relative Wavelength at Various Angles of Incidence of a Typical 28 Periods Bragg Reflector.

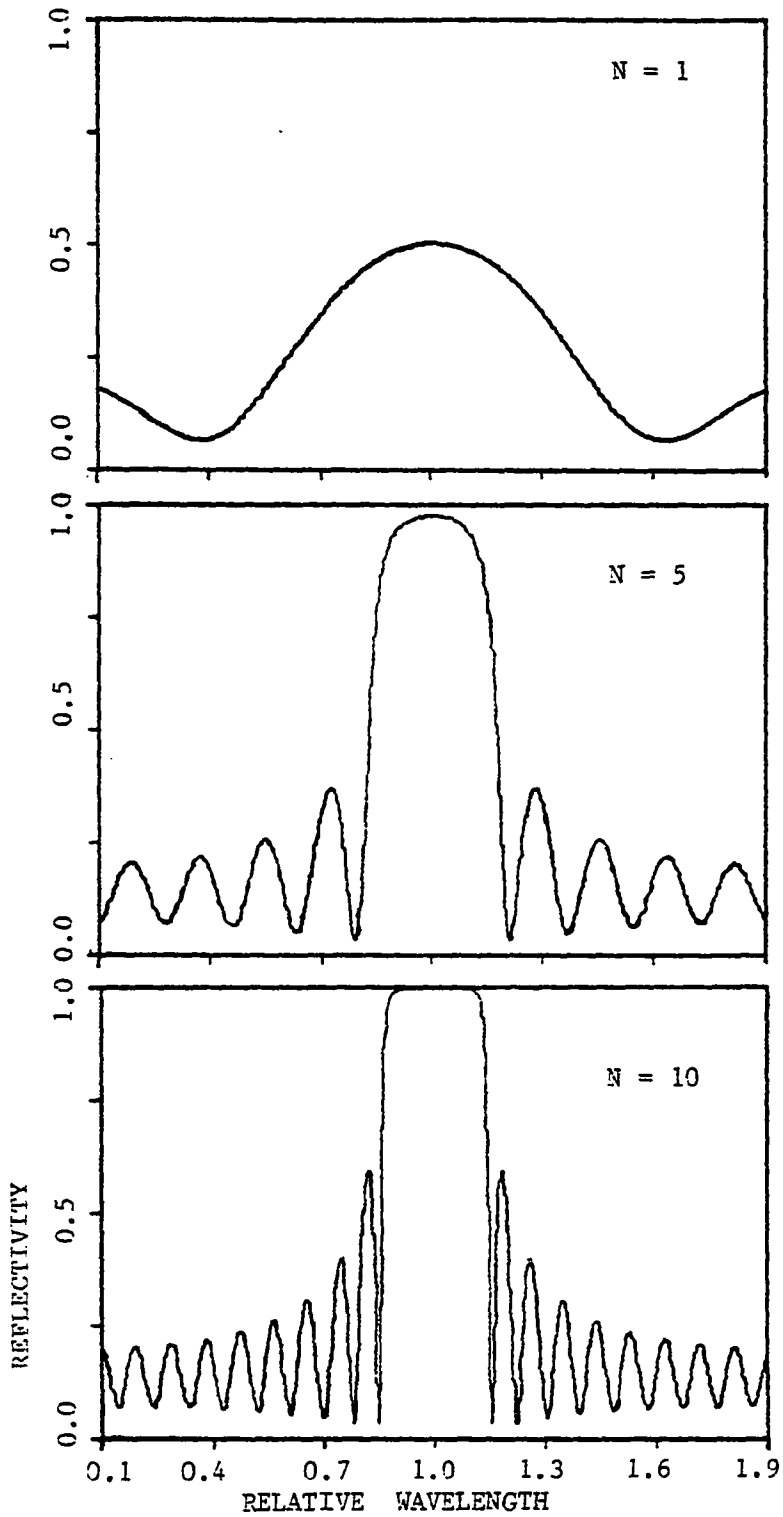


Figure 4.2. Reflectivity for Double $\lambda_0/4$ Layer Periodic Bragg Reflector as a Function of λ_0/λ .
 $n_1 = 3.62$, $n_2 = 3.44$, $n_s = 3.62$, $n_g = 3.34$, $\theta = 80^\circ$.

the minima depend on the outermost bounding media. In particular for $n_g = n_s$ the minima are all zero.

Consider a triple structure, which has a basic period $(\frac{n_1}{4} \frac{n_1}{4} \frac{n_2}{4})$, where $\frac{n_1}{4}$ and $\frac{n_2}{4}$ represent quarter wavelength layers with refractive index n_1 and n_2 . The computed reflectivity for $n_1 = 3.45$, $n_2 = 3.24$, $n_g = 3.24$, and $n_s = 3.45$ is shown in Figure 4.3(a). The first and second high reflectance zones occur at relative wavelength $2/3$ and $4/3$, respectively. Reflectivities for quadruple and quintuple structure which have a basic period of various combination of $(\frac{n_1}{4})$ and $(\frac{n_2}{4})$ are plotted in Figure 4.3(b),(c). The number and maxima of the subsidiary are proportional to the number of periods. So far we have considered the reflective spectrum for which all the layers in basic period are tuned at one quarter wavelength. It is obvious that with an increased number of layers in basic period, the reflectivity within the stop zone converges slowly to unity. And also with increasing layers in the basic period, the stop-band width for a given ratio of index decreases.

Reflectivity spectra shown in Figure 4.4 are for a symmetric triple layered periodic Bragg reflector made up of eighth-wave, quarter-wave and eighth-wave layer combination with $n_1 = 3.45$, $n_2 = 3.24$. For the $(\frac{n_1}{8} \frac{n_2}{4} \frac{n_1}{8})$ structure, the subsidiary maxima in longer wave side are smaller than those on the shorter wave side. The symmetric structure $(\frac{n_2}{8} \frac{n_1}{4} \frac{n_2}{8})$ case the situation is reversed. In most application of Bragg reflector in Integrated Optics, the ratio of indices of refraction in various layers is close to unity (typically $n_1/n_2 = 1.05$), thus reflective spectrum near grazing angle of incident is affected much by the refractive index of guiding layer. To be able to compare the effect of n_g

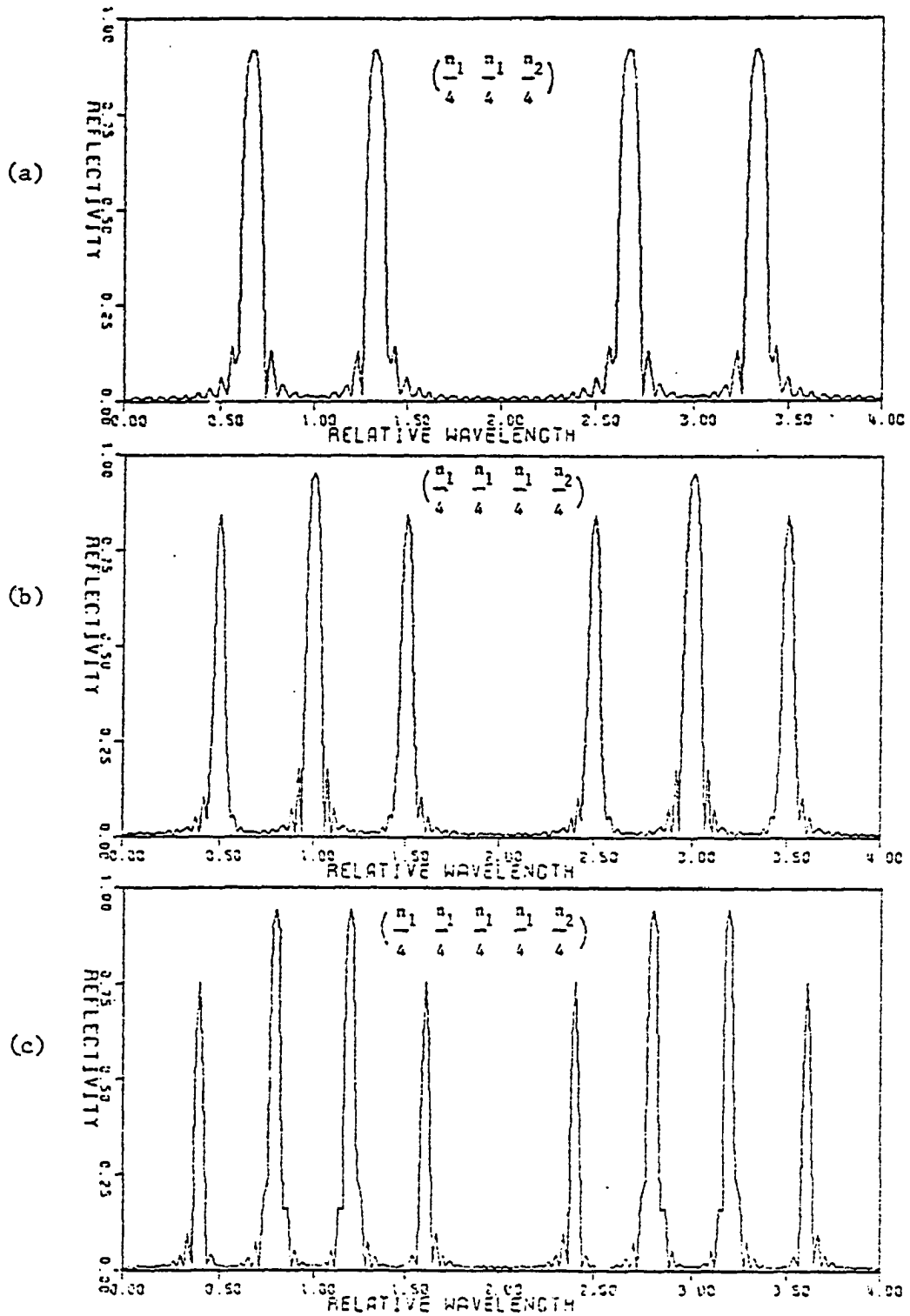


Figure 4.3. Reflectivity for Tuned $\lambda_0/4$ Triple (a),
 Quadruple (b), and Quintuple (c) with $n_1 = 3.45$,
 $n_2 = 3.24$, $N = 10$ and $\theta = 60^\circ$.

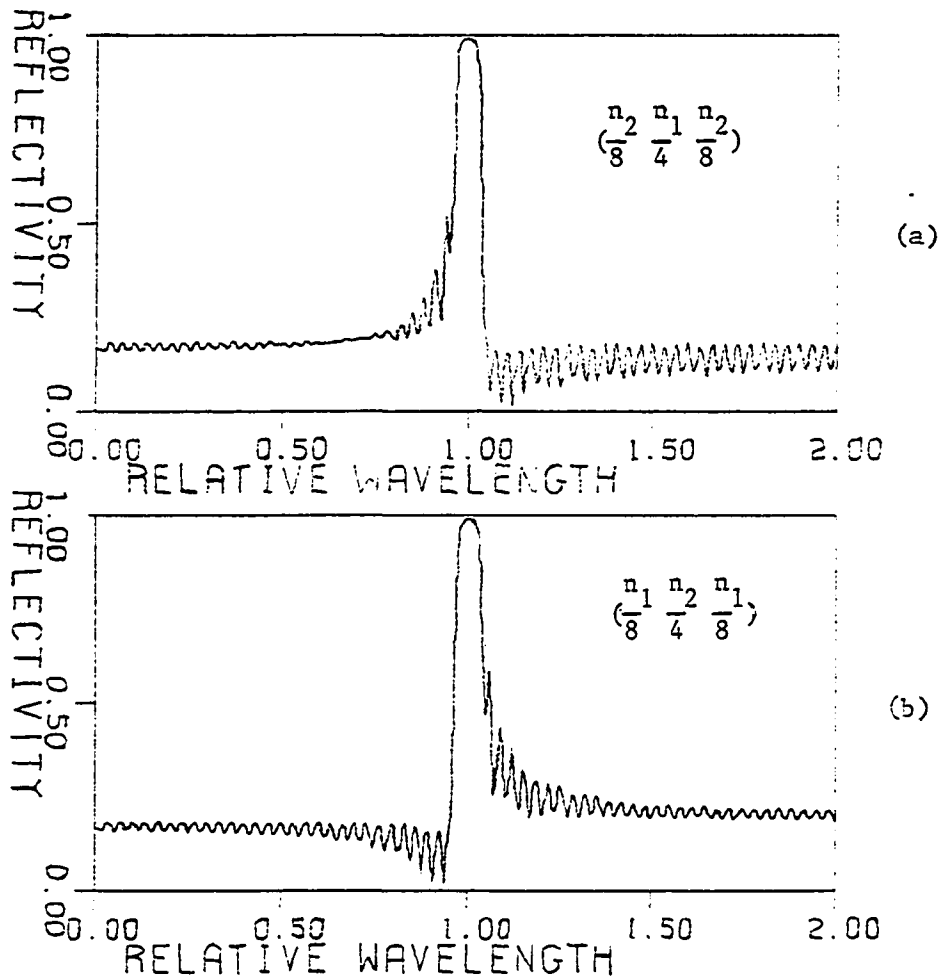


Figure 4.4. Reflective Spectra for Triple Layered Bragg Reflector with $N = 30$, $n_1 = 3.45$, $n_2 = 3.42$ and $\theta = 80^\circ$. (a) $(\frac{n_2}{8} \frac{n_1}{4} \frac{n_2}{8})$.
 (b) $(\frac{n_1}{8} \frac{n_2}{4} \frac{n_1}{8})$.

on the reflectivities, the reflectivities are calculated as n_g is varied from 3.20 to 3.44. Figure 4.5 shows the effect of n_g on reflectivities for the quarter wave double layered periodic Bragg reflector at incident angle $\theta = 80^\circ$ with $n_1 = 3.24$, $n_2 = 3.45$ and $n_s = 3.45$. A broader bandwidth is obtained as n_s and n_g approach to n_2 .

4.3. Reflectivity at the Center of Stopband

In practice, the problem of designing a Bragg reflector with given substrate, the incident media and reflectivity require to calculate the number of layers which are needed. For normal incidence in quarter wave tuned layered structure, the characteristics equation (3.25) turn out to be simple. But at non-normal incident in non-quarter wave multilayered structure calculation is of complicated. The primary purpose of this section is to present the reflectivity characteristics of double, triple quadruple and quintuple layered periodic reflector structure. Three useful parameters for reflectivity are: (1) number of periods, (2) refractive index ratio in basic period, (3) incident angles.

Throughout this discussion reference wavelength and the outermost indices used are $\lambda_0 = 1.15 \mu\text{m}$, $n_s = 3.45$, $n_g = 3.24$. These values represent $\text{Ga}_{1-x}\text{Al}_x\text{As}$ that could be used for making an optical waveguide. For $(\frac{n_1}{4} \frac{n_2}{4})$ basic period, reflectivity was calculated as a function of number of periods N ; the results are plotted in Figure 4.6 in which the upper and lower set of curves were obtained by choosing Bragg angle = 80° and 60° , respectively.

The curves in Figure 4.7 show the reflectivity as a function of periods N for the Bragg reflector made up of basic period of $(\frac{n_1}{6} \frac{n_2}{6} \frac{n_1}{6})$

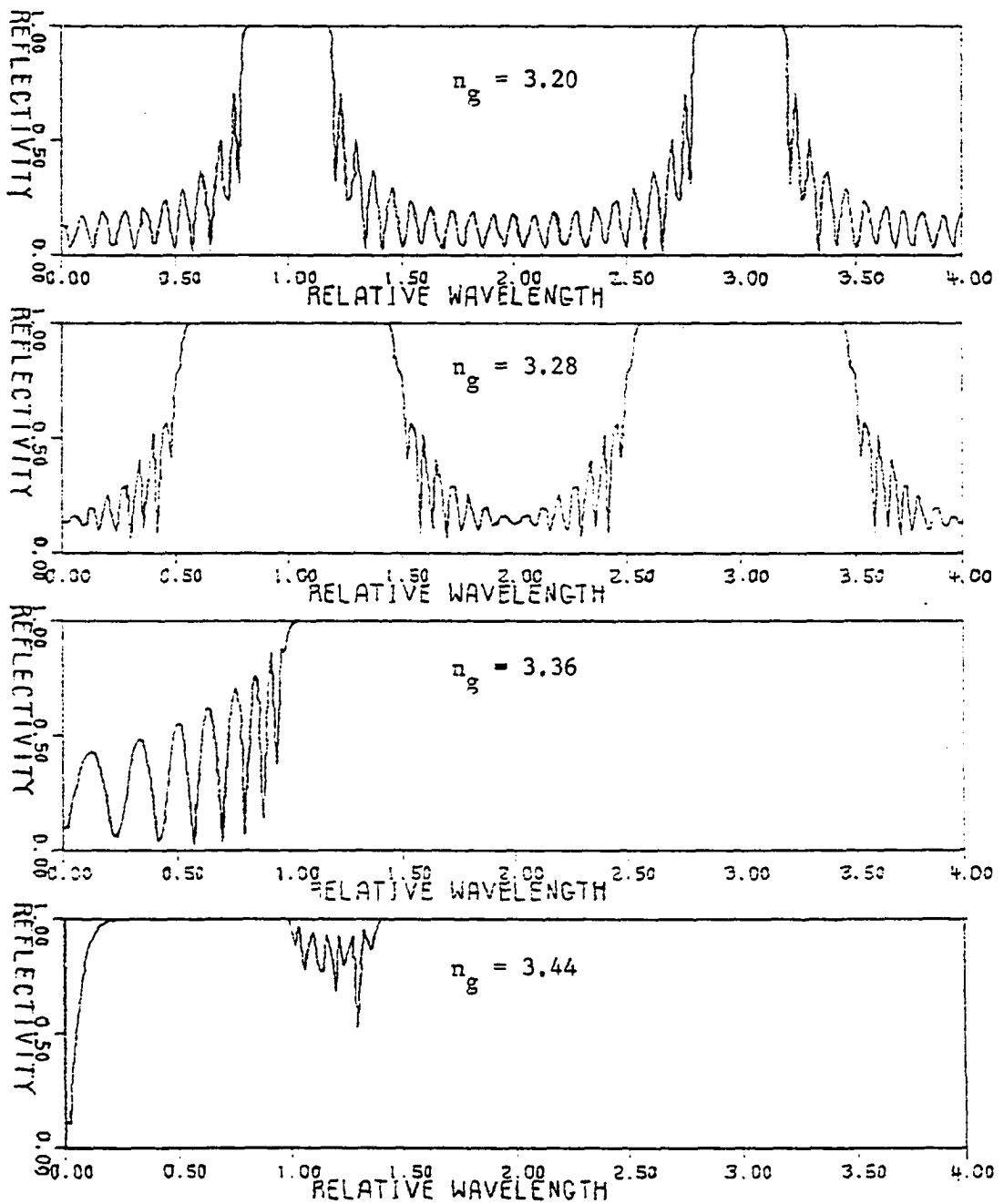


Figure 4.5. Reflectivity vs. Relative Wavelength for Several Values of Guiding Layer's Refractive Index n_g with $\theta = 80^\circ$

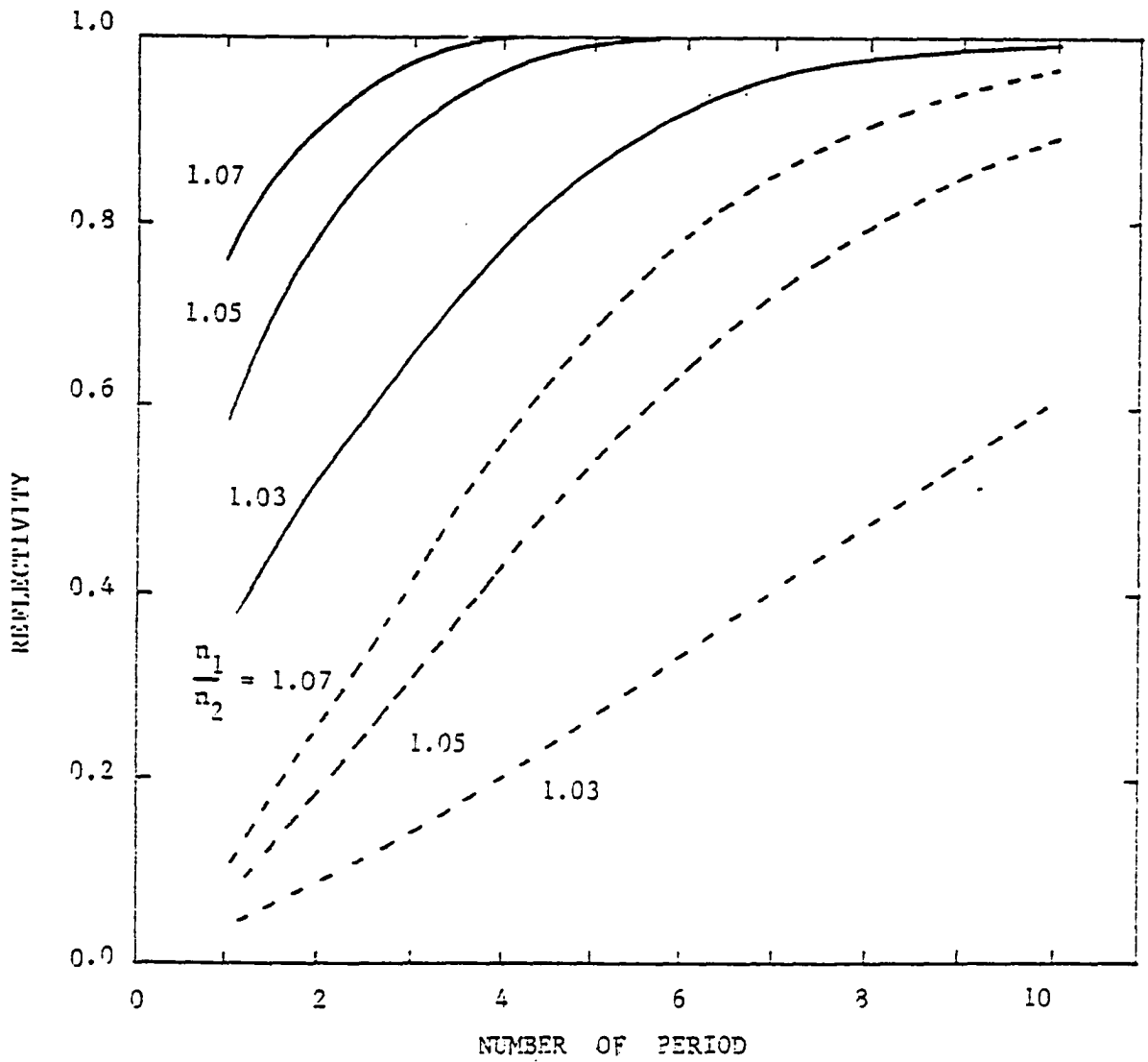


Figure 4.6. Reflectivity as a Function of Period N for a Quarter Wave Double Structure
 Solid Curves: Bragg Angle 80°
 Broken Curves: Bragg Angle 60°

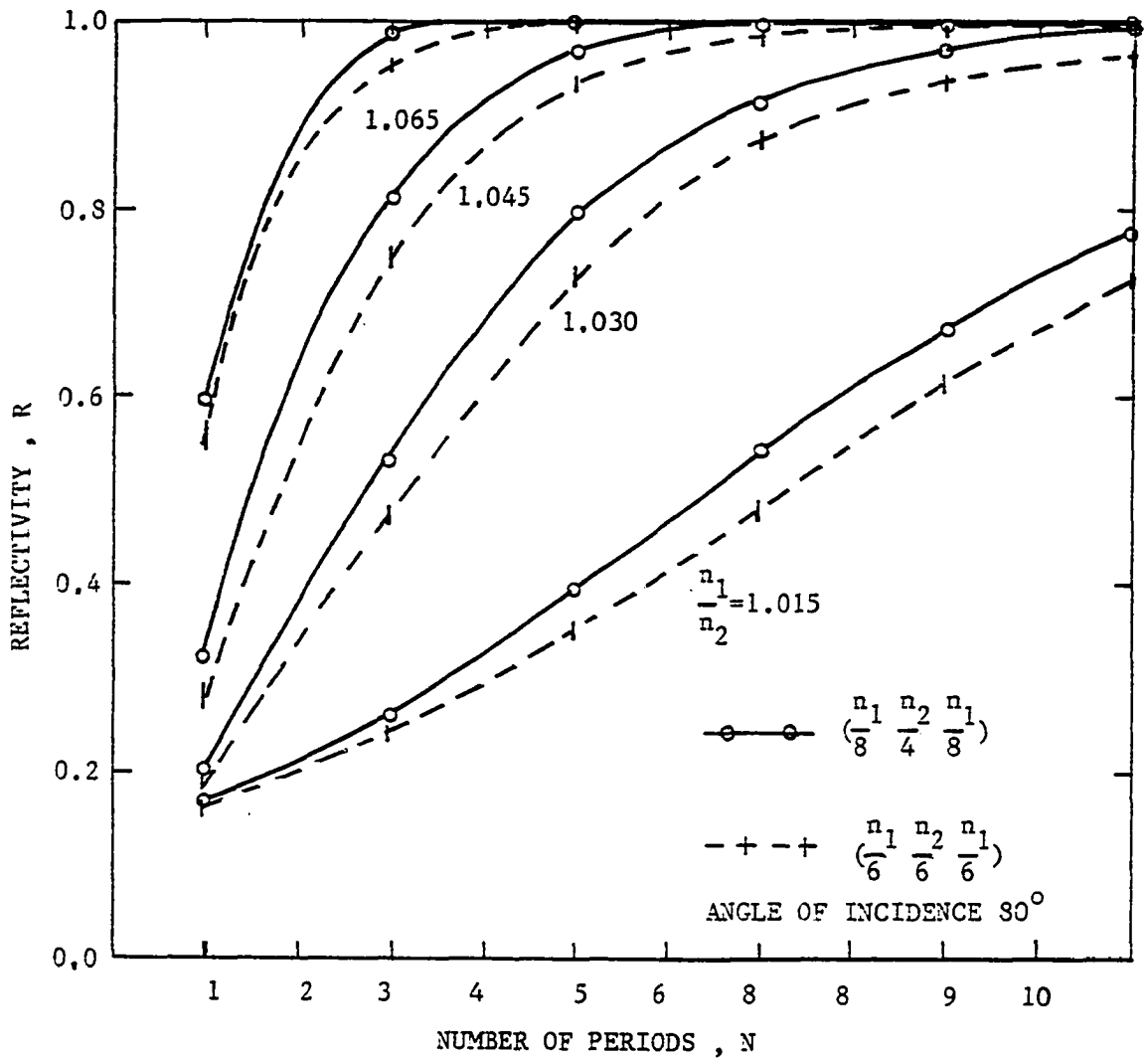


Figure 4.7. Reflectivity as a Function of Period N for Reflector with Basic Period of $(\frac{n_1}{6} \frac{n_2}{6} \frac{n_1}{6})$ and $(\frac{n_1}{8} \frac{n_2}{4} \frac{n_1}{8})$.

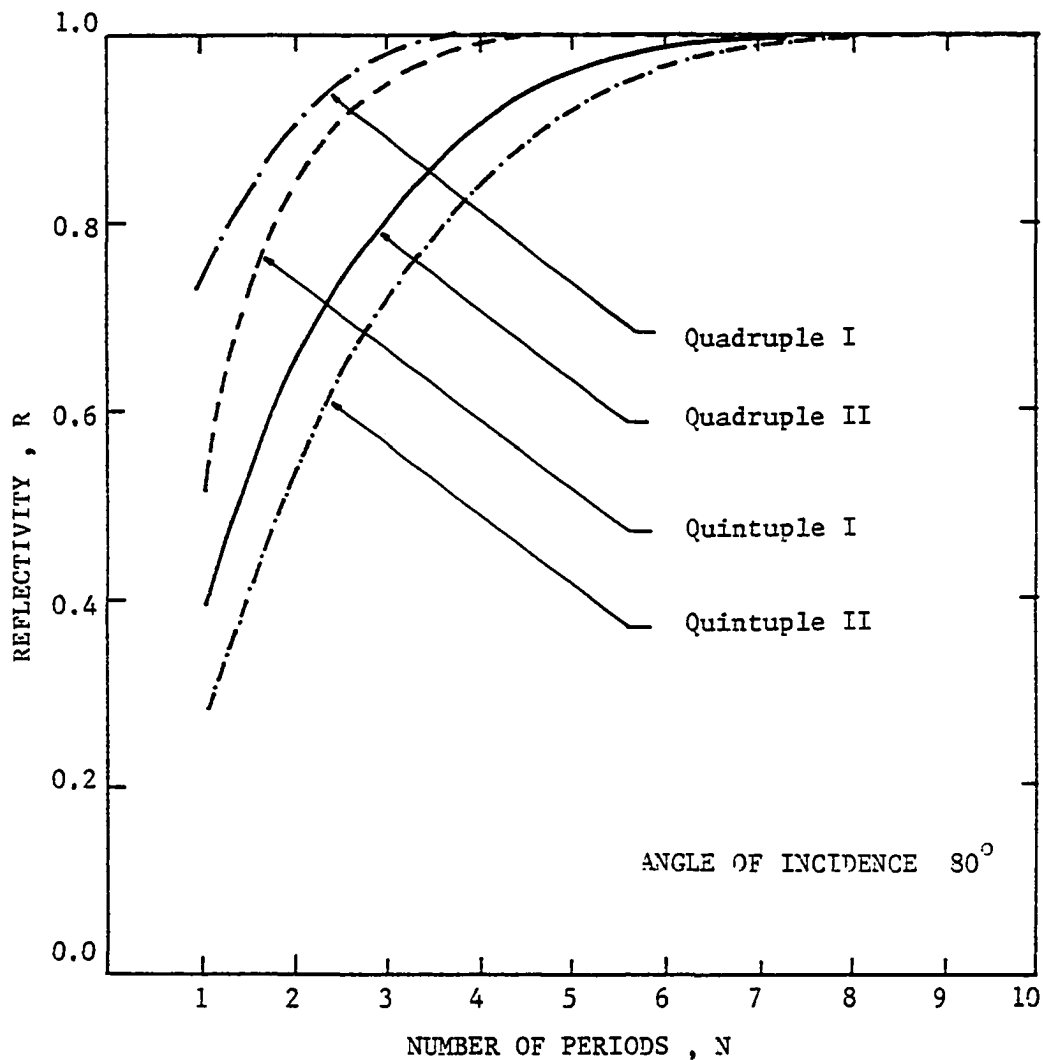


Figure 4.8. Reflectivity at the Center of Stopzone vs. Periods N for Quadruple and Quintuple Basic Period Reflector.

$$\text{Quadruple I : } \left(\frac{3.45}{4} \frac{3.45}{4} \frac{3.45}{4} \frac{3.24}{4} \right)$$

$$\text{Quadruple II: } \left(\frac{3.45}{8} \frac{3.40}{8} \frac{3.36}{8} \frac{3.28}{8} \right)$$

$$\text{Quintuple I : } \left(\frac{3.24}{8} \frac{3.40}{8} \frac{3.44}{2} \frac{3.40}{8} \frac{3.24}{8} \right)$$

$$\text{Quintuple II: } \left(\frac{3.28}{10} \frac{3.38}{10} \frac{3.44}{10} \frac{3.38}{10} \frac{3.28}{10} \right)$$

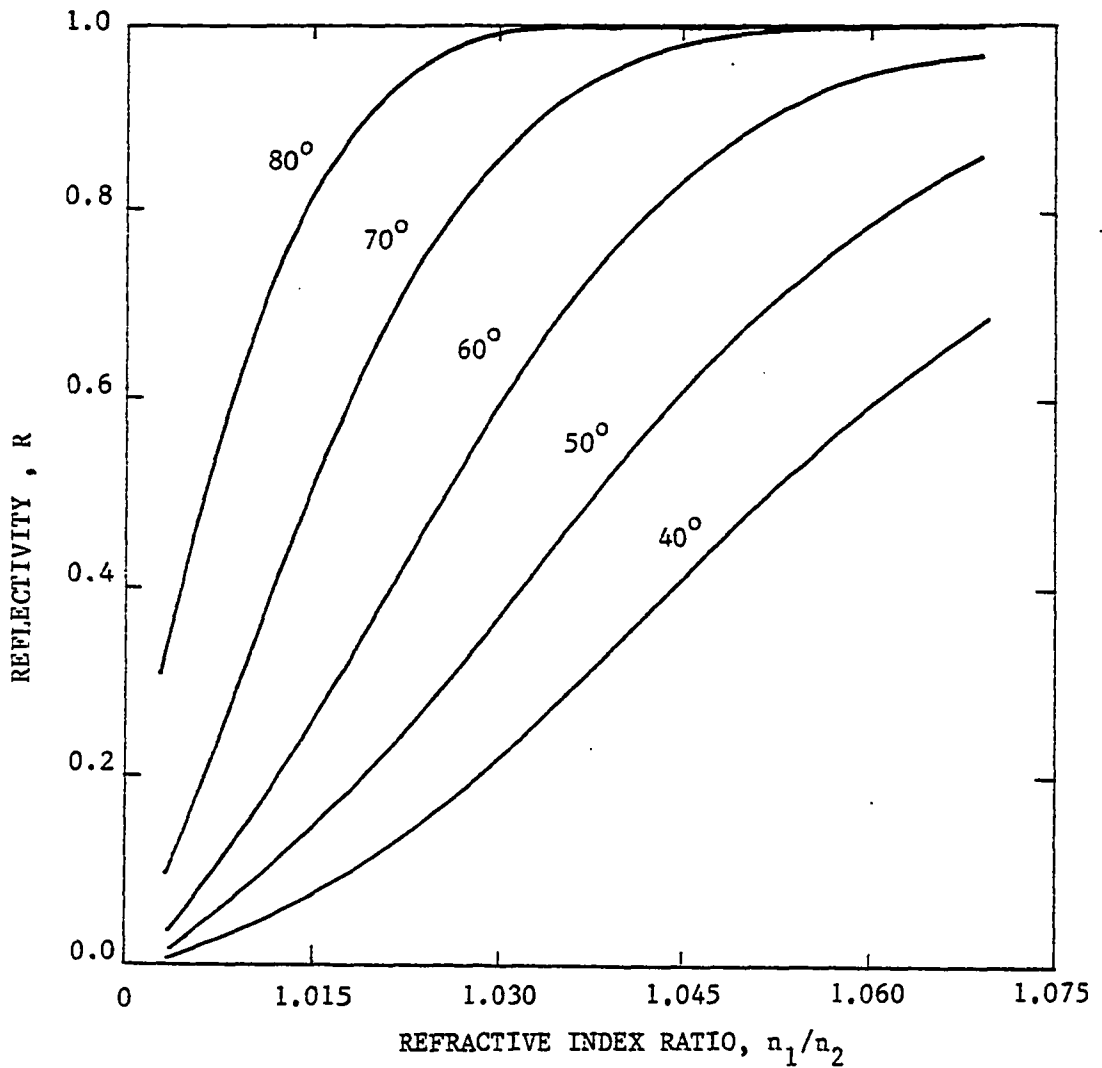


Figure 4.9. The Effect of Index Ratio n_1/n_2 on Reflectivity for $(\frac{n_1}{4} \frac{n_2}{4})$ Double Structure at Several Different Incident Angles. Total Number of Periods is 10.

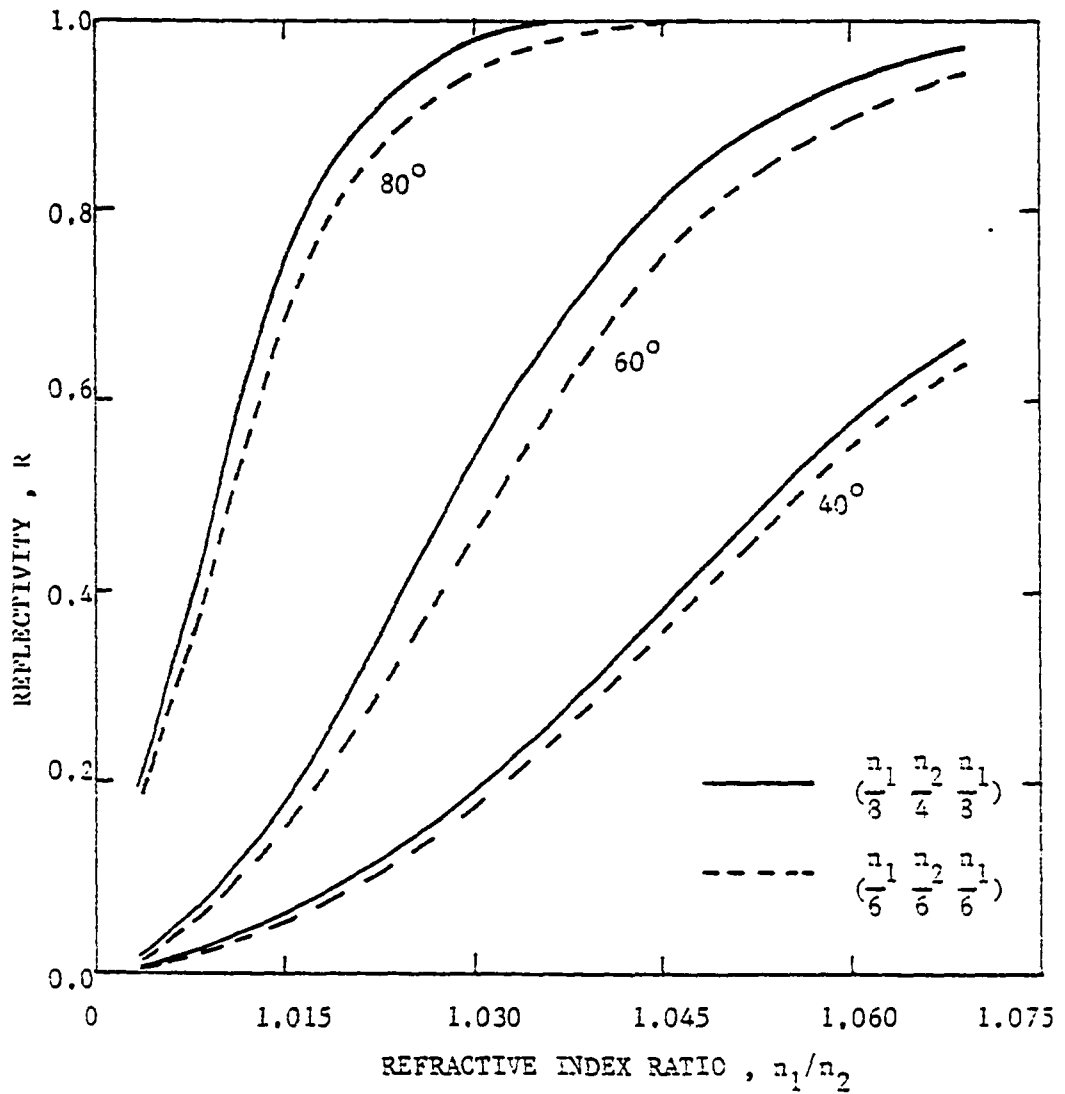
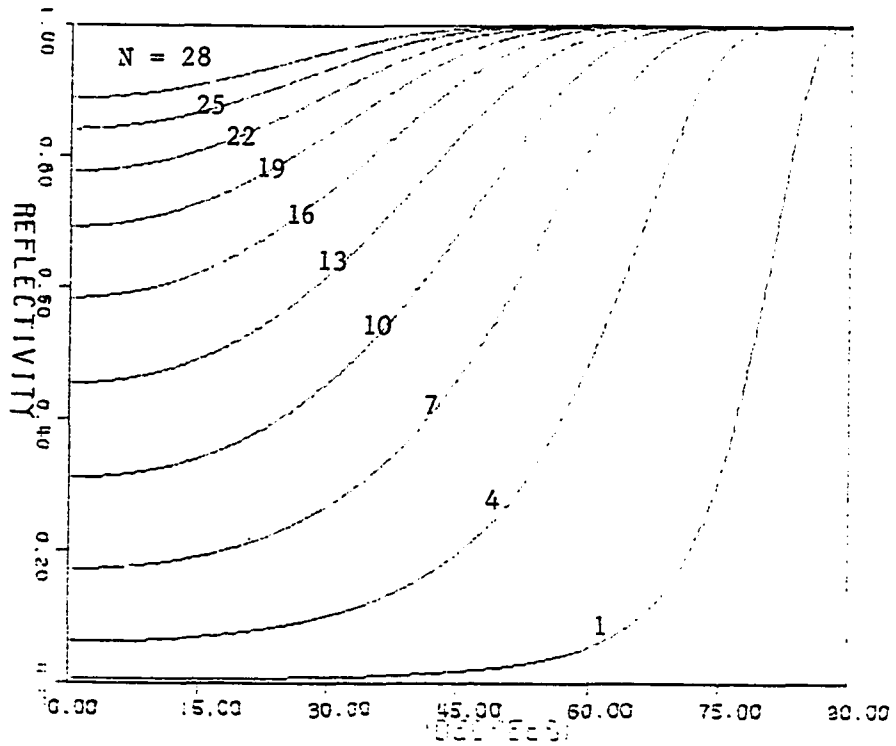
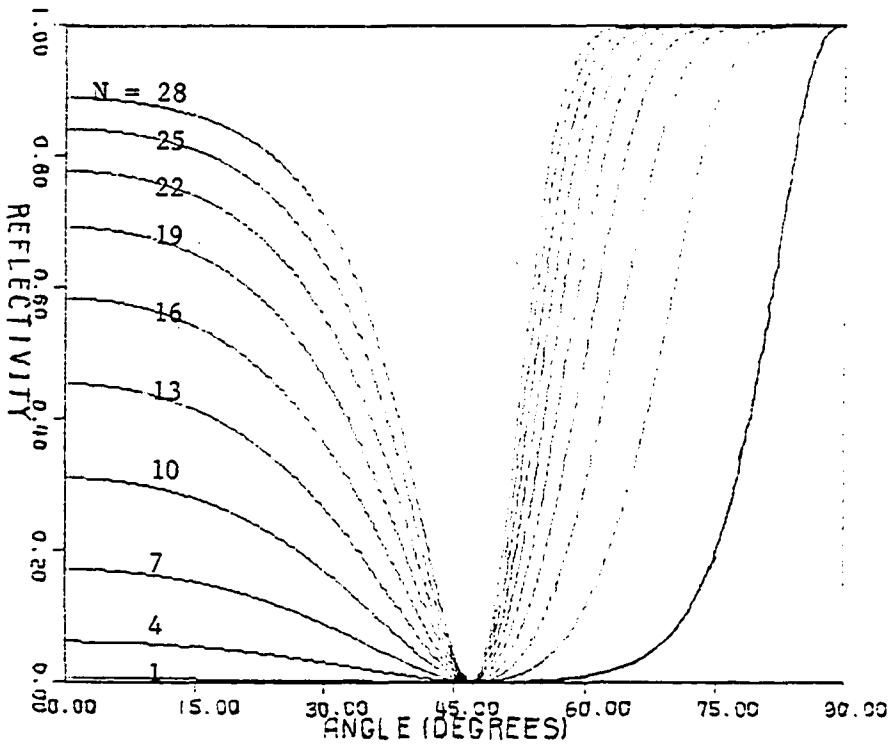


Figure 4.10. The Effect of Index Ratio n_1/n_2 on Reflectivity for Triple Structure at Incident Angles 40° , 60° , 80° .

Reflector Parameter: $n_1 = 3.45$, $n_2 = 3.24$, $N = 10$.



(a)



(b)

Figure 4.11. The Effect of Incidence Angle on Reflectivity of TE Waves (a) and TM Waves (b) Triple Layered Bragg Reflector of $(\frac{n_1}{8} \frac{n_2}{4} \frac{n_1}{8})$ Structure with $n_1 = 3.45$ $n_2 = 3.24$.

and $(\frac{n_1}{8} \frac{n_2}{4} \frac{n_1}{8})$ triple layers. The reflectivity vs. periods N for quadruple and quintuple structure are shown in Figure 4.8.

The effect of index ratio in periodic layer was examined by calculating the reflectivity vs. n_1/n_2 . Figure 4.9 represents the results of a series of calculation for a double structure. Figure 4.10 is shown the reflectivity vs. n_1/n_2 for a triple structure. As noted before, at a given ratio of refractive index, a $(\frac{n_1}{8} \frac{n_2}{4} \frac{n_1}{8})$ basic period symmetric triple structure exhibits a large reflectivity compared to other symmetric structure.

The effect of different incident angle was investigated by plotting reflectivities of triple structures, period up to 28. The graphs of Figure 4.11 indicate that TE and TM waves show different characteristics in reflectivity. Reflectivity of TE waves increases with increasing angle of incident and member of periods. The most interesting features of TM waves are the zeros of reflectivity. This zero of reflectivity for TM waves indicates the Brewster angle given by Equation (4.1). This condition are applicable and useful to design of reflecting polarized waveguide. On the other hand, polarization insensitive beam splitting waveguide structure may be obtained at the intersection points of TM and TE branches.

4.4. Selectivity of Multilayer Bragg Reflector

The width of stop zone is of importance in application of a Bragg Reflector to a wavelength selective waveguide structure. The Abeles's approach⁽⁷⁻⁹⁾, mentioned in section 3.3, the approximate representation of stop zone width, is expected to be valid for the structure with the

infinite number of periods. In Figure 4.12 we have plotted the stop zone width of a typical double layered Bragg reflector against the refractive indices ratio in a basic period. The results of both the exact numerical calculation and the Equation (3.47) are shown. The solid curves are obtained by using Equation (3.47), and the dotted curves by the exact numerical calculation. There are large differences between results obtained by the two methods. It is observed that the differences in the values of stop zone width calculated by two methods are getting large as long as the refractive index ratio is small. For a small number of periods with a small refractive indices ratio (smaller than 1.07), Equation (3.47) could not yield a sufficiently accurate value for the stop zone of the Bragg waveguide. It is therefore necessary to use the exact numerical approach to calculate the stop zone width when the number of periods is not large. In Figure 4.13 we have plotted the selectivity of a typical double layer Bragg reflector as a function of the number of periods for three different ratio of refractive indices. Figure 4.13 indicates that as the number of period increases, the selectivity decreases hyperbolically, and selectivity increases with the ratio of refractive index. But it is also important to note that an increase in the number of period not only increases reflectivity but also increases the values of subsidiary maxima and brings the subsidiary maxima on both sides of stop zone closer to the center. Figure 4.14 is a plotting of the selectivity of triple structure Bragg reflector against number of periods. The solid curves are for Bragg reflector having basic period of $(\frac{n_1}{8} \frac{n_2}{4} \frac{n_1}{8})$ and dotted curves for Bragg reflector which have a basic period of $(\frac{n_1}{4} \frac{n_2}{8} \frac{n_3}{8})$. The value of refractive indices n_1 and n_3 are

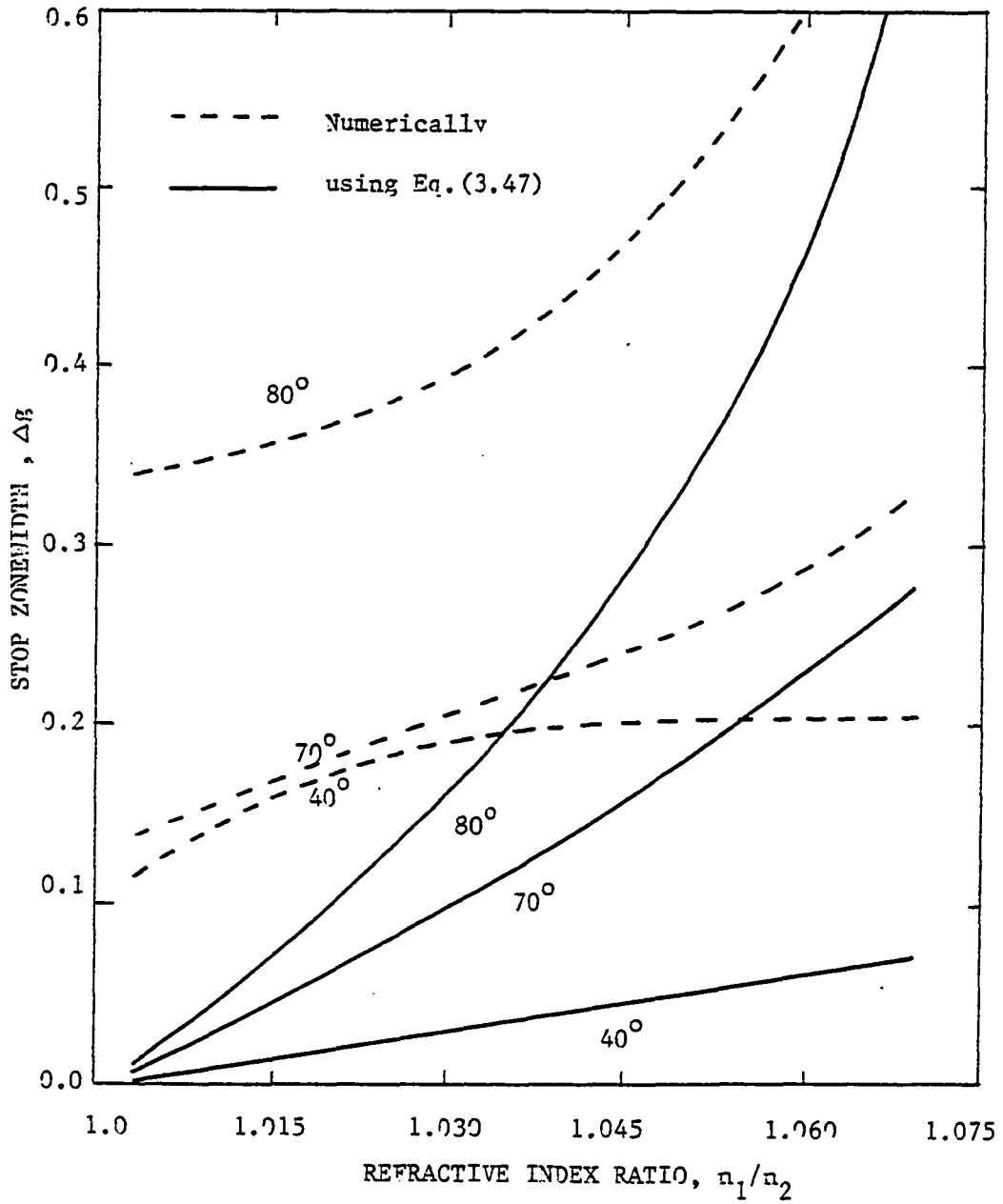


Figure 4.12. Stopzone Widths of Double Layer Bragg Reflector Against the Refractive Indices Ratio at Several Incident Angles. Dotted Curves: Exact Calculation: Solid Curves: Using Equation (3.47). Reflector Parameter: $n_1 = 3.45$, Fixed n_2 is From 3.20 to 3.45, $N = 10$, $\lambda_0 = 1.15$ (μm), $n_g = 3.24$, $n_s = 3.45$.

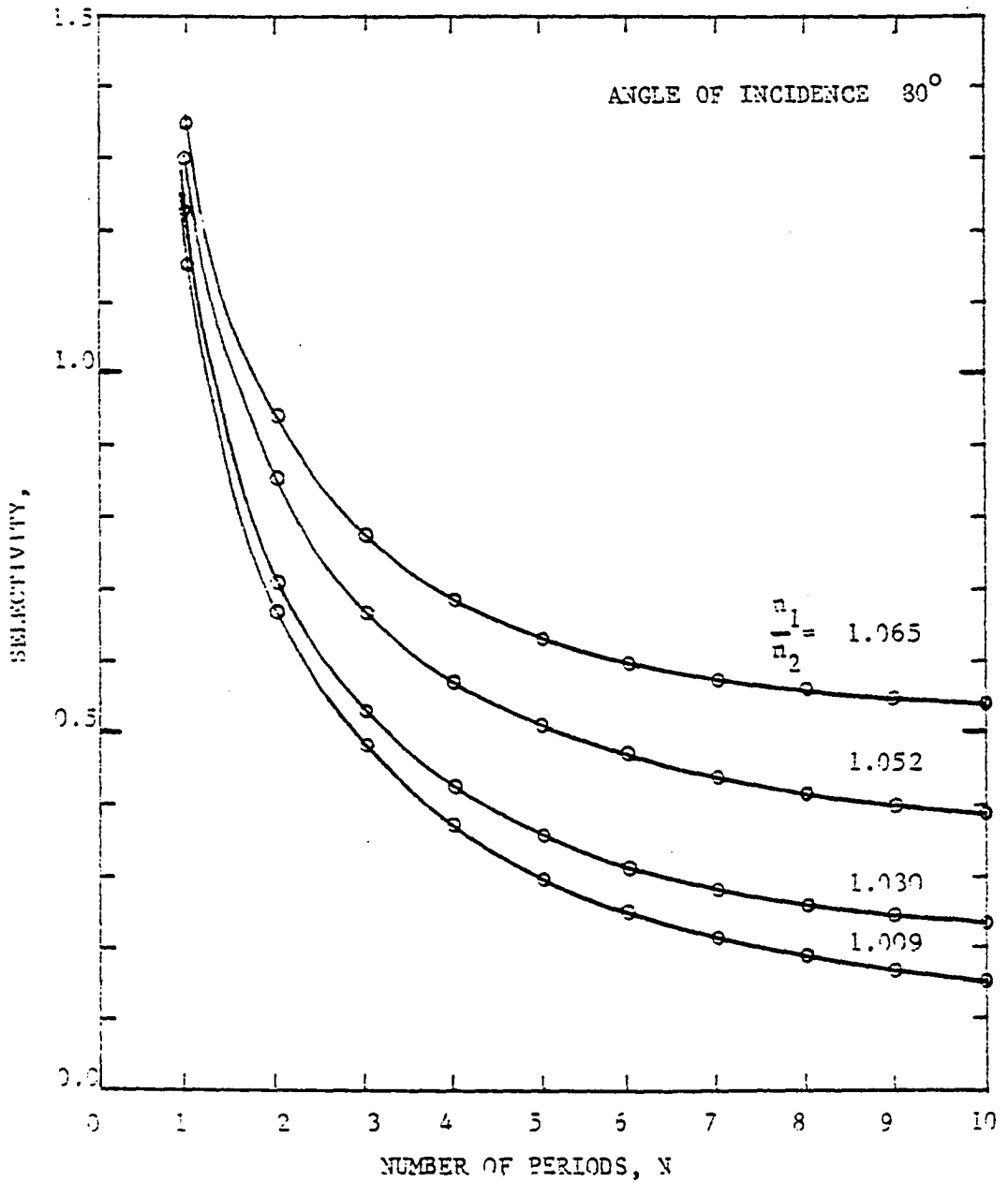


Figure 4.13. Selectivity of Double Layer Bragg Reflector as Function of N . Reflector Parameter $n_1/n_2 = 1.065, 1.052, 1.030, 1.009$, $\lambda_0 = 1.15$ (μm), $n_g = 3.24$, $n_s = 3.45$.

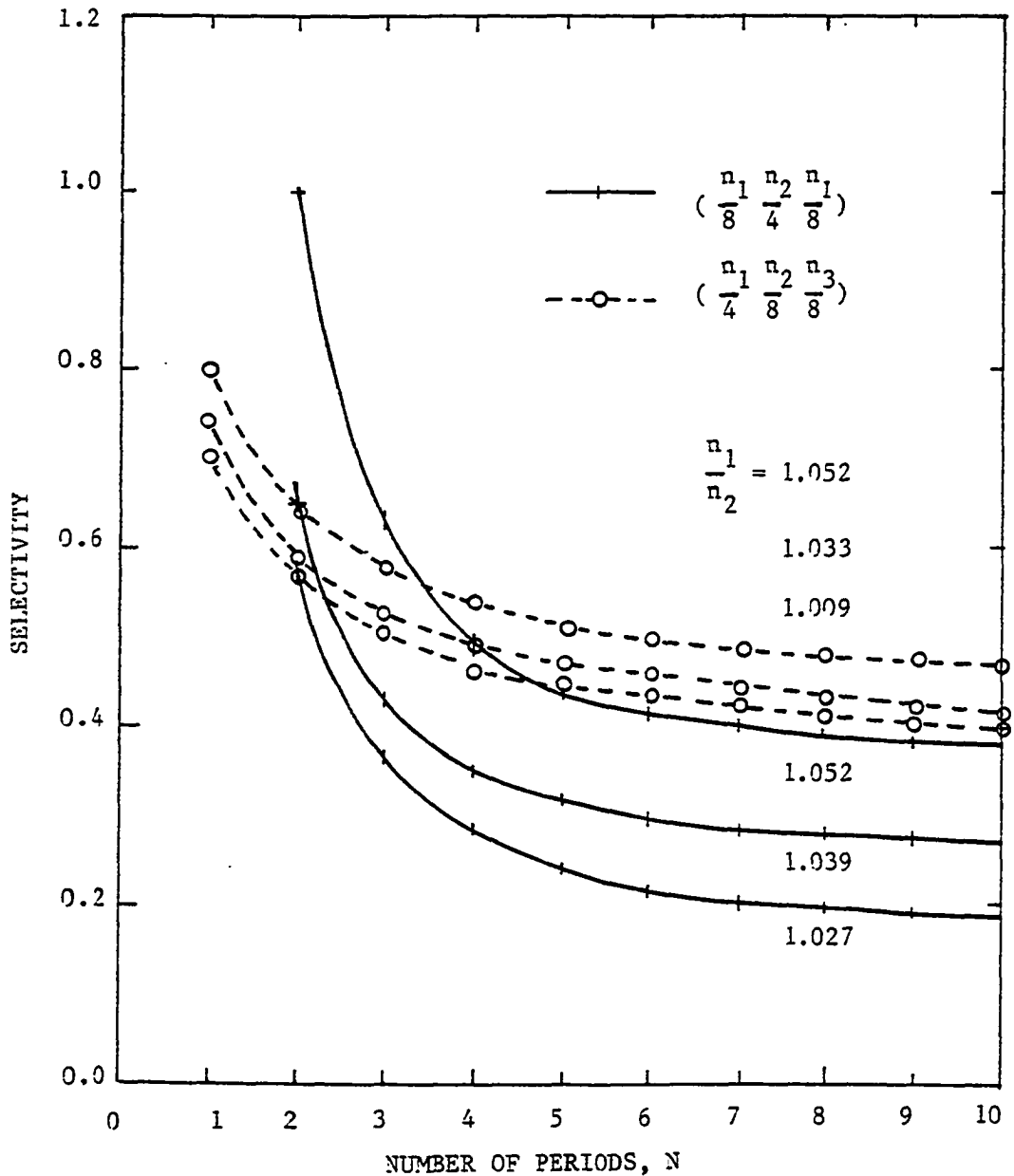


Figure 4.14. Selectivity of Untuned Triple Structure Bragg Reflector. Solid Curves: $(\frac{n_1}{8}, \frac{n_2}{4}, \frac{n_1}{8})$, Dotted Curves:

$$(\frac{n_1}{4}, \frac{n_2}{8}, \frac{n_3}{8}). \quad n_1 = 3.45, \quad n_3 = 3.24, \quad n_s = 3.45$$

$$n_g = 3.24, \quad \lambda_0 = 1.15 \text{ } (\mu\text{m}).$$

fixed at 3.45 and 3.24, respectively in both case. In Figure 4.14 it is apparent that a lower selectivity can be obtained by $(\frac{n_1}{8} \frac{n_2}{4} \frac{n_3}{8})$ structure rather than $(\frac{n_1}{4} \frac{n_2}{8} \frac{n_3}{8})$. Whereas the latter structure has a higher reflectivity, the former structure offers a significant advantage over all other structure. As mentioned in section 4.2, $(\frac{n_1}{8} \frac{n_2}{4} \frac{n_1}{8})$ and $(\frac{n_2}{8} \frac{n_1}{4} \frac{n_2}{8})$ basic period structure where $n_1 > n_2$, have tendency to suppress the subsidiary maximum in long wavelength side and in short wavelength side, respectively. (see also Figure 4.4). This unique characteristics of those basic structure can be utilized to realize a short wavelength or long wavelength passing waveguide system.

In Table 4.1, the comparison of the selectivity of various different basic period reflector composed of more than four layers are given.

Table 4.2 shows a relation between the reflectivity and selectivity of the $(\frac{n_1}{8} \frac{n_2}{4} \frac{n_1}{8})$ structure for several values of the number of period. This data will be referred to later when the Bragg waveguide is evaluated.

4.5. Effect of Incidence Angle Variation

In considering the application of a periodic Bragg reflector in wavelength reflective guiding structure, one of the most important characteristics, yet generally overlooked, is the center wavelength shift and stopzone width change due to variation of an angle of incidence. Figure 4.15 shows the effects of incidence angle on the center wavelength of a typical double layered periodic Bragg reflector. In the figure vertical axis represents λ_0/λ_θ where λ_0 and λ_θ denote the center wavelength at normal incident and at incident angle θ , respectively. A remarkable shift in center wavelength is seen to occur at large angle of incidence. And also the shift in center wavelength of reflector with small refractive

Basic Period	Selectivity	Stopband Center	Parameter
$(\frac{n_1}{4} \frac{n_1}{4} \frac{n_1}{4} \frac{n_2}{4})$	0.08	λ_0	$n_1 = 3.45, n_2 = 3.24, \theta_g = 60^\circ$
$(\frac{n_1}{8} \frac{n_2}{8} \frac{n_3}{8} \frac{n_4}{8})$	0.258	λ_0	$n_1 = 3.45, n_2 = 3.40, \theta_g = 80^\circ$ $n_3 = 3.36, n_4 = 3.28$
$(\frac{n_1}{10} \frac{n_2}{10} \frac{n_3}{10} \frac{n_4}{10} \frac{n_5}{10})$	0.32	λ_0	$n_1 = 3.28, n_2 = 3.38, \theta_g = 80^\circ$ $n_3 = 3.44, n_4 = 3.38, n_5 = 3.28$
$(\frac{n_1}{8} \frac{n_2}{8} \frac{n_3}{2} \frac{n_4}{8} \frac{n_5}{8})$	0.134	λ_0	$n_1 = 3.28, n_2 = 3.38, \theta_g = 80^\circ$ $n_3 = 3.44, n_4 = 3.38, n_5 = 3.28$
$(\frac{n_1}{4} \frac{n_1}{4} \frac{n_1}{4} \frac{n_1}{4} \frac{n_2}{4})$	0.06	$\frac{5}{4}\lambda_0$	$n_1 = 3.45, n_2 = 3.24, \theta_g = 60^\circ$

All Structure have $n_s = 3.45, n_g = 3.24$ at Wavelength $\lambda_0 = 1.15$ (μm)
and 10 Periods.

Table 4.1. Selectivity of Various Reflector Consisted of Basic Period of More than 4 Layers.

Number of Period N		5	10	15	20	25	30
$\frac{n_1}{n_2} = \frac{3.45}{3.35}$ $\Lambda = 0.30 \mu\text{m}$	R	0.1985	0.5396	0.7841	0.9081	0.9624	0.9841
	$\frac{\lambda_2 - \lambda_1}{\lambda_0}$	0.189	0.116	0.095	0.088	0.081	0.074
$\frac{n_1}{n_2} = \frac{3.45}{3.24}$ $\Lambda = 0.73 \mu\text{m}$	R	0.9994	1.0	1.0	1.0	1.0	1.0
	$\frac{\lambda_2 - \lambda_1}{\lambda_0}$	0.606	0.553	0.550	0.549	0.546	0.539

All structures have $n_s = 3.45$, $n_g = 3.24$ at wavelength $\lambda_0 = 1.15 \mu\text{m}$.

Table 4.2. Reflectivity and Selectivity of the

$(\frac{n_1}{8} \frac{n_2}{4} \frac{n_1}{8})$ Symmetric Structure.

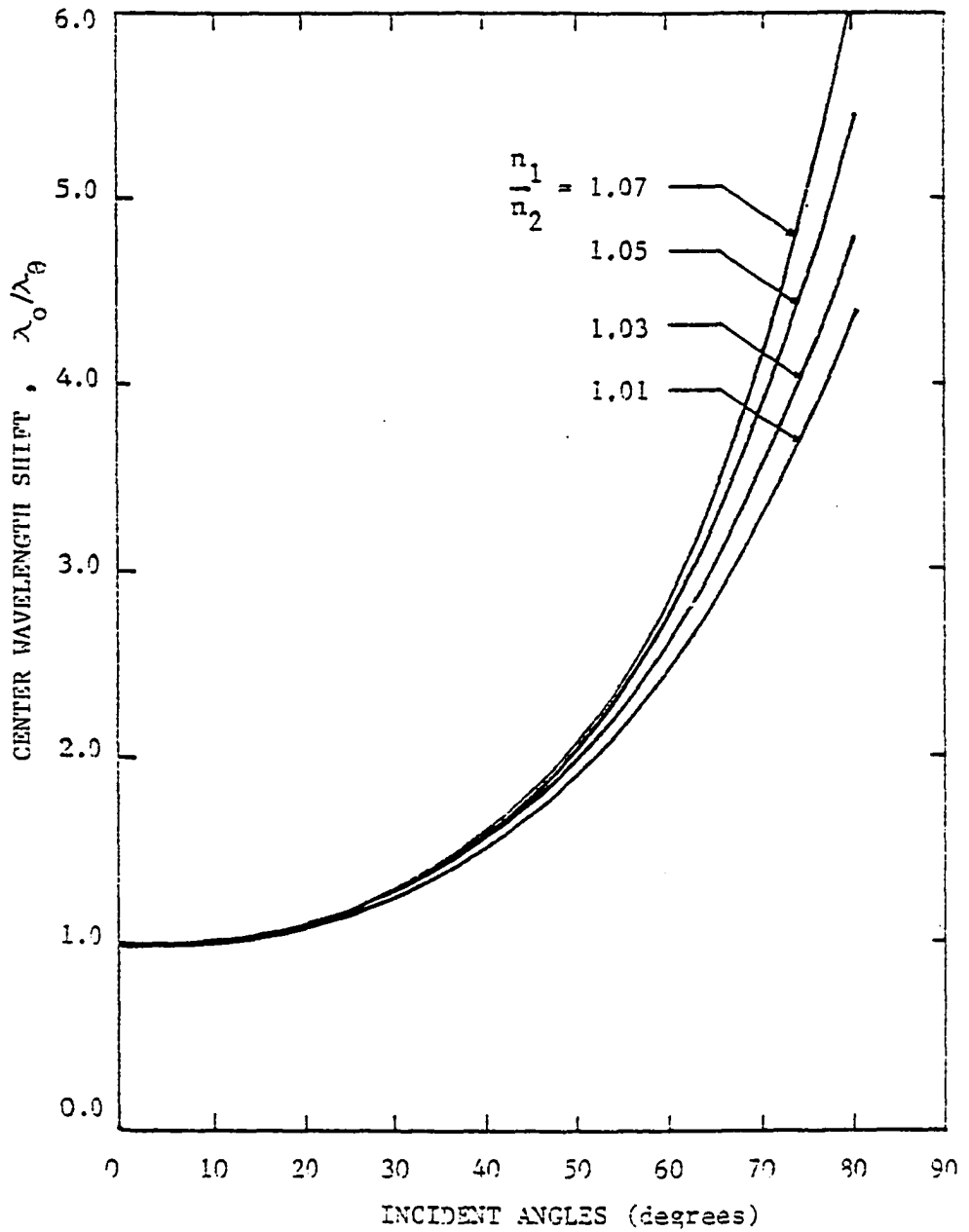


Figure 4.15. Center Wavelength Shift (λ_0/λ_θ) of a Double $\frac{\lambda_0}{4}$ Layer Periodic Bragg Reflector.

index ratio is less than that of large refractive index ratio. An investigation is made on the center wavelength shift owing to incident angle variation in triple, quadruple and quintuple basic period. The results are shown in Figure 4.16 with reflector parameters. From the various plots of center wavelength shift in Figure 4.15 and 4.16 we note following features: the slope of center wavelength shift is very steep at large incident angle; the magnitude of the shift is dependent, generally, on the type of basic period structure, refractive index ratio. The possible reason for these features is that the optical thicknesses of each layer decrease with an increase of angle of incidence, consequently a multilayer's center wavelength shifts toward shorter wavelength as an angle of incidence is increased.

Figure 4.17 shows theoretical effects of incidence angle variation on the bandwidth of double, triple and quadruple basic period which have same reflector parameter as that of Figure 4.16. We see that remarkable change in selectivity as any of the three structure is seen to occur over a wide range of angles. This is a quite different results compare to bandwidth variation of narrow bandpass interference filter reported by M.L. Baker and V.C. Yen ⁽⁵³⁾. These changes can be understood by considering small refractive index ratio and increased mismatch in the optical thickness of layers.

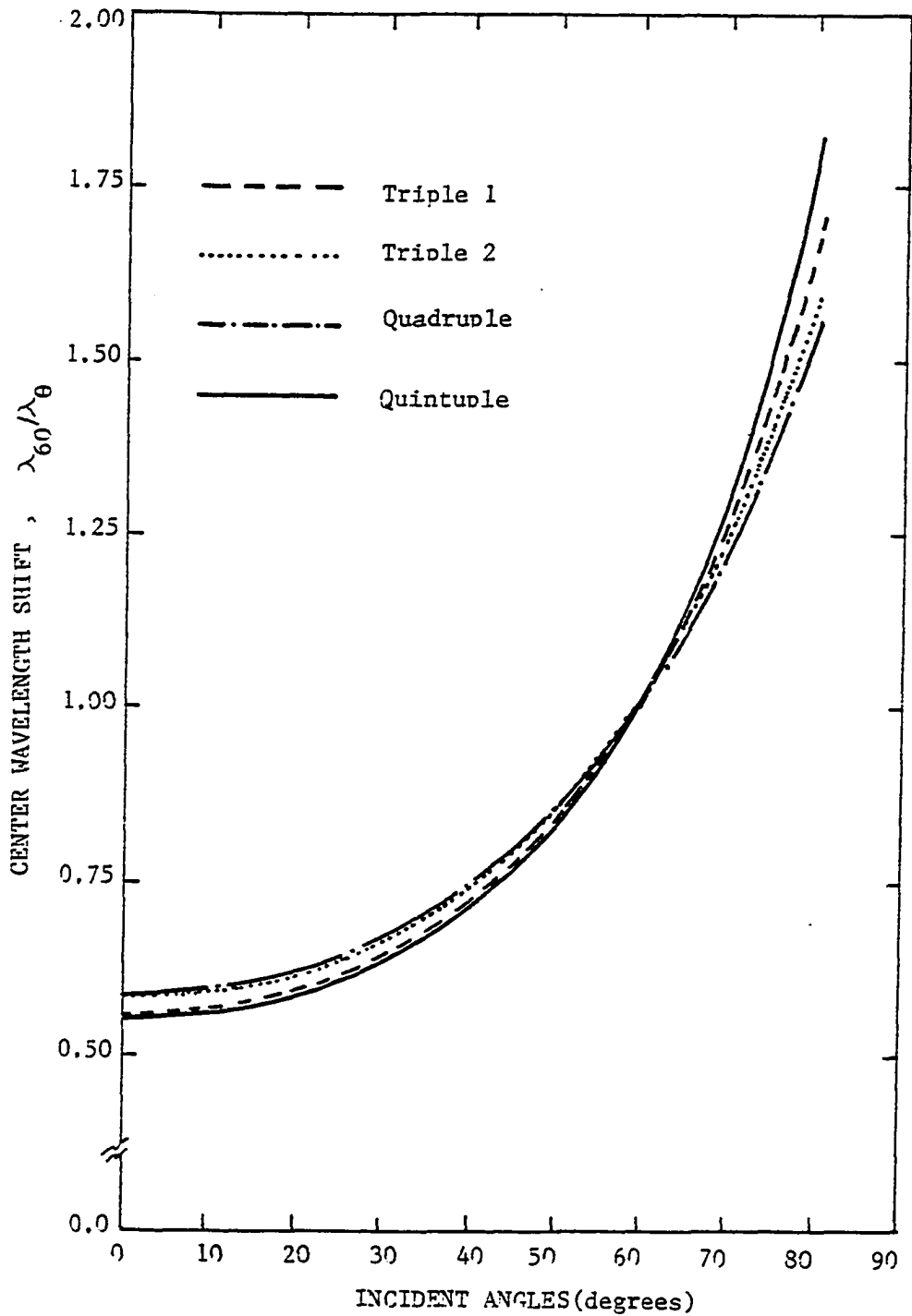


Figure 4.16. Center Wavelength Shift of a Typical Bragg Reflector with 20 Periods of Triple, Quadruple and Quintuple Basic Structure. Reflector Parameter: $(\frac{3.45}{4} \frac{3.40}{8} \frac{3.24}{8})$, $(\frac{3.45}{8} \frac{3.40}{4} \frac{3.45}{8})$, $(\frac{3.45}{4} \frac{3.45}{4} \frac{3.45}{4} \frac{3.40}{4})$, $(\frac{3.28}{10} \frac{3.38}{10} \frac{3.44}{10} \frac{3.38}{10} \frac{3.28}{10})$, Bragg Angle is 60° .

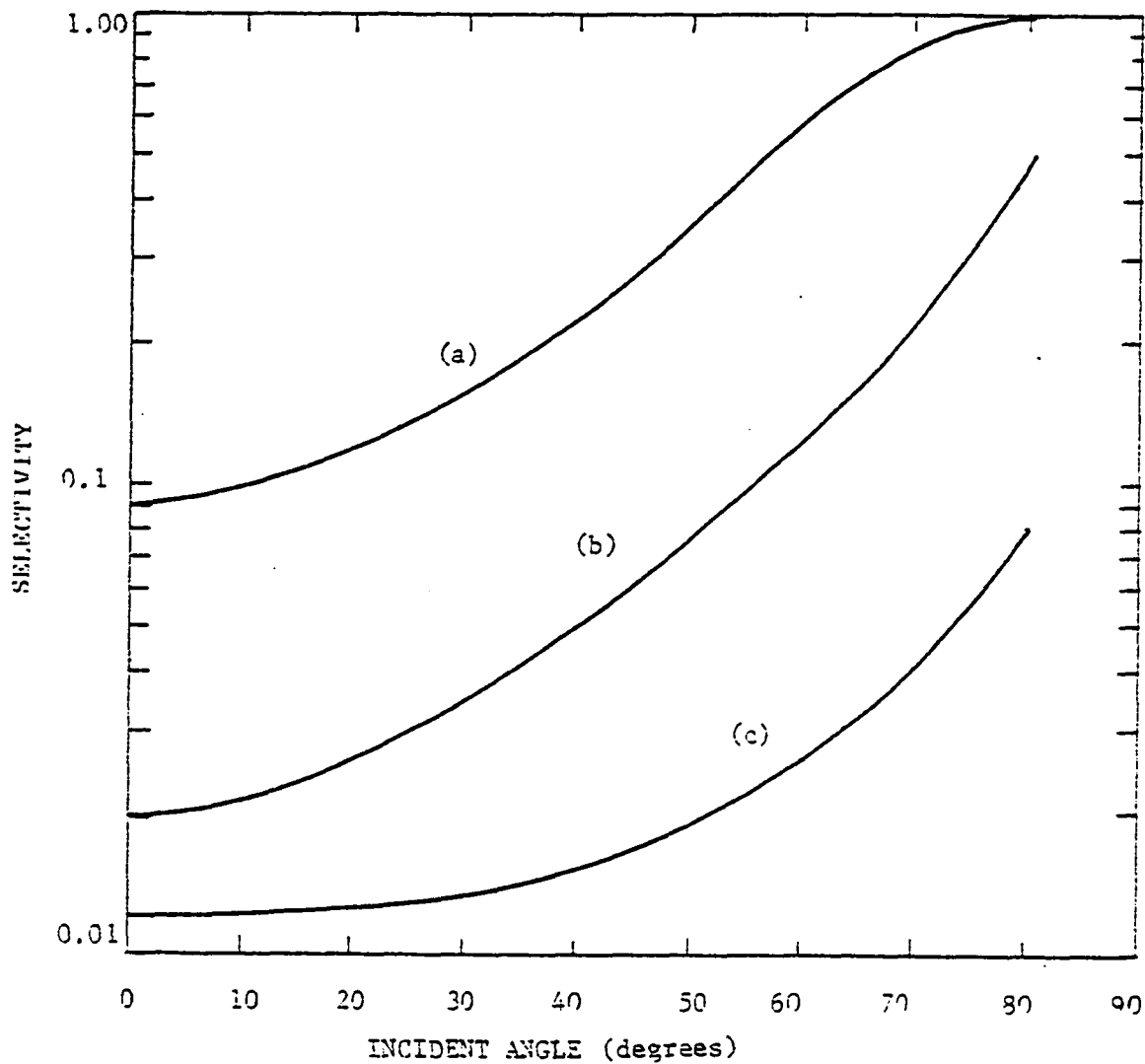


Figure 4.17. Selectivity Variation Against Incident Angle

Reflector Parameter: (a) $(\frac{3.45}{4} \frac{3.35}{4})$

(b) $(\frac{3.45}{4} \frac{3.40}{8} \frac{3.24}{8})$, (c) $(\frac{3.45}{4} \frac{3.45}{4} \frac{3.45}{4} \frac{3.40}{4})$.

CHAPTER V

TRIPLE LAYERED PERIODIC BRAGG WAVEGUIDE

5.1 Introduction

Since the advent of the solid, gas and semiconductor laser two decades ago, there has been immense advances in Integrated Optics. Optical modulation ⁽⁵⁴⁾, frequency mixing ⁽⁵⁵⁾, and parametric oscillation ⁽⁵⁶⁾ has been extensively studied. Recently, however, the introduction of low loss fiber ⁽⁵⁷⁾ and heterojunction laser ⁽⁵⁸⁾ and development of optical signal processing have raised the important questions concerning the future needs of totally integrated optical system ⁽⁵⁹⁾. As far as optical systems are concerned certain features of the thin film devices appear to have definite advantage. First, all the elements of a thin film devices are exposed on the surface and are easily accessible for probing, measurement, or modifications. Secondly, the thin film optical devices can be made small enough to place one next to the other on a single substrate, forming an optical system which is naturally more compact, less vulnerable to the environmental changes, and more economical. Thirdly, since the thin film has a thickness comparable to the optical wavelength and since most of the light energy is confined within the film, the light intensity inside the film can be very large even at moderate power level. This large power density is important in nonlinear interactions. Finally, the phase velocity of a light wave in a thin film waveguide depends on the thickness of the film and the mode

of propagation. This provides important design possibilities.

Many optical devices that have been reported show two basic dielectric waveguide structures which are in form of a planar film or strip with a refractive index higher than that of substrate. The optical confinement in waveguide is provided by two or three dielectric layers, having a higher refractive index layer surrounded by cladding layers of lower refractive index material. This condition is necessary to obtain an imaginary transverse propagation constant which corresponds to an evanescent decay of the mode field in the bounding media.

Recently another type of dielectric optical guiding structure with periodic layered Bragg reflector has been introduced ⁽⁶⁾. Such a Bragg waveguide which consists of alternating layers of material with high and low refractive indices has been demonstrated ⁽¹⁹⁾. The application of such Bragg reflector has also been recently reported in the operation of injection laser ^(20,21).

All the Bragg waveguides reported to date have double layered structure which require a large number of periodic layers to process, and thus have inherent disadvantages in cost effective production.

The recent work of electromagnetic wave propagation in double layered periodic dielectric structure by Yeh, et. al., ⁽⁶⁾ described Bloch waves in Bragg waveguide with help of Floquet's theorem. In their studies, two bounding media of Bragg reflector were assumed to have same refractive index as one of periodic layers. This assumption inherently impose limitation to more general application.

The main purpose of this chapter is to derive generalized wave propagation characteristic of a triple layered periodic Bragg waveguide.

This proposed method can be applied to any combination of layer with different refractive indices bounding medium. Also presented are the closed form expression for dispersion relation and the complete characterization of the triple layered periodic Bragg waveguide.

5.2 Transform Matrix of a Triple Layered Periodic Bragg Reflector

Consider a triple layered periodic Bragg waveguide structure shown in Figure 5.1. Guiding layer and Bragg reflector are sandwiched between a semi-infinite substrate (n_s) and a semi-infinite super-strate (n_a). The Bragg reflector are composed of N number of basic period with triple layeres of refractive indices n_1 , n_2 and n_3 . The cartesian coordinate system is chosen that x axis is normal to the interfaces. The position of each layer of reflector is specified by coordinate x_i , the upper boundary of each material. The thicknesses of each layer in basic period are given by

$$d_i = x_{i+1} - x_i, \quad i = 1, 2, \dots, 3N \quad (5-1)$$

and note that

$$d_{3p+q} = d_q$$

where

$$p = 1, 2, 3, \dots, N \text{ and } q = 1, 2, 3$$

and period is,

$$\Lambda = d_1 + d_2 + d_3 \quad (5-2)$$

The index profile in basic period is given by

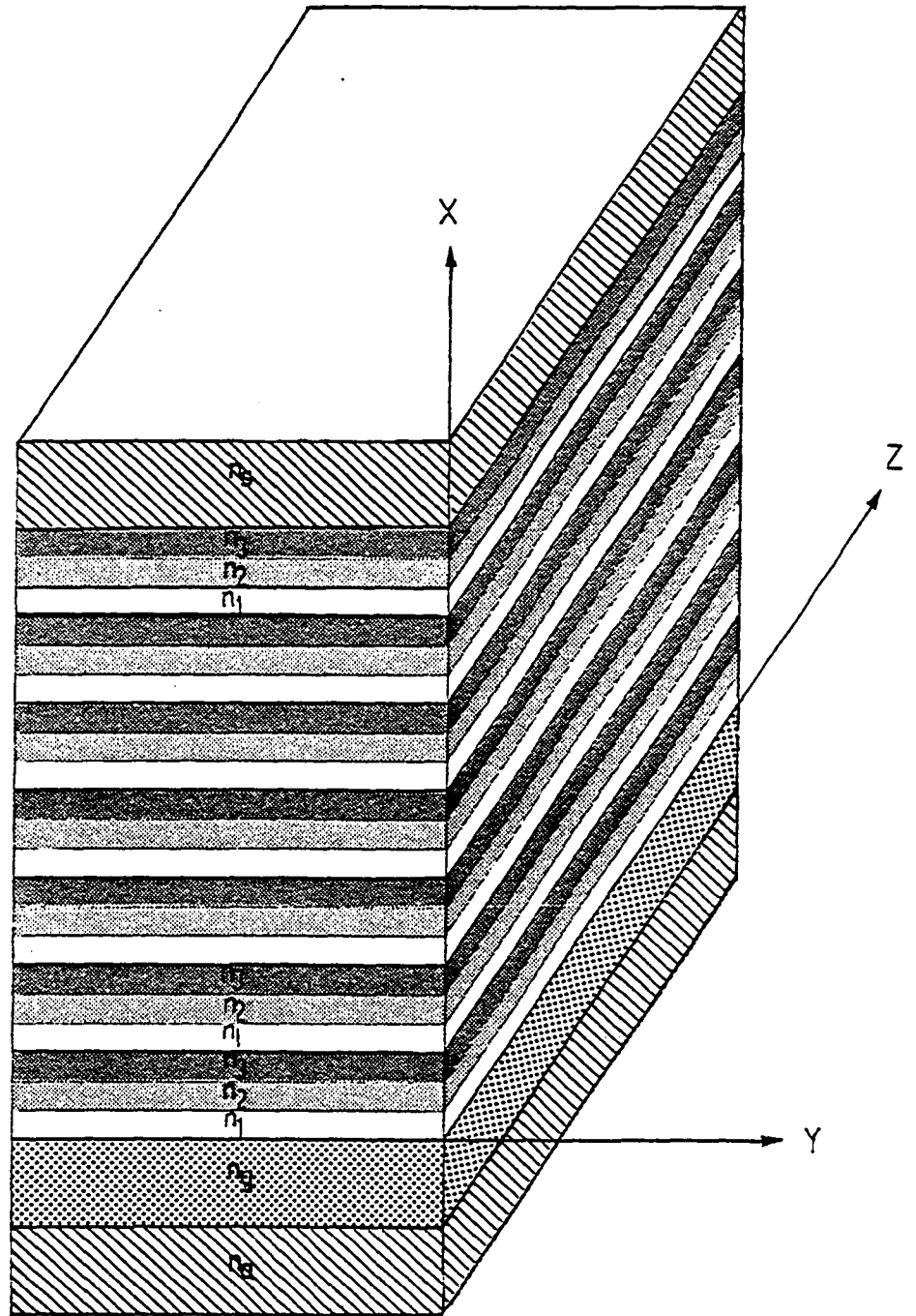


Figure 5.1. Triple Layered Dielectric Periodic Bragg Waveguide Structure with Semi-infinite Outer Media.

$$n(x) = \begin{cases} n_1 & 0 \leq x \leq d_1, \\ n_2 & d_1 \leq x \leq d_2, \\ n_3 & d_2 \leq x \leq d_3, \end{cases} \quad (5.3)$$

with

$$n(x + \Lambda) = n(x).$$

It is assumed that the incident light is monochromatic plane polarized and the individual layers are homogeneous, isotropic, nonmagnetic, and lossless. Also assume that layers are infinitely long in y and z directions.

The electric field distribution in each layer of Bragg reflector may be written by

$$E(x) = a'_{p,q} \exp\{jk_q(x-x_i)\} + b'_{p,q} \exp\{jk_q(x-x_i)\}, \quad (5.4)$$

where

$$k_q = k \sqrt{n_q^2 - n_e^2}, \quad q = 1, 2, 3$$

$a'_{p,q}$: incident complex amplitude at q^{th} interface of p^{th} period

$q = 1, 2, 3$ and $p = 1, 2, \dots, N$,

$b'_{p,q}$: reflected complex amplitude at q^{th} interface of p^{th} period,

n_q : refractive index in q^{th} layer of each period,

$n_e = \frac{\beta\lambda_0}{2\pi}$: normalized propagation constant (or effective refractive index),

β : propagation constant in z direction,

λ_0 : optical wavelength,

i : $3(p-1) + q$.

In Equation (5.4) a factor $\exp(j\beta z - j\omega t)$ has been suppressed.

We are now ready to use the matrix method derived in Chapter III for analyzing the propagation of plane waves in triple periodic Bragg reflector. In case of TE modes, applying Equation (3.10) to Equation (5.4), amplitude constants in each interface within the same period are related to

$$\begin{bmatrix} a'_{p,1} \\ b'_{p,1} \end{bmatrix} = V_1^{-1} V_2 U_2 \begin{bmatrix} a'_{p,2} \\ b'_{p,2} \end{bmatrix} \quad (5.6)$$

$$\begin{bmatrix} a'_{p,2} \\ b'_{p,2} \end{bmatrix} = V_2^{-1} V_3 U_3 \begin{bmatrix} a'_{p,3} \\ b'_{p,3} \end{bmatrix}$$

The incident and reflected complex amplitudes in the layer of refractive index n_i of a period to the corresponding layer of the same refractive index in the next period are obtained, using the Equation (3.10).

$$\begin{bmatrix} a'_{p,1} \\ b'_{p,1} \end{bmatrix} = V_1^{-1} V_2 U_2 V_2^{-1} V_3 U_3 V_3^{-1} V_1 U_1 \begin{bmatrix} a'_{p+1,1} \\ b'_{p+1,1} \end{bmatrix} \quad (5.7)$$

here V_i , U_i are admittance and phase matrix of i^{th} layer, respectively, and given by Equation (3.11) and (3.13) in Chapter III with appropriate parameters.

The electric field distribution equation can be rewritten as the following form

$$E(x) = a_{p,q} \exp\{jk_q(x - p\Lambda)\} + b_{p,q} \exp\{-jk_q(x - p\Lambda)\} \quad (5.8)$$

where we define,

$$\begin{aligned} a_{p,1} &\equiv a'_{p,1} \exp(jk_1 d_0), & b_{p,1} &\equiv b'_{p,1} \exp(-jk_1 d_0), \\ a_{p,2} &\equiv a'_{p,2} \exp(jk_2 d_3), & b_{p,2} &\equiv b'_{p,2} \exp(-jk_2 d_3), \\ a_{p,3} &\equiv a'_{p,3}, & b_{p,3} &\equiv b'_{p,3}. \end{aligned}$$

And x_i is substituted by

$$\begin{aligned} x_{3(p-1) + 1} &= (p-1)\Lambda + d_1, & x_{3(p-1) + 2} &= (p-1)\Lambda + d_0, \\ x_{3(p-1) + 3} &= (p-1)\Lambda. \end{aligned}$$

here

$$\Lambda = t_1 + t_2 + t_3 \text{ and } d_0 = d_2 + d_3.$$

The incident and reflected complex amplitudes at each interface within basic period are related to the following expression,

$$\begin{bmatrix} a_{p,2} \exp(-jk_2 d_0) \\ b_{p,2} \exp(jk_2 d_0) \end{bmatrix} = \frac{1}{2} \begin{bmatrix} (1 + \frac{\eta_1}{\eta_2}) & (1 - \frac{\eta_1}{\eta_2}) \\ (1 - \frac{\eta_1}{\eta_2}) & (1 + \frac{\eta_1}{\eta_2}) \end{bmatrix} \cdot \begin{bmatrix} a_{p,1} \exp(-jk_1 d_0) \\ b_{p,1} \exp(jk_1 d_0) \end{bmatrix}, \quad (5.9)$$

$$\begin{bmatrix} \bar{a}_{p,3} \exp(-jk_3 d_3) \\ \bar{b}_{p,3} \exp(jk_3 d_3) \end{bmatrix} = \frac{1}{2} \begin{bmatrix} \left(1 + \frac{n_2}{n_3}\right) & \left(1 - \frac{n_2}{n_3}\right) \\ \left(1 - \frac{n_2}{n_3}\right) & \left(1 + \frac{n_2}{n_3}\right) \end{bmatrix} \cdot \begin{bmatrix} \bar{a}_{p,2} \exp(-jk_2 d_3) \\ \bar{b}_{p,2} \exp(jk_2 d_3) \end{bmatrix} \quad (5.10)$$

The matrix Equation (5.7) represents the linear transformation of the complex amplitude in layer 1 of a basic period to the corresponding layer 1 in next period. Manipulating the admittance and phase matrix in Equation (5.7) and introducing new notation, we obtained the following matrix.

$$\begin{bmatrix} \bar{a}_{p,1} \\ \bar{b}_{p,1} \end{bmatrix} = \begin{bmatrix} T_{11} & T_{12} \\ T_{21} & T_{22} \end{bmatrix} \begin{bmatrix} \bar{a}_{p+1,1} \\ \bar{b}_{p+1,1} \end{bmatrix} \quad (5.11)$$

The elements of transform matrix are

$$\begin{aligned} T_{11} = & \left\{ \cos k_1 d_1 \cos k_2 d_2 - \frac{1}{2} \left(\frac{k_2}{k_1} + \frac{k_1}{k_2} \right) \sin k_1 d_1 \sin k_2 d_2 \right. \\ & - \frac{j}{2} \left[\left(\frac{k_2}{k_3} + \frac{k_3}{k_2} \right) \cos k_1 d_1 \sin k_2 d_2 \right. \\ & \left. \left. + \left(\frac{k_3}{k_1} + \frac{k_1}{k_3} \right) \sin k_1 d_1 \cos k_2 d_2 \right] \right\} \exp(-jk_3 d_3) \end{aligned} \quad (5.12a)$$

$$\begin{aligned} T_{12} = & \left\{ \frac{1}{2} \left(\frac{k_2}{k_1} - \frac{k_1}{k_2} \right) \sin k_1 d_1 \sin k_2 d_2 \right. \\ & + \frac{j}{2} \left[\left(\frac{k_3}{k_1} - \frac{k_1}{k_3} \right) \sin k_1 d_1 \cos k_2 d_2 \right. \\ & \left. \left. + \left(\frac{k_3}{k_2} - \frac{k_2}{k_3} \right) \cos k_1 d_1 \sin k_2 d_2 \right] \right\} \exp(jk_3 d_3) \end{aligned} \quad (5.12b)$$

$$\begin{aligned}
T_{21} = & \left\{ \frac{1}{2} \left(\frac{k_2}{k_1} - \frac{k_1}{k_2} \right) \sin k_1 d_1 \sin k_2 d_2 \right. \\
& - \frac{j}{2} \left[\left(\frac{k_3}{k_1} - \frac{k_1}{k_3} \right) \sin k_1 d_1 \cos k_2 d_2 \right. \\
& \left. \left. + \left(\frac{k_3}{k_2} - \frac{k_2}{k_3} \right) \cos k_1 d_1 \sin k_2 d_2 \right] \right\} \exp(-jk_3 d_3)
\end{aligned} \tag{5.12c}$$

$$\begin{aligned}
T_{22} = & \left\{ \cos k_1 d_1 \cos k_2 d_2 - \frac{1}{2} \left(\frac{k_2}{k_1} + \frac{k_1}{k_2} \right) \sin k_1 d_1 \sin k_2 d_2 \right. \\
& + \frac{j}{2} \left[\left(\frac{k_2}{k_3} + \frac{k_3}{k_2} \right) \cos k_1 d_1 \sin k_2 d_2 \right. \\
& \left. \left. + \left(\frac{k_3}{k_1} + \frac{k_1}{k_3} \right) \sin k_1 d_1 \cos k_2 d_2 \right] \right\} \exp(jk_3 d_3)
\end{aligned} \tag{5.12d}$$

It can be easily proved that the determinant of transform matrix is unity, that is unimodular.

$$T_{11}T_{22} - T_{12}T_{21} = 1 \tag{5.13}$$

Note that there are some symmetric relations among those 4 matrix elements of the transform matrix.

$$T_{11} = T_{22}^* \tag{5.14}$$

$$T_{12} = T_{21}^*$$

These symmetric relations are very useful in simplifying the matrix manipulation as well as in numerical calculations. This advantage vanishes for dielectric layers having a complex refractive index.

The inverse of transform matrix is obtained by simple transposing the matrix itself,

$$\begin{bmatrix} \overline{T}_{11} & \overline{T}_{12} \\ \overline{T}_{21} & \overline{T}_{22} \end{bmatrix}^{-1} = \begin{bmatrix} \overline{T}_{22} & -\overline{T}_{21} \\ -\overline{T}_{12} & \overline{T}_{11} \end{bmatrix} \quad (5.15)$$

This is due to the fact that the transform matrix is unimodular (Equation 5.13).

By successive application of Equation (5.11) to the Bragg reflector which is composed of N numbers of basic period, we have

$$\begin{bmatrix} \overline{a}_{1,1} \\ \overline{b}_{1,1} \end{bmatrix} = \begin{bmatrix} \overline{T}_{11} & \overline{T}_{12} \\ \overline{T}_{21} & \overline{T}_{22} \end{bmatrix}^{N-1} \begin{bmatrix} \overline{a}_{N,1} \\ \overline{b}_{N,1} \end{bmatrix} \quad (5.16)$$

The square matrix in Equation (5.16) is the system transform matrix which relates the complex amplitudes of incident plane waves and the reflected plane waves in the first layer of the first period to those of the first layer in the last period. The relations between the amplitude of each layers within period are given by Equation (5.9) and (5.10).

By using Equation (5.15), the Equation (5.16) can be rewritten as the following form.

$$\begin{bmatrix} \overline{a}_{N,1} \\ \overline{b}_{N,1} \end{bmatrix} = \begin{bmatrix} \overline{T}_{22} & -\overline{T}_{21} \\ -\overline{T}_{12} & \overline{T}_{11} \end{bmatrix}^{N-1} \begin{bmatrix} \overline{a}_{1,1} \\ \overline{b}_{1,1} \end{bmatrix} \quad (5.17)$$

Thus we can specify the field distribution in the Bragg reflector uniquely by determine $\overline{a}_{1,1}$ and $\overline{b}_{1,1}$.

5.3 Floquet's Theorem and Bloch Wave Function

The field distribution in periodic layers can be expressed in more simple form using the Floquet's Theorem⁽⁶⁰⁾. The complex amplitude related by the matrix equation (5.18) in fore section may also be written as

$$\begin{bmatrix} a_{N,1} \\ b_{N,1} \end{bmatrix} = T^{(N-1)} \begin{bmatrix} a_{1,1} \\ b_{1,1} \end{bmatrix} \quad (5.18)$$

here T' denotes inverse of square matrix in Equation (5.16). Imposing the requirements that wave function must remain finite as N approaches infinity. This is most conveniently discussed in terms of the eigenvalue problem of the matrix T' . The eigenvalues of T' are given by roots of characteristic equation,

$$t^2 - t(\text{trace of } T') + \det T' = 0. \quad (5.19)$$

The roots are

$$t = \frac{1}{2} \left[(\text{trace of } T') \pm \sqrt{(\text{trace of } T')^2 - 4} \right] \quad (5.20)$$

If $(\text{trace of } T') < 2$, the eigenvalue t has real and imaginary part, and may be written as

$$t = e^{\pm jK(N-1)\Lambda}$$

this condition denote the propagation waves. When $(\text{trace of } T') > 2$, $K = \frac{m\pi}{\Lambda} + jK_i$ and t has only a real part so that the wave is evanescent. These are so called stop band of periodic medium. The band edge are the regions where $\frac{(\text{trace } T')}{2} = 1$. The parameter K is given by

$$e^{jK\Lambda} = \frac{T_{11} + T_{22}}{2} \pm \sqrt{\left(\frac{T_{11} + T_{22}}{2}\right)^2 - 1}. \quad (5.21)$$

We also note that (trace of T') = (trace of T).

By substituting Equation (5.12a) and (5.12d) to above equation we have,

$$\begin{aligned} \frac{T_{11} + T_{22}}{2} &= \cos k_1 d_1 \cos k_2 d_2 \cos k_3 d_3 \\ &\quad - \frac{1}{2} \left(\frac{k_2}{k_1} + \frac{k_1}{k_2} \right) \cos k_3 d_3 \sin k_1 d_1 \sin k_2 d_2 \\ &\quad - \frac{1}{2} \left(\frac{k_2}{k_3} + \frac{k_3}{k_2} \right) \cos k_1 d_1 \sin k_2 d_2 \sin k_3 d_3 \\ &\quad - \frac{1}{2} \left(\frac{k_3}{k_1} + \frac{k_1}{k_3} \right) \cos k_2 d_2 \sin k_1 d_1 \sin k_3 d_3 \end{aligned} \quad (5.22)$$

Note that Equation (5.22) is same as the Equation (3.33), which is related to stop zone width in Section 3 of Chapter III with appropriate values of m_{11} and m_{22} for triple layered period.

Using the property of Floquet's theorem, wave in n_1 layer of the p^{th} period can be written,

$$E(x) = \exp(jKx)E_K(x), \quad (5.23)$$

where

$$\begin{aligned} E_K(x) &= \{ a_{p,1} \exp[jk_1(x - p\Lambda)] \\ &\quad + b_{p,1} \exp[-jk_1(x - p\Lambda)] \} \exp[-jK[x - (p-1)\Lambda]], \end{aligned} \quad (5.24)$$

here K known as Bloch wave number is given by Equation (5.22). $a_{p,1}$ and $b_{p,1}$ are obtained by Equation (5.19) with eigenvalue as the following form,

$$\begin{bmatrix} \bar{a}_{p,1} \\ \bar{b}_{p,1} \end{bmatrix} = e^{jK(p-1)\Lambda} \begin{bmatrix} \bar{a}_{1,1} \\ \bar{b}_{1,1} \end{bmatrix} \quad (5.25)$$

5.4 Electric Field and Dispersion Equation

Multilayered periodic media present high reflectivity to incident monochromatic radiation.

Fox ⁽⁵⁾ has suggested that such reflection can be used in a new type of dielectric waveguide in which conventionally used substrate is replaced by a structure of periodic layers. Yeh, et. al., ⁽⁶⁾ used a Bloch wave formulation of propagation in double layered media to obtain a dispersion relation of Bragg waveguide and showed the property of confined mode in the guiding layer which has a lower index of refraction than that of the periodic layers.

The Bragg waveguide considered here consists of a guiding layer of refractive index n_g surrounded by a index of refraction n_a and triple layered periodic reflector. Figure 5.1 shows the coordinate system and guide dimension.

In case of TE modes the field component are E_y , H_x and H_z . Each of these components, satisfies the wave equation, for $E_y(x)$,

$$\frac{\partial^2 E_y(x)}{\partial x^2} + (k_0^2 n^2(x) - \beta^2) E_y(x) = 0,$$

here we assume

$$E(x,y,z) \exp(-j\omega t) = E_y(x) \exp j(\beta z - \omega t)$$

Finally, the solution in all the regions are given by

$$E(x) = \begin{cases} a_a \exp q_a (x + d) & x \leq -d, \\ a_o \exp(jk_g x) + b_o \exp(-jk_g x) & -d \leq x \leq 0, \\ E_k(x) \exp(iKx), & 0 \leq x \leq N\Lambda, \\ a_s \exp(jk_s x) & x \geq N\Lambda, \end{cases} \quad (5.26)$$

where

$$\beta = k n_g \sin \theta_g$$

$$k = \frac{2\pi}{\lambda_o}$$

$$q_a = (\beta^2 - k^2 n_a^2)^{\frac{1}{2}}, \quad (5.27)$$

$$k_\ell = (k^2 n_\ell^2 - \beta^2)^{\frac{1}{2}}, \quad \ell = g, s$$

N = number of periods,

$$\Lambda = d_1 + d_2 + d_3$$

Here we assume that $n_a < n_g < n_1, n_2, n_3$. The assumed solution in superstrate and guiding layer is similar to the conventional slab dielectric waveguide as in section 4 of Chapter II. The wave expression in triple layered reflector, $E_k(x) \exp(iKx)$, is given by Equation (5.24) and the electric field in substrate are assumed only transmitted waves.

In order to obtain the complete solution of the plane wave for the mode of waveguide shown in Figure 5.1, we must apply the appropriate continuity conditions at the interfaces of the structure. Using Equation (3.10), a_o and b_o are related to

$$\begin{bmatrix} a_{1,1} \exp(-jk_1 \Lambda) \\ b_{1,1} \exp(jk_1 \Lambda) \end{bmatrix} = \frac{1}{2} \begin{bmatrix} (1 + \frac{n_g}{n_1}) & (1 - \frac{n_g}{n_1}) \\ (1 - \frac{n_g}{n_1}) & (1 + \frac{n_g}{n_1}) \end{bmatrix} \begin{bmatrix} a_0 \\ b_0 \end{bmatrix} \quad (5.28)$$

The continuity condition at $x = -d$ turn out to be the following simple form,

$$\tan(k_g d - \theta) = j \frac{b_0/a_0 - 1}{b_0/a_0 + 1}, \quad (5.29)$$

here

$$\theta = \tan^{-1}(q_a/k_g).$$

We note that b_0/a_0 in Equation (5.29) is the reflection coefficient of Bragg reflector given by Equation (3.35) in Chapter III. Equation 5.29 is called the dispersion relation of Bragg waveguide. The left hand side contains only the parameter of the guiding layer refractive index (n_g) and superstrate refractive index (n_a) while the right hand side depends only on the reflection coefficient of the periodic reflector. For guided propagation β , q_a and k_g are real so that the left hand side of Equation (5.29) is a real number. The right hand side is real if and only if the propagation conditions in the reflector fall within one of the forbidden gaps and a_0 is equal to the complex conjugate of b_0 .

The solutions of dispersion equation can be used to determine the value of the propagation constant β that correspond to a confined waveguiding. These values of β can then be used to calculate the mode dispersion curves for a particular Bragg waveguide.

5.5 Confinement Factor and Loss

All Bragg waveguide reported up to this date have large number of periods. In practical process, they have inherent disadvantages in cost effective production. Although the current molecular beam technology can fabricate as many layers as needed. In practice, the time invested in the growth is proportional to the number of periods. Typical growth rate is about $1 \mu\text{m/hr}$ (61).

Also the confinement factor play an important role in injection laser. For instance the threshold current density depends on the confinement factor (62).

We will calculate the confinement factor of the triple layer periodic Bragg waveguide. The confinement factor is defined as the ratio of the light intensity within guiding layer to the sum of light intensity both within and outside the guiding layer.

The confinement factor Γ for the triple layer periodic Bragg waveguide is expressed by

$$\begin{aligned} \Gamma = & \frac{\int_{-d}^0 \{a_0 \exp(jk_g x) + b_0 \exp(-jk_g x)\} \{a_0 \exp(jk_g x) + b_0 \exp(-jk_g x)\}^* dx}{\left[\int_{-\infty}^{-d} \{a_a \exp q_a(x+d)\} \{a_a \exp q_a(x+d)\}^* dx \right.} \\ & + \int_{-d}^0 \{a_0 \exp(jk_g x) + b_0 \exp(-jk_g x)\} \{a_0 \exp(jk_g x) + b_0 \exp(-jk_g x)\}^* dx \\ & + \int_0^{NA} \{E_k(x) \exp(iKx)\} \{E_k(x) \exp(iKx)\}^* dx \quad (5.30) \\ & \left. + \int_{NA}^{d_s} \{a_s \exp(jk_s x)\} \{a_s \exp(jk_s x)\}^* dx \right] \end{aligned}$$

here we assumed substrate has thickness d_s and considered TE mode only. After some manipulation of above equation, confinement factor Γ is

given by

$$r = \left[1 + \frac{(1 - e^{-2NK_i\Lambda})}{1 - e^{-2K_i\Lambda}} \left(\frac{S_a + S_{11} + S_{12} + S_{13} + S_s d_s}{S_g} \right) \right]^{-1} \quad (5.31)$$

here

$$S_a = \frac{a_0 a_0^* + b_0 b_0^*}{2q_a} + \frac{1}{2q_a} \left[a_0^* b_0 e^{2jk_g d} + (a_0^* b_0 e^{2jk_g d})^* \right] \quad (5.32a)$$

$$S_g = (a_0 a_0^* + b_0 b_0^*)d + \frac{\sin k_g d}{k_g} \left[a_0^* b_0 e^{jk_g d} + (a_0^* b_0 e^{jk_g d})^* \right] \quad (5.32b)$$

$$S_{11} = (a_{1,1} a_{1,1}^* + b_{1,1} b_{1,1}^*)d_1 + \frac{\sin k_1 d_1}{k_1} \left[a_{1,1}^* b_{1,1} e^{jk_1(d_1 + 2d_0)} + (a_{1,1} b_{1,1} e^{jk_1(d_1 + 2d_0)})^* \right] \quad (5.32c)$$

$$S_{12} = (a_{1,2} a_{1,2}^* + b_{1,2} b_{1,2}^*)d_2 + \frac{\sin k_2 d_2}{k_2} \left[a_{1,2}^* b_{1,2} e^{jk_2(d_2 + 2d_3)} + (a_{1,2} b_{1,2} e^{jk_2(d_2 + 2d_3)})^* \right] \quad (5.32d)$$

$$S_{13} = (a_{1,3} a_{1,3}^* + b_{1,3} b_{1,3}^*)d_3 + \frac{\sin k_3 d_3}{k_3} \left[a_{1,3}^* b_{1,3} e^{jk_3 d_3} + (a_{1,3} b_{1,3} e^{jk_3 d_3})^* \right] \quad (5.32e)$$

$$S_s = \left(\frac{2\eta_3}{\eta_3 + \eta_s} \right) a_{1,3} a_{1,3}^* e^{-2(N-1)K_i\Lambda} \quad (5.32f)$$

All Bragg waveguides have loss due to the finite number of periods in the periodic layers. In practice, it is impossible to fabricate an infinite number of periods, thus the minimum number of periods should be calculated for an acceptable loss.

The following calculation is to find out the attenuation constant

for each mode. The time averaged flux of energy is given by the real part of the complex Poynting vector

$$S = \frac{1}{2} \text{Re}(E \times H^*) \quad (5.33)$$

The total power flow P is given by integration of the z component of S over the cross sectional area A .

$$P = \int_A S \cdot dA \quad (5.34)$$

The power loss due to the energy flow into the substrate is given by

$$P_{\text{loss}} = \int_w S \cdot dw, \quad (5.35)$$

where w is the wall area. The power flow along the guide can be

$$p(z) = P_0 \exp(-2\alpha z). \quad (2.36)$$

Therefore the attenuation constant is written by

$$2\alpha = - \frac{1}{p} \left(\frac{dp}{dz} \right) \quad (5.37)$$

where $-\left(\frac{dp}{dz}\right)$ can be interpreted as the power loss per unit length of the guide. By combining Equations (5.32), (5.34), (5.35), and (5.36), the attenuation constant can be described by

$$\alpha = \frac{S_x}{2 \int S_z dx} \quad (5.38)$$

here S_x and S_z represent the x and z component of the Poynting vector S . Using Equation (5.32) and Equation (5.38), the attenuation constant is given by

$$\alpha = \frac{k_s}{2\beta} \frac{\left(\frac{2n_3}{n_3 + n_s}\right)^2 a_{13} a_{13}^* e^{-2(N-1)K_i \Lambda}}{S_a + S_g + (S_{11} + S_{12} + S_{13}) \left(\frac{1 - e^{-2NK_i \Lambda}}{1 - e^{-2K_i \Lambda}}\right)} \quad (5.39)$$

5.6 Numerical Results

In this section some numerical results about dispersion relation, electric field profile, confinement factor and loss due to finite number of period are presented.

Operationally the eigenmode is calculated by substituting suitable range of values for n_e (i.e., $n_a < n_e < n_g$) into Equation (5.29). And since the left hand side of Equation (5.29) is a real number, if the resulting values of T_{11} and T_{22} correspond to stop zone and the number of period N is sufficient to obtain unit reflectivity, then right hand side of the dispersion Equation (5.29) is a real number. The number of period N to achieve unity reflectivity is estimated from the results of Chapter IV. The calculated dispersion relations and envelope decay factor of two different Bragg waveguides are shown in Figure 5.2 and 5.3. In each case, the substrate index $n_s = 3.45$, guiding layer index $n_g = 3.24$, reference wavelength $\lambda_0 = 1.15 \mu\text{m}$ are used. And the reflector parameters are given in Table 5.1. These are representative values that could be used in Bragg waveguide with $\text{Ga}_x\text{Al}_{1-x}\text{As} - \text{GaAs}$ combination.

In Figure 5.2 and 5.3, the solid curves represent the normalized thickness of guiding layer d/λ_0 versus the normalized propagation constant n_e (or effective index of refraction) and the broken curve represents the envelope decay factor $\exp(-K_1\Lambda)$ versus n_e . In addition, each mode is represented by a separate curve with mode label $m = 0, 1, 2, 3, \dots$. In a conventional slab waveguide the n_e for confined mode vary continuously from maximum of refractive indices of two cladding medium to refractive index of core material (See Figure 2.5). It is

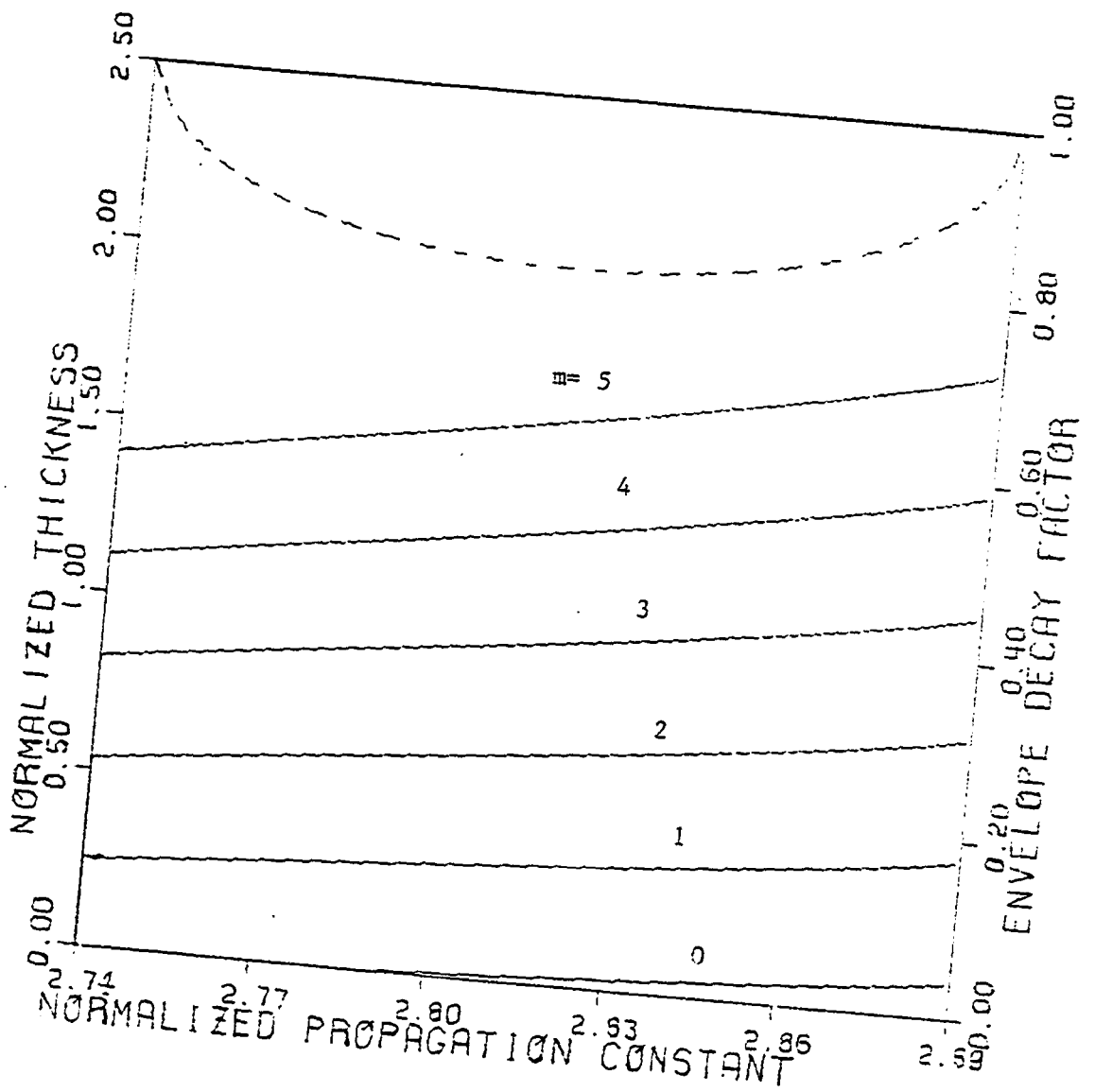


Figure 5.2. Dispersion Relation for Bragg Waveguide II of Table 5.1.
 Solid Curves: d/λ_0 vs. n_e
 Broken Curve: $\exp(-K_1\Lambda)$ vs. n_e

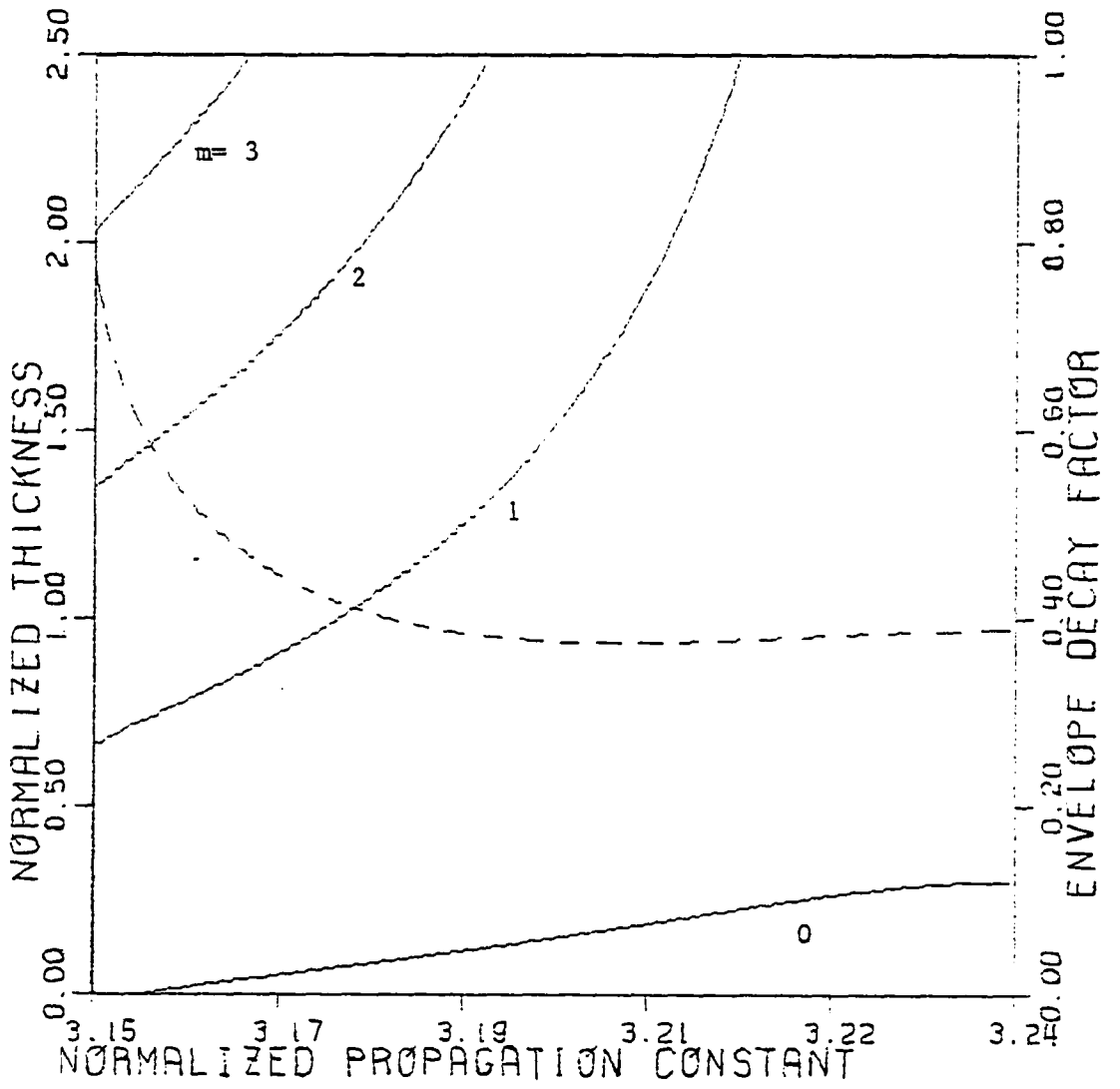


Figure 5.3. Dispersion Relation for Bragg Waveguide I of Table 5.1.

Solid Curve: d/λ_0 vs. n_e

Broken Curve: $\exp(-K_1\Lambda)$ vs. n_e

Type	Number of Periods	Indices of Refraction			Thickness [μm]			Thickness of Basic Period Λ [μm]
		n_1	n_2	n_3	d_1	d_2	d_3	
I	5	3.45	3.24	3.45	0.11	0.51	0.11	0.73
II	30	3.45	3.35	3.45	0.07	0.16	0.07	0.30

- 1) Bragg waveguide I and II satisfy the Bragg condition at $\theta_0 = 80^\circ, 60^\circ$, respectively.
- 2) $n_g = 3.24$ $n_s = 3.45$.
- 3) Both waveguide have a reflector of triple layered basic $(\frac{n_1}{8} \frac{n_2}{4} \frac{n_1}{8})$ structure.

Table 5.1. Bragg Waveguide Parameters

noted in Figure 5.2 and 5.3 that the n_e for confined mode in Bragg waveguide can only vary within the stop zone, $(T_{11} + T_{22})/2 > 1$. For the outside of stopzone, the waveguide modes change to substrate modes.

An interesting feature of Figure 5.2 is the single transverse mode operation for waveguide thickness that would support many transverse mode in a conventional slab waveguide such as one shown in Figure 2.5 in Chapter II. This is possible only when the thickness of each layer in reflector is adjusted to satisfy Bragg condition at small angle.

The result in Figure 5.3 which represents the dispersion relation for 80° matching angle show the possibilities of allowing several high modes in a certain guide thickness. However, if thickness is selected so that the loss for higher order mode is higher than that of a lower order mode, then the higher mode will eventually leak into the substrate. This mode selective capability could be applied to various fields of Integrated Optics. It is observed in Figure 5.3 that the envelope decay factor $\exp(-K_i \Lambda)$ is minimum at the center of the stopzone. The value of $K_i \Lambda$ governs the amplitude of light wave in reflector. The Bloch wave constant vs. n_e for a typical triple layered Bragg waveguide is shown in Figure 5.4. It is clearly seen that K_i is maximum at center of stop zone.

Figure 5.5 shows the electric field profiles of fundamental TE mode with $d = 0.23 \mu\text{m}$ and the higher order mode with $d = 2.35 \mu\text{m}$. The waveguide parameters are the same as those used for obtaining Figure 5.3. Those figures show the effect of envelope decay factor on

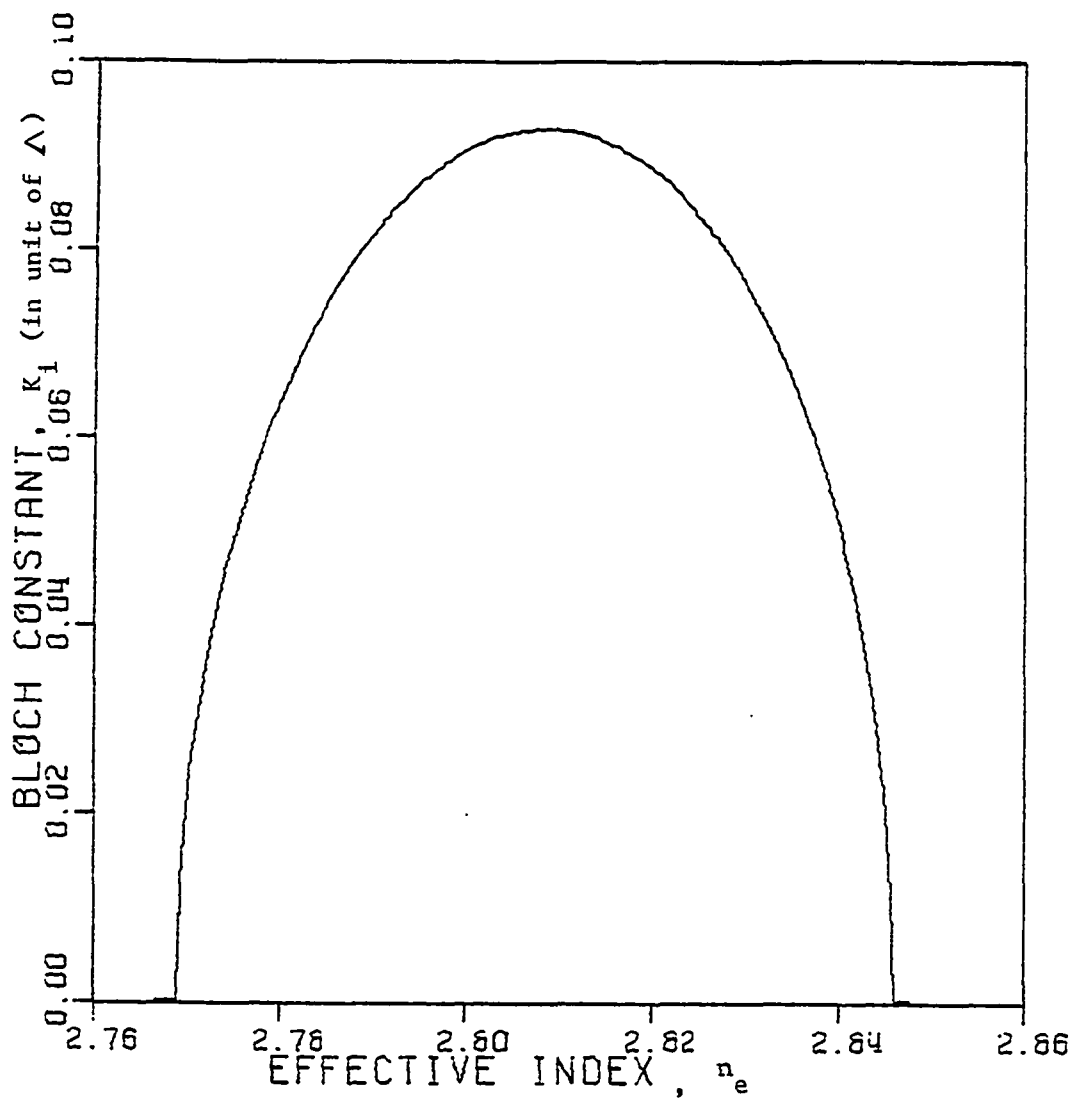


Figure 5.4. Bloch Wave Constant vs. Normalized Propagation Constant.

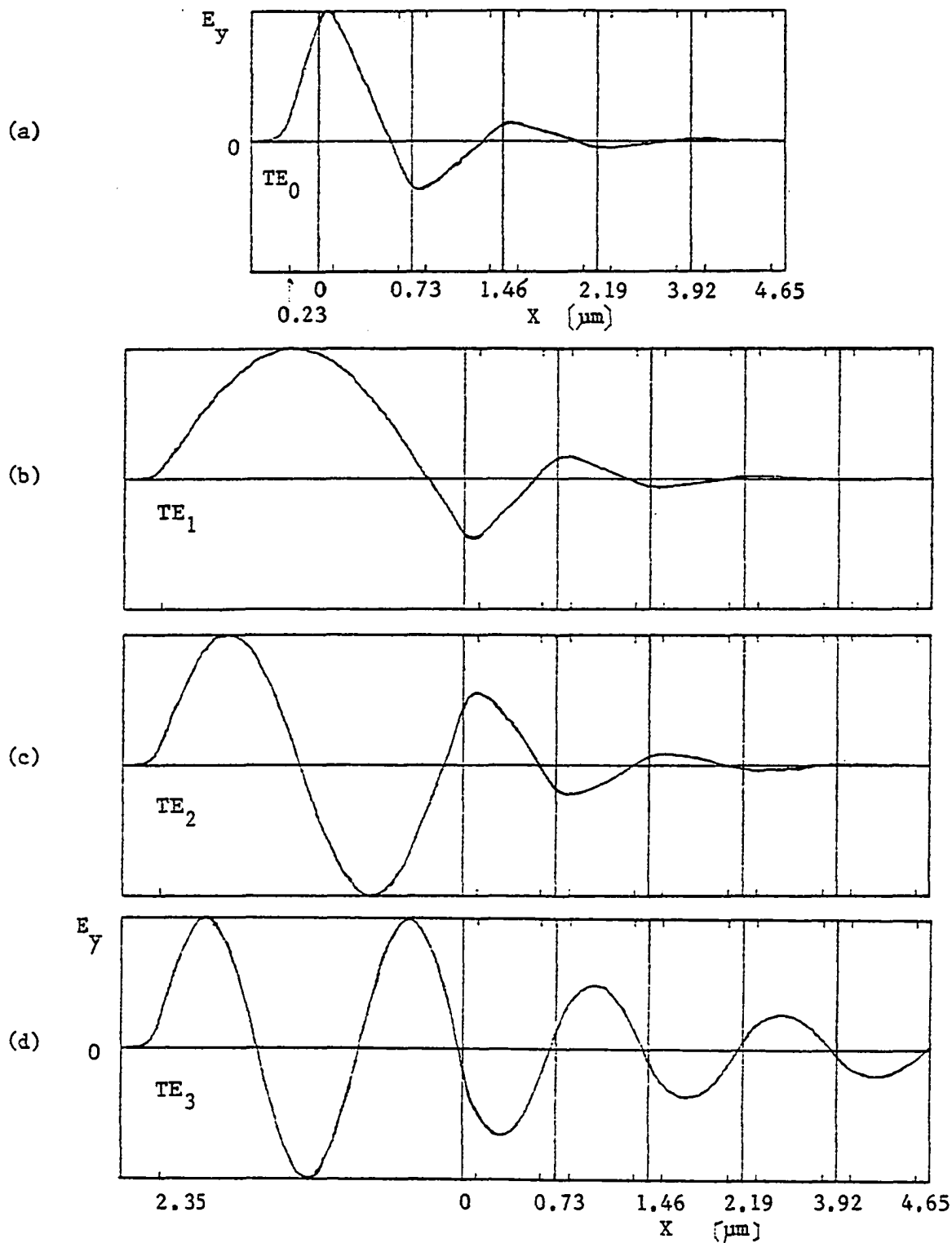


Figure 5.5. Electric Field Distribution of Bragg Waveguide I.

a) TE_0 mode for $d = 0.23 \mu\text{m}$

b) TE_1 c) TE_2 d) TE_3 with $d = 2.35 \mu\text{m}$

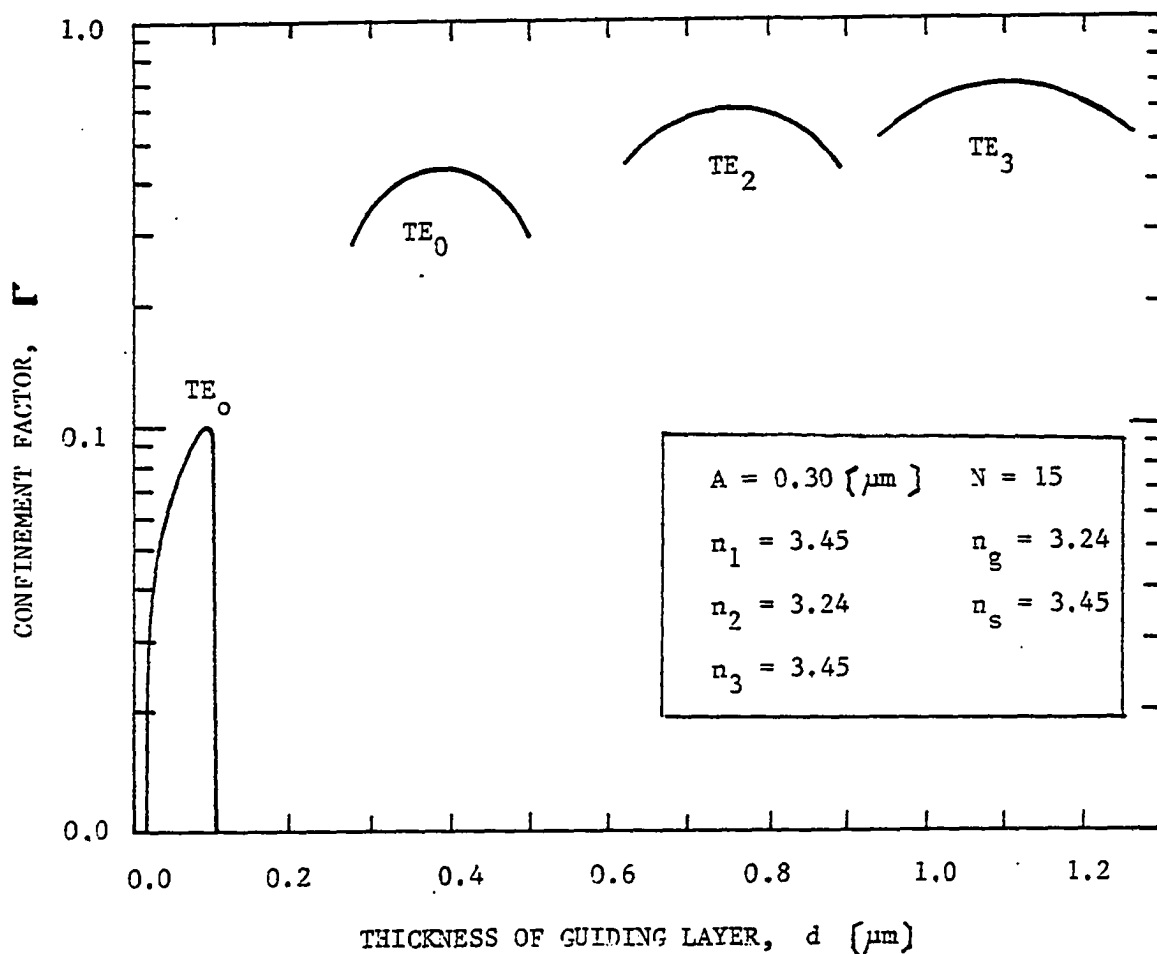


Figure 5.6. Confinement Factor for the Fundamental, First -, Second -, and Third - Order TE Mode as a Function of Guiding Layer Thickness.

amplitude of electric field in periodic reflector for different order of mode.

It is readily seen that field confinement in guiding layer for fundamental mode is small compared to that of higher order mode. For a case of larger d , where higher order modes are permitted, Figure 5.5 (b), (c), (d) show that, as the mode order increases, more of light intensity is outside of guiding layer. Therefore the lower the mode order, the greater the confinement.

The variation of confinement factor Γ for fundamental, first -, second - , and third - order TE mode against guiding layer thickness is plotted in Figure 5.6. Γ decreases when d is less than or greater than d_{opt} and becomes maximum at $d = d_{opt}$, where d_{opt} denotes the optimum thickness of guiding layer at a given incident condition. This Bragg waveguide mode confinement characteristics differs from the conventional heterostructure in which Γ for higher order mode is small near cutoff and approach the value for the fundamental mode as d is increased.

The attenuation constants as a function of the number of period N for TE modes are plotted in Figure 5.7. The Bragg waveguide have $(\frac{n_1}{8} \frac{n_2}{4} \frac{n_1}{8})$ basic period with same refractive indice as that of Table 5.1. In the figure, solid graph and broken graph represent for $\Lambda = 0.42$ and $0.73 \mu\text{m}$, respectively. The attention constant of the Bragg waveguide decreases rapidly as the number of periods of reflector increases. And this figure also shows the larger Λ has less loss due to higher reflectivity of Bragg reflector as discussed in Chapter IV. The results for the triple structure shown in Figure 5.7

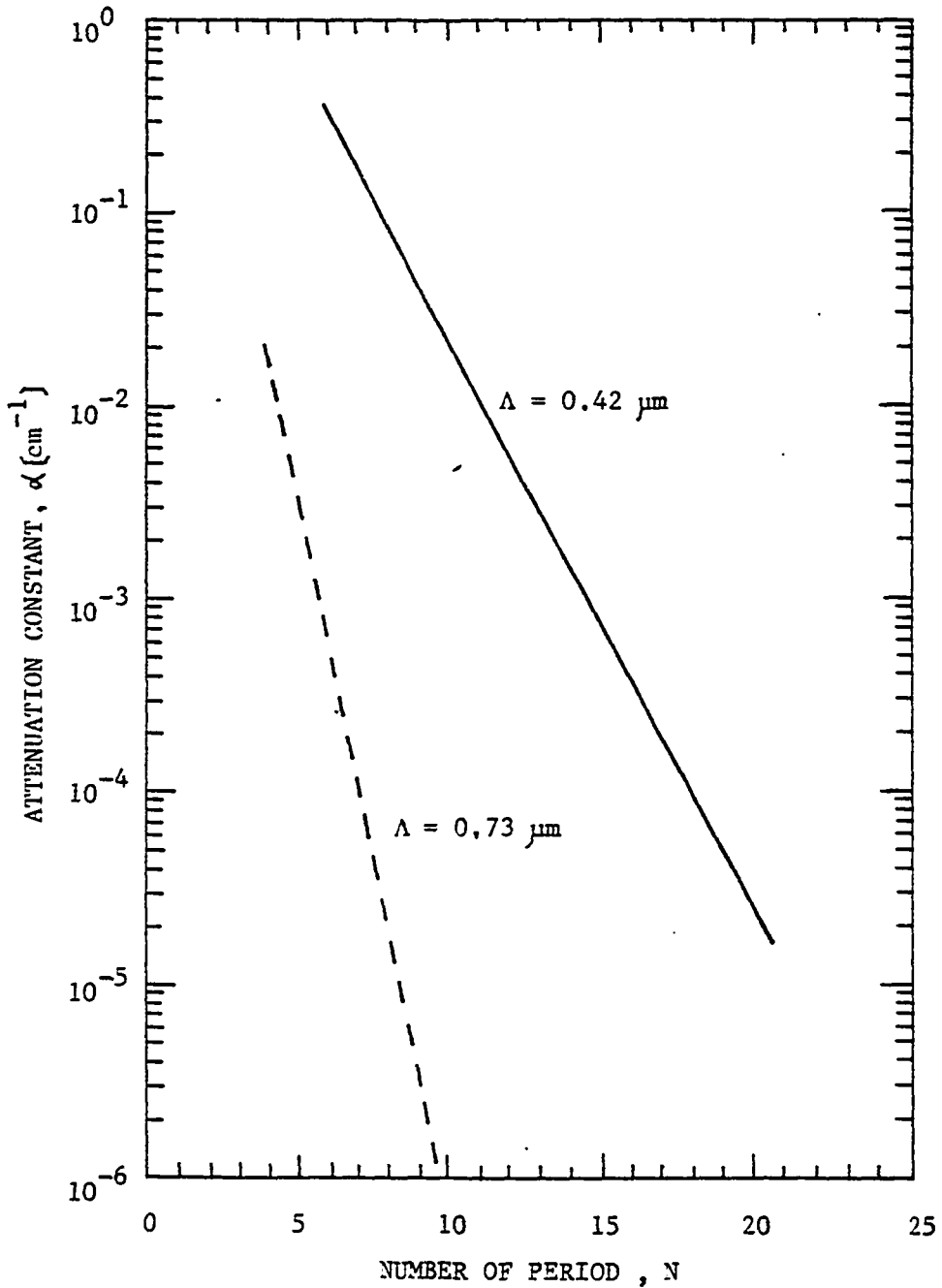


Figure 5.7. The Attenuation Constant vs. Number of Period for TE Mode in Bragg Waveguide with $n_1 = 3.45$ and $n_2 = 3.24$.

Solid Graph: $\Lambda = 0.42 \mu\text{m}$

Broken Graph: $\Lambda = 0.73 \mu\text{m}$

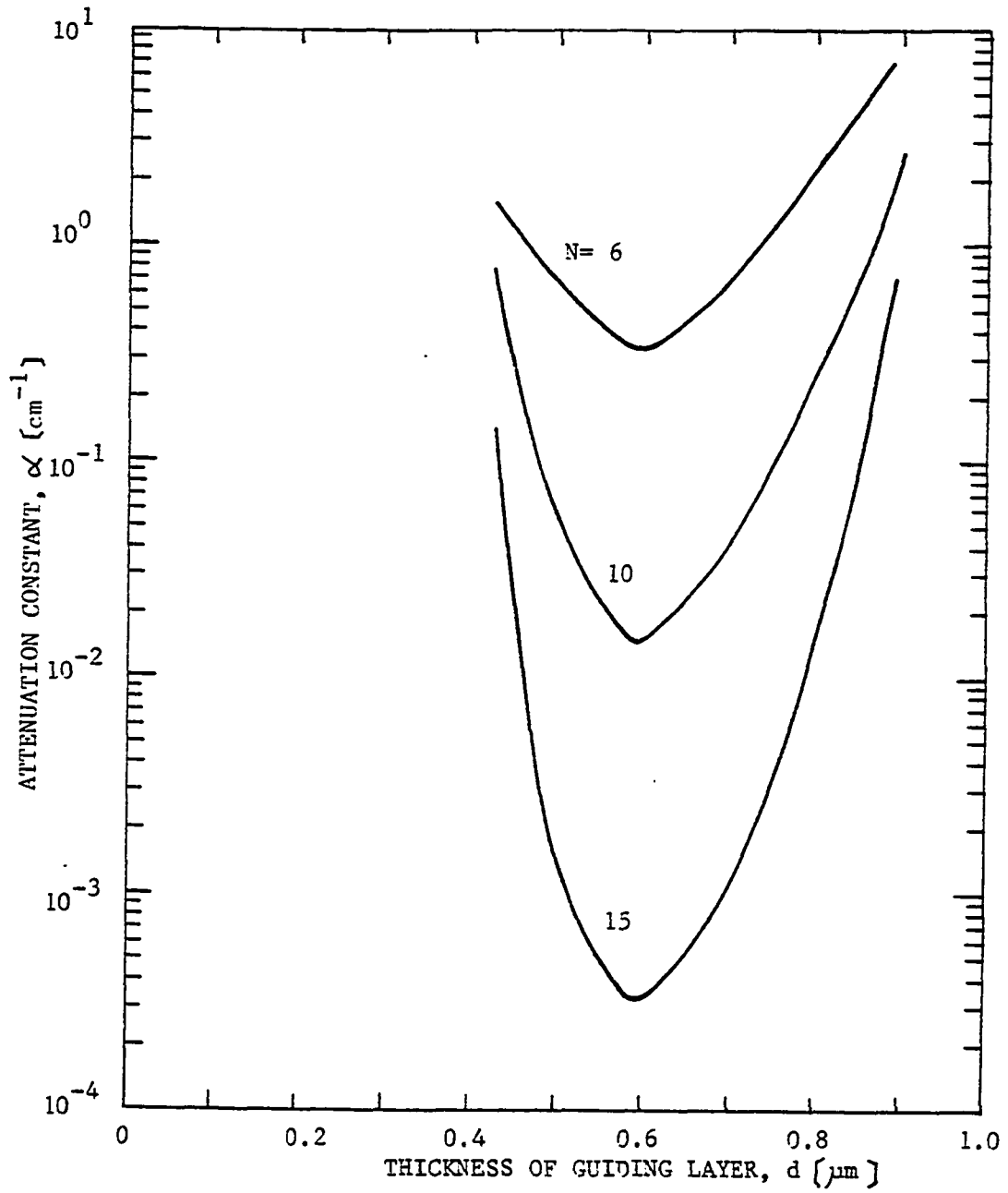


Figure 5.8. The Attenuation Constant α as a Function of Guiding Layer Thickness d for Three Different Number of Period N .

exhibit lower loss than that of the double structure reported by A.Y. Cho, et.al (19). Figure 5.8 describes the effect of guiding layer thickness on loss as a parameter of number of period for the TE mode in waveguide I given in Table 5.1. Regardless to number of period, the attenuation constant becomes minimum at the optimum thickness corresponding to the center of the allowed range of guiding layer thickness. It is clear from Figure 5.7 and 5.8 that the maximum confinement and minimum loss is accomplished with the optimum guiding layer thickness.

In Table 5.2, the attenuation constant and selectivity for the TE₁ mode for two different configurations of the Bragg waveguide are listed. The waveguide parameters are same as those of Table 5.1. For higher selectivity, it is necessary not only to choose the layer thicknesses to satisfy the Bragg condition at small angle but also to adjust the refractive index differences between layer as small as possible.

Waveguide Type*	Number of Period	Attenuation Constant α [cm ⁻¹]	Selectivity $\frac{\lambda_2 - \lambda_1}{\lambda_0}$
II	30	0.57×10^{-1}	0.074
I	5	0.18×10^{-1}	0.539

*Waveguide parameters are given in Table 5.1

Table 5.2. Attenuation Constant and Selectivity for the TE₁ Mode of the Bragg Waveguide I and II.

CHAPTER VI

CONCLUSIONS

A generalized closed form expression for reflectivity of multi-layered Bragg reflector is presented with expression of dispersion relationship, electric field distribution, optical confinement factor, and loss of triple layered Bragg waveguide. These expressions are valid for any orientation of a polarization and any values of a layer thickness, wavelength, refractive indices of outermost bounding medium and an angle of incidence.

With the numerical data, comparison and discussion of some important characteristics such as reflectivity and selectivity of a double, triple, quadruple and quintuple layered periodic reflector are extensively analyzed.

Addition of a number of layer in basic period has no significant effect on the magnitude of reflectance, while adjusting and controlling refractive index and thickness in each layer build up complexities in practical fabrication process. But with regard to bandwidth, the selectivity is drastically improved as the number of $\lambda_0/4$ layer in basic period increases.

Among several structure investigated, a symmetric triple basic period exhibits unique property such as long wavelength or short wavelength pass characteristics. In addition to above aspects, the

calculated reflectivity would place this triple structure in a range that would make it more superior to the double structure Bragg waveguide, which have been reported.⁽¹⁹⁾ It was observed that $(\frac{n_1}{8} \frac{n_2}{4} \frac{n_1}{8})$ basic structure has largest stopband among other symmetric structures for a given indices of refraction.

Finally, Bragg waveguides composed of a triple layered periodic reflector have been studied thoroughly with regard to mode characteristics, field profiles in each layer, optical confinement and loss due to wave leaking into substrate. Arbitrary low loss waveguide is achieved with 5 periods of a triple layer.

The attenuation constant becomes minimum at the optimum thickness corresponding to the center of the allowed range of guiding layer thickness and decreases exponentially with number of period. A possible single mode Bragg waveguide at a thickness which is a few times larger than the wavelength could be used as a coupling device to optical fiber.

The Brewster condition on the TM mode is applicable to reflecting polarized waveguide. On the other hand, the characteristics of TM and TE reflectivity against the angle of incidence may be utilized in beam splitting waveguide structure.

Moreover, one of the important and useful application of a triple layered Bragg waveguide is wavelength division multiplexing for a future optical transmission system⁽⁶³⁾.

REFERENCES

- 1) H. Kogelnik, "An Introduction to Integrated Optics," IEEE Trans. on Microwave Theory and Techniques, Vol. MTT-23, No.1, pp. 2-15, Jan. 1975.
- 2) R.O. Miles, "Characteristics of a Hollow Core Distributed Feedback CO₂ Laser," IEEE J. Quantum Electronics, Vol. QE-14, No. 1, pp. 275-283, Apr. 1978.
- 3) M.B. Klein, "Enhancement of Third Harmonic Generation in Metal Dielectric Waveguide," Applied Optics, Vol. 18, No. 16, pp. 2733-2734. Aug. 1979.
- 4) R.O. Miles, R.W. Gros, "Propagation Losses at 10.6 μm in Hollow Core Rectangular Waveguides for Distributed Feedback Applications," IEEE J. Quantum Electronics, Vol. QE-15, No. 12, pp. 1396-1401, Dec. 1979.
- 5) E.A. Ash, "Grating Surface Waveguide", Presented at Int. Microwave Symp., New Beach, California, 1970.
- 6) P. Yeh, A. Yariv, C. Hong, "Electromagnetic Propagation in Periodic Media," J. Opt. Soc. Am. Vol. 67, No. 4, pp. 423-438, Apr. 1977.
- 7) O.S. Heavens, Optical Properties of Thin Films, Butter Worth Scientific Pub. Co., London, 1955.
- 8) Z. Knittel, Optics of Thin Films, John Wiley & Sons, New York, 1976.
- 9) G. Hass, Physics of Thin Film, Vol. 2, Academic Press, New York, 1964.
- 10) F. Abeles, Ann. Phys., Vol. 12, No. 5, pp. 596-604, 1950.
- 11) C.E. Curry, Electromagnetic Theory of Light, MacMillan, London, 1950.
- 12) L. Brillouin, Wave Propagation in Periodic Structure, McGraw Hill, New York, 1946.
- 13) G. Allen, "Band Structure of One Dimensional Crystal with Square Well Potential," Phys. Rev., Vol. 91, No. 4, pp. 531-533, Apr. 1956.

- 14) S. Barone, Analysis of Periodic Structure, Inst. of Brooklyn, Rep. R-486-56, Apr. 1956.
- 15) D. Kossel, "Analogies Between Thin Film Optics and Electron Band Theory," J. Opt. Soc. Am. Vol. 56, No. 10, pp. 1434, Oct. 1966.
- 16) L.R. Lewis, A. Hessel, "Propagation Characteristics of Periodic Array of Dielectric Slab," IEEE Trans. on Microwave Theory and Techniques, Vol. MTT-19, No. 3, 276-286, Mar. 1971.
- 17) J.A. Arnaud, M. Saleh, "Guidance of Surface Wave," Appl. Opt. Vol. 13, No. 1, pp. 2343-2345, Oct. 1974.
- 18) A.J. Fox, "The Grating Guide--A Component for Integrated Optics," Proc. IEEE Vol. 62, No. 5, pp. 644-645, May, 1974.
- 19) A.Y. Cho, A. Yariv, P. Yeh, "Observation of Confined Propagation in Bragg Waveguide," Applied, Phys. Lett., Vol. 30, No.9, pp. 471-472, May 1977.
- 20) J.B. Shellan, et. al., "Transverse Bragg reflector Injection Lasers," Opt. Lett., Vol. 2, No. 5, pp. 136-138, May, 1978.
- 21) R.D. Dupuis, P.D. Darkus, "Preparation and Properties of $Ga_{1-x}Al_xAs$ - GaAs Heterostructure Laser Grown by Metalorganic Chemical Vapor Deposition," IEEE J. Quantum Electronics, Vol. QE-15, No. 3, pp. 128-135, Mar. 1979.
- 22) S.E. Miller, "Integrated Optics: An Introduction," Bell Sys. Tech. J., Vol. 48, No. 9, pp. 2059-2069, Sept. 1969.
- 23) J.E. Goell, "A Circular Harmonic Computer Analysis of Rectangular Dielectric Waveguide," Bell Sys. Tech. J., Vol. 48, pp. 2133-2160, Sept. 1969.
- 24) P.K. Tien, "Light Waves in Thin Films and Integrated Optics," Appl. Opt., Vol. 10, No. 22, pp. 2395-2400, Nov. 1971.
- 25) D. Marcuse, "Power Distribution and Radiation Losses in Multimode Dielectric Slab Waveguide," Bell Sys. Tech. J., Vol. 51, pp. 1819-1836, Oct. 1972.
- 26) E.A. Mincatille, "Dielectric Rectangular Waveguide and Dielectric Coupler for Integrated Optics," Bell Sys. Tech. J., Vol. 48, pp. 2071-2102, Sept. 1969.
- 27) D. Marcuse, ed., Integrated Optics, IEEE Press, New York, 1973.
- 28) H.F. Taylor, A. Yariv, "Guided Wave Optics," Proc. IEEE, Vol. 62, No. 8, pp. 1044-1060, Aug. 1974.

- 29) D. Marcuse, Theory of Dielectric Optical Waveguide, Academic Press, New York, 1974.
- 30) D.F. Nelson, J. McKenna "Electromagnetic Modes of Anisotropic Dielectric Waveguide at P-N Junction," J. Appl. Phys., Vol. 38, pp. 4057-4074, 1967.
- 31) J. McKenna, "The Excitation of Planar Structure Dielectric Waveguide at P-N Junction," Bell Sys. Tech., Vol. 46, pp. 1491-1566, 1967.
- 32) L. Brillouin, Wave Propagation in Periodic Structure, 2nd Ed., Dover Pub., New York, 1953.
- 33) J.R. Wait, Electromagnetic Waves in Stratified Media, Pergamon Press, New York, 1962.
- 34) L.M. Brekhoushikh, Waves in Layered Media, Academic Press, New York, 1960.
- 35) H.A. Macleod, Thin Film Optical Filters, Hilger Ltd., London, 1969.
- 36) P.H. Berning, "Theory and Calculation of Optical Thin Films", Physics of Thin Film, G. Hass ed., Vol. I, Academic Press, New York, 1963.
- 37) W. Weinstein, "Computation in Thin Film Optics," Vacuum, Vol. IV, No. 1, pp. 3-19, Jan. 1954.
- 38) G.B. Airy, Trans. Cambridge Phil. Soc. Vol. 4, pp. 409-500, 1832.
- 39) A.W. Crook, "The Reflection and Transmission of Light by any System of Parallel Isotropic Films," J. Opt. Soc. Am., Vol. 38, No. 5, pp. 954, 1948.
- 40) See Reference (36).
- 41) K.D. Mielenz, "Use of Chebyshev Polynomial in Thin Film Computation," J. Res. Nat'l Bureau Standard (A), Vol. 63A, No. 3, pp. 297-300, Nov. 1959.
- 42) M. Abramowitz, I.A. Stegun, ed., Handbook of Mathematical Function, Dover, New York, 1972.
- 43) A. Herpin, Compt. Rend. Vol. 225, pp. 182, 1947.
- 44) See reference (35).
- 45) L.I. Epstein, "The Design of Optical Filter," J. Opt. Soc. Am., Vol. 42, No. 11, pp. 806-810, Nov. 1952.

- 46) R. Ulrich, R. Zengerle, "Optical Bloch Waves in Periodic Planar Waveguides," Topical Meeting on Integrated and Guided-Wave Optics, Incline Village, Nevada, 1980.
- 47) H.M. Stoll, W.E. Soady, "Bragg-Effect Polarizer/Analyzers and Lensless Waveguide Beam Expanders," Topical Meeting on Integrated and Guided-Wave Optics, Incline Village, Nevada, 1980.
- 48) P. Yeh, A. Yariv, A.Y. Cho, "Optical Surface Waves in Periodic Layered Media," Appl. Phys. Lett. Vol. 32, No. 2, pp. 104-105, Jan. 1978.
- 49) D.D. Sell, H.C. Casey, K.W. Wecht, "Concentration Dependence of the Refractive Index for N- and P-type GaAs between 1.2 and 1.8 eV," J. Appl. Phys., Vol. 45, No. 6, pp. 2650-2657, Jun. 1974.
- 50) H. Kressel, H.F. Lockwood, J.K. Butter, "Measurement of Refractive Index Step and of Carrier Confinement at (AlGa)As - GaAs Heterojunction" , J. Appl. Phys., Vol. 44, No. 9, pp. 4095-4097, Sept. 1973.
- 51) H.C. Casey, D.D. Sell, M.B. Parrish, "Refractive Index of $\text{Al}_x\text{Ga}_{1-x}\text{As}$ between 1.2 and 1.8 eV," Appl. Phys. Lett., Vol. 24, No. 2, pp. 63-65, Jan. 1974.
- 52) J.J. Vera, "Some Properties of Multi-layer films with Periodic Structure," Optica Acta, Vol. 11, pp. 315-333, 1964.
- 53) M.L. Baker, V.C. Yen, "Effect of the Variation of Angle of Incidence and Temperature on Infrared Filter Characteristics," Appl. Optics, Vol. 6, No. 8, pp. 1343-1351, Aug. 1967.
- 54) I.P. Kaminow, "Optical Waveguide Modulator," IEEE Trans. on Microwave Theory and Techniques, Vol. MTT-23 No. 1, pp. 57-69, Jan. 1975.
- 55) J.R. Tucker, "Quantum Limited Detection in Tunnel Junction Mixers," IEEE J. Quantum Electronics, Vol. QE-15, No. 11, pp. 1234-1257, Nov. 1979.
- 56) R. Fischer, L.A. Kuleskii, "Optical Parametric Oscillators," J. Quantum Electron., Vol. 7, pp. 135-159, 1977.
- 57) See for example, Special Issue on Quantum Electronic Devices for Optical-Fiber Communications, IEEE Trans. on Quantum Electronics, Vol. QE-14, No. 11, Nov. 1978.
- 58) H. Kressel, J.K. Butler, Semiconductor Lasers and Heterojunction LEDs, Academic Press, New York, 1977.

- 59) C.M. Verber, "Integrated Optical Data Processor," Laser Focus, Vol. 15, No. 12, pp. 68-69, Dec. 1979.
- 60) E. Merzbacher, Quantum Mechanics, John-Wiley, New York, 1970.
- 61) A.Y. Cho, J.R. Arthur, "Molecular Beam Epitaxy," in Progress in Solid State Chemistry, J. McCaldin, G. Somorjai, ed., Vol. 10, pt. 3, pp. 157-191, 1975.
- 62) H.C. Casey, M.B. Parrish, Heterostructure Lasers, Academic Press, New York, 1978.
- 63) T. Miki, H. Ishio, "Viabilities of the Wavelength Division Multiplexing Transmission System," IEEE Trans. on Communication Vol. COM-26, No. 7, pp. 7, July 1978.

APPENDIX

1. COMPUTER PROGRAM TO CALCULATE REFLECTIVITY AS A FUNCTION OF A RELATIVE WAVELENGTH FOR THE MULTI-LAYERED REFLECTOR IN CHAPTER IV

```

CCCCCCCCCCCCCCCCCCCCCCCCCCCCCCCCCCCCCCCCCCCCCCCCCCCCCCCCCCCCCCCCCCCC
C
C           REFLECTIVITY VS RELATIVE WAVELENGTH           C
C
C
CCCCCCCCCCCCCCCCCCCCCCCCCCCCCCCCCCCCCCCCCCCCCCCCCCCCCCCCCCCCCCCCCCCC
C
      IMPLICIT COMPLEX*16(A-F),REAL*8(Q-S)
      DIMENSION WJD(200),WN(10),T(10),WNR(10),WNI(10)
      2,AK(10),CH(10,2,2),CC(2,2),C(2,2),CF(2,2)
      3,GND(10,200),EP(10),EE(10),EM(10)

C
C      WS ; LOWER LIMIT OF RELATIVE WAVELENGTH SCALE
C      WE ; UPPER LIMIT OF RELATIVE WAVELENGTH SCALE
C      JT ; NUMBER OF POINT IN RELATIVE WAVELENGTH
C      MD ; MODE , MD=1 TE MODE,      MD=2, TM MODE
C

DATA WS,WE,JT,MD /0.0,2.0, 200, 1 /
PI=3.141592856
NP=0

C
C      READ DATA
C      N ; NUMBER OF PERIOD
C      LM ; NUMBER OF LAYERS IN EACH PERIOD,LESS THAN 7
C      ZANG ; INCIDENT ANGLE IN DEGREES
C      W0 ; REFERENCE WAVELENGTH IN VACUUM ,( UM)
C      WNG ; INDEX OF REFRACTION OF SUPERSTRATE
C      WNS ; INDEX OF REFRACTION OF SUBSTRATE
C      T(LX) ; DIMENSIONED OPTICAL THICKNESS OF LAYER (NORMALIZED
C              BY REFERENCE WAVELENGTH W0 )
C      WN(LX) ; DIMENSIONED INEX OF REFRACTION OF LAYER
C
54 READ(5,55,END=56)N,LM, ZANG,W0,WNG,WNS,(T(LX),WN(LX),LX=1,6)
55 FORMAT(12,1X,12,1X,F2.0,1X,F4.3,1X,2(F3.2,1X),6(F2.0,1X,F3.2
1,1X))
      NP=NP+1
      SITA=PI*ZANG/180.
      DO 2222 L=1,LM

```

```

WRITE(6,666) LW,WC,T(LW)
666  FORMAT(/,40X,'OPTICAL THICKNESS OF LAYER ',11.5X,F5.3
2. / ',F5.2,' UM')
WED=WN(LW)
WEG=WNG*DSIN(SITA)
IF(WED-WEG) 770,775,775
775  WNEF=FNK(WED,WEG)
GO TO 778
776  WNEF=FNK(WEG,WED)
778  T(LW)=W0/(T(LW)* WNEF)
2222 CONTINUE
LD=LM+1

C
C      PX : LENGTH OF X AXIS , INCH
C      PY : LENGTH OF Y AXIS , INCH
C      F : PLOTTER SCALE FACTOR
C      HL : CHARACTER HEIGHT IN INCH
C
DATA PY,PX,F,HL/4.,2.,1.0,0.10/
CALL PLTDT(W0,N,LM,F,WN,T,WNG,WNS,HL,ZANG,MD)
PN=N
RHI=ZANG*2.*PI/360.
C      WL DEFINED AS RELATIVE WAVELENGTH W0/W
DO 20 M=1,JT
WL=WS+M*(WE-WS)/JT
WJD(M)=YL
RKZ=(PI*2./W0)*WL
WNE=WNG*DSIN(RHI)
WN(LD)=WNS
DO 79 I=1,LD
IF(WN(I)-WNE) 90,91,91
91  WNT=WN(I)
WNR(I)=FNK(WNT,WNE)
WNI(I)=0.
GO TO 799
90  WNT=WN(I)
WNI(I)=FNK(WNE,WNT)
WNR(I)=0.
799 AK(I)= CMPLX(WNR(I),WNI(I))
79  CONTINUE
AI=CMPLX(0.,1.)
DO 12 L=1,LM
BP(L)=RKZ*T(L)*AK(L)
EE(L)= AK(L)
EM(L)=WN(L)*WN(L)/AK(L)
12  CONTINUE
ZWN=WNG*DCOS(RHI)
BK=AK(LD)
IF(MD .EQ. 2) GO TO 202
DO 22 L=1,LM
AC12=CDSIN(EP(L))/EE(L)
AC21=EE(L)*CDSIN(EP(L))
CH(L,1,1)=CCOS(3P(L))
CH(L,1,2)=-AI*AC12
CH(L,2,1)=-AI*AC21
CH(L,2,2)=CDCOS(3P(L))
22  CONTINUE
GO TO 204
202  ZWN=WNG/DCOS(RHI)
BK=WN(LD)*WN(LD)/AK(LD)

```

```

      DC 23 L=1,LM
      AC12=CDSIN(BP(L))/EM(L)
      AC21=EM(L)*CDSIN(BP(L))
      CH(L,1,1)=CDCOS(BP(L))
      CH(L,1,2)=-AI*AC12
      CH(L,2,1)=-AI*AC21
      CH(L,2,2)=CDDCS(BP(L))
23    CONTINUE
204   LC=LM-1
      DO 661 IC=1,2
      DO 661 JC=1,2
661   CC(IC,JC)=CH(1,IC,JC)
      DO 301 IM=1,LC
      IP=IM+1
      DO 71 I=1,2
      DO 71 J=1,2
      C(I,J)=CMPLX(0.,0.)
      DO 71 K=1,2
      C(I,J)=C(I,J)+CC(I,K)*CH(IP,K,J)
71    CONTINUE
      DO 72 IA=1,2
      DO 72 JA=1,2
      CC(IA,JA)=C(IA,JA)
72    CONTINUE
301   CONTINUE
      ARG=(CC(1,1)+CC(2,2))/2.
      RG=DREAL(ARG)
      RR=DABS(RG)
      IF(RR=0.1D 1 ) 401,402,303
401   SHI=DARCOS(RG)
      SHM=SHI*(N-1)
      SHN=SHI*N
      RDN=DSIN(SHI)
      RSN=DSIN(SHN)/RDN
      RSM=DSIN(SHM)/RDN
      GO TO 305
402   RDM=N-1
      RDN=N
      GO TO 305
303   SQA=(RG*RG)-1.
      SQR=DSQRT(SQA)
      IF(RG.LE.0.) GO TO 92
      PQA=RG+SQR
      GO TO 1100
82    PQA=RG-SQR
1100  SXN=1.
      SXP=1.
      N1=N-1
      RQA=(0.1D 1 )/PQA
      RDD=PQA-RQA
      IF(N1.EQ.0) GO TO 994
      DC 99 IS=1,N1
      SXP=SXP+PQA
      SXN=SXN/PQA
99    CONTINUE
994   RSM=(SXP-SXN)/RDD
      RSN=((SXP*PQA)-(SXN/PQA))/RDD
305   CFF=CC(1,1)*RSN-RSM
      CFS=CC(1,2)*RSN
      CSF=CC(2,1)*RSN

```

```

CSS=CD(2,2)*FSH-RSM
EM=CFF+CFS*BK
CM=CSP+CSS*BK
CY=CX/LM
CREF=(ZLN-CY)/(ZLN+CY)
RF=CDABS(CREF)
REF=RF*RF
GND(NP,1)=REF
20  CONTINUE
    IF(MD.EQ.2) GO TO 109
    WRITE(6,614)
614  FORMAT(//,50X,'TE MODE ',//)
    GO TO 119
109  WRITE(6,613)
613  FORMAT(//,50X,'TM MODE ',//)
119  WRITE(6,668) N,LM,ZANG
668  FORMAT(//,50X,'NUMBER OF PERIODS',5X,I2, /
2,50X,'NUMBER OF LAYERS',15X,I2, /
5,50X,'DESIGN ANGLE ',5X,F4.1,' ( DEGREES )',//)
    DO 103 K2=1,LM
    WRITE(6,669) K2,T(K2),K2,WN(K2)
669  FORMAT(20X,'T',I1,5X,F7.4,10X,'N',I1,5X,F7.4 )
103  CONTINUE
    WRITE(6,667) WNG,WNS
667  FORMAT(40X,'WNG ',F7.4,5X,' WNS ',F7.4, //)
    XDT=1/PX
    YDT=WE/PY
    CALL PLOT(0.,0.,-3)
    CALL PLCT(0.0,1.0,-3)
    CALL FACTOR(F)
    X=0.15
    CALL PLOT(X,0.,-3)
    CALL PLOT(0.,PY,2)
    CALL PLCT(PX,PY,2)
    CALL PLOT(PX,0.,2)
    CALL PLOT(0.,0.,2)
    CALL PLOT(PX,0.,-3)
    XST=GND(NP,1)*PX
    CALL PLOT(-XST,0.,3)
    DO 52 IP=1,JT
    PPY=IP*PY/JT
    PPX=GND(NP,IP)*PX
    CALL PLOT(-PPX,PPY,2)
52  CONTINUE
    CALL AXIS(-PX,0., ' REFLECTIVITY',-15,PX,0.,1.,-XDT)
    CALL AXIS(0.,0., 'RELATIVE WAVELENGTH',-15,PY,90., WS,YDT)
    XSH=HL*3./F
    CALL PLOT(XSH,-1.,-3)
    GO TO 54
56  WRITE(6,1007)
1007 FORMAT(2X,'RELATIVE',5X,3(4X,'REFLECTIVITY',5X), /
2,2X,'WAVELENGTH ',//)
    DO 1005 IP=1,JT
    WRITE(6,1006) WJD(IP),(GND(MP,IP),MP=1,NP)
1006 FORMAT(2X,F8.5,5X,10(F7.4,2X) )
1005 CONTINUE
    CALL PLOT(0.,0.,999)
    STOP
    END
    FUNCTION FNKIFN,SN)

```



```

DO 103 I4=1,10
CALL NUMBER(0.,0.,HI,T(I4),90.,4)
CALL SYMSQL(0.,999.,HI,'(MICRONS)',90.,9)
CALL PLOT(HX2,0.,-3)
103 CONTINUE
   ORGN=HY*2.+HYS
   CALL PLOT(0.,-ORGN,-3)
   RETURN
END

```

2. COMPUTER PROGRAM TO CALCULATE ELECTRIC FIELD DISTRIBUTION FOR A TRIPLE LAYERED PERIODIC BRAGG WAVEGUIDE IN CHAPTER V

```

CCCCCCCCCCCCCCCCCCCCCCCCCCCCCCCCCCCCCCCCCCCCCCCCCCCCCCCCCCCCCCCCCCCCCCCCCCCC
C
C          ELECTRIC FIELD DISTRIBUTION
C          TRIPLE LAYERED PERIODIC BRAGG WAVEGUIDE
C
CCCCCCCCCCCCCCCCCCCCCCCCCCCCCCCCCCCCCCCCCCCCCCCCCCCCCCCCCCCCCCCCCCCCCCCCCCCC
C
  IMPLICIT COMPLEX*16(A-C)      ,REAL*8(P-S)
  DIMENSION T(4),WN(4)
  DATA LM,MX,MY,F/3,2,2,0.5/

C
C      N : NUMBER OF PERIOD
C      ZANG : DESIGN ANGLE ,DEGREES
C      WO : WAVELENGTH IN VACUUM, UM
C      WNA : INDEX OF REFRACTION OF SUPERSTRATE
C      WNG : INDEX OF REFRACTION OF GUIDE
C      WNS : INDEX OF REFRACTION OF SUBSTRATE
C      WNE : EFFECTIVE INDEX OF REFRACTION
C      T : OPTICAL THICKNESS OF EACH LAYERS IN BASIC PERIOD
C      WN : INDEX OF REFRACTION OF EACH LAYERS IN BASIC PERIOD
C      NMD : MODAL NUMBER, 0, 1, 2, 3, .....
C
  PI=3.141592856
54  READ(5,55,END=56) N,ZANG,WO,WNA,WNG,WNS,WNE
  1,T(1),*N(1),T(2),WN(2),T(3),WN(3),NMD
55  FORMAT(12,1X,F4.2,1X,4(F4.3,1X),F6.5,1X,3(F4.2,1X,F4.3,1X),12)
  ZITA=      PI*ZANG/180.
  DO 626 LD=1,LM
  WRITE(6,666) LD,*C,T(LD)
666  FORMAT( 40X,'OPTICAL THICKNESS OF LAYER ',I2,' = ',F5.3,'/'
  1,F5.3,' , UM ')
  WEG=WNG*SIN(ZITA)
  WED=WN(LD)
  IF(WED=*WEG) 776,775,775
775  WNEF=FNK(WED,WEG)
  GO TO 778

```

```

776 WNEF=FNK(WEG,WED)
778 T(LD)=WO/(T(LD)*WNEF)
626 CONTINUE
WRITE(6,992) NMD
992 FORMAT('1',,////////,3JX,'TRIPLE LAYERED PERIODIC BRAGG WAVEGUIDE',
1 ,,,,,, 50X,'TE ',I2,////)
WRITE(6,668) LM,N ,ZANG ,WO
668 FORMAT(///,50X,'NUMBER OF LAYER',15X,I2,///,50X
1 , 'NUMBER OF PERIODS',5X,I2,///
5,50X,'DESIGN ANGLE ',5X,F4.1,' ( DEGREES )',///
6,50X,'DESIGN WAVELENGTH' ,5X,F6.3,' (MICRONS)',// )
DO 103 K2=1,LM
WRITE(6,669) K2,T(K2),K2,WN(K2)
669 FORMAT(40X,'T',I1,5X,F7.4,10X,'N',I1,5X,F7.4 )
103 CONTINUE
WRITE(6,667) WNG,WNS ,WNA,WNE
667 FORMAT(43X,'WNG ',F7.4,5X,'NS ',F7.4,/,
1 43X,'WNA ',F7.4, 5X,'WNE ',F7.4,/)
CALL ANGPT(MX,MY,F, WNG,WNS,ZANG,WO, TT, JT,N,LM,T,WN,WNA
1, NMD,WNE,CAZ,CBZ,FG)
WN3=WN(3)
WN2=WN(2)
WNI=WNI(1)
T3=T(3)
T2=T(2)
T1=T(1)
CALL WFLD(N, WO,TT,WNE,WNA,WNG,WNI,WN2,WN3
1, T1,T2,T3,CAZ,CBZ,FG,MX,MY,F,NMD)
GO TO 54
56 CALL PLOT(0..0..999)
STOP
END
FUNCTION FNK(FN,SN)
DOUBLE PRECISION ANK
ANK=(FN*FN)-(SN*SN)
FNK=DSORT(ANK)
RETURN
END
SUBROUTINE ANGPT(KX,KY,F,WNG,WNS,ZANG,WO,TT,JT,N
1, LM,T,WN,WNA,NMD,WNE,CAZ,CBZ,FG)
IMPLICIT COMPLEX*16(A-E),REAL*8(P-S)
REAL MX,MY
DIMENSION WN(4),T(3),WNR(4),WNI(4)
2,AK(4),CH(3,2,2),CO(2,2),C(2,2),CF(2,2),BP(3),EE(3)
PN=N
MY=KY
LD=1 +LM
MX=KX*2.
PI=3.141592856
* S=WO
WL=WS
LMX=LM
PDWG=WNE/WNG
RHI=DARSIN(PDWG)
RANG=RHI*180./PI
RKZ=2.*PI/WL
WN(LD)=WNS
DO 79 I=1,LD
IF(WN(I)-WNE) 90,91,91
91 WNT=WN(I)

```

```

WNR(I)=FNK(WNT,WNE)
WNI(I)=0.
GO TO 799
90  WNT=WN(I)
    WNI(I)=FNK(WNE,WNT)
    WNR(I)=0.
799  AK(I)=    CMPLX(WNR(I),WNI(I))
79  CONTINUE
    AI=CMPLX(0.,1.)
    DO 12 L=1,LM
    BP(L)=RKZ*T(L)*AK(L)
    EE(L)=    AK(L)
12  CONTINUE
    ZWN=WNG*DCOS(RHI)
    BK=AK(LD)
    DO 22 L=1,LM
    AC12=CDSIN(BP(L))/EE(L)
    AC21=EE(L)*CDSIN(BP(L))
    CH(L,1,1)=CDCOS(BP(L))
    CH(L,1,2)=AI*AC12*(-1.)
    CH(L,2,1)=AI*AC21*(-1.)
    CH(L,2,2)=CDCOS(BP(L))
22  CONTINUE
    LO=LM-1
    DO 661 IO=1,2
    DO 661 JO=1,2
661  CO(IO,JO)=CH(1,IO,JO)
    DO 301 IM=1,LO
    IP=IM+1
    DO 71 I=1,2
    DO 71 J=1,2
    C(I,J)=CMPLX(0.,0.)
    DO 71 K=1,2
    C(I,J)=C(I,J)+CO(I,K)*CH(IP,K,J)
71  CONTINUE
    DO 72 IA=1,2
    DO 72 JA=1,2
    CO(IA,JA)=C(IA,JA)
72  CONTINUE
301  CONTINUE
    ARG=(CO(1,1)+CO(2,2))/2.
    RG=DREAL(ARG)
    RR=DABS(RG)
    IF(RR-0.1D 1) 401,402,303
401  SHI=DARCOS(RG)
    SHN=SHI*#N
    SHM=SHI*(N-1)
    RDN=DSIN(SHI)
    RSM=DSIN(SHM)/RDN
    RSN=DSIN(SHN)/RDN
    GO TO 305
402  RDM=N-1
    RDN=N
    IF(N1 .EQ. 0) GO TO 994
303  SQA=(RG*FG)-1.
    SQR=DSQRT(SQA)
    IF(RG .LE. 0.)    GO TO 82
    PQA=RG+SQR
    GO TO 1100
82  PQA=RG-SQR

```

```

1100  SXN=1.
      SXP=1.
      PQA=(0.1D 1 )/PQA
      RQJ=PQA-FQA
      NI=N-1
      IF(NI .EQ. 0) GO TO 994
      DO 99 IS=1,NI
      SXP=SXP*PQA
      SXN=SXN/PQA
99     CONTINUE
994    FSM=(SXP-SXN)/FDD
      FSN=((SXP*PQA)-(SXN/PQA))/RDD
305   CFF=CD(1,1)*FSN-RSM
      CFS=CD(1,2)*FSN
      CSF=CD(2,1)*FSN
      CSS=CD(2,2)*FSN-FSM
      BM=CFF+CFS*BK
      CM=CSF+CSS*BK
      CY=CM/BM
      CREF=(ZWN-CY)/(ZWN+CY)
      RF=CDABS(CREF)
      REF=RF*RF
      CAZ=ZWN+CY
      CBZ=ZWN-CY
      ZWA=WNE*WNE-WNA*WNA
      GG=RKZ*WNG*DCOS(RHI)
      QA=RKZ*SQRT(ZWA)
      CALL THCK(GG,QA,CAZ,CBZ,TT,PI,NMD,TAB,TCD)
      PG=GG
      SZR=0.
      CKG=DCMPLX(PG,SZP)*TT
      CRHU=GG*((1.-CREF)*CDCOS(CKG)-AI*(1.+CREF)*CDSIN(CKG))
      CRHD=(1.+CREF)*CDCOS(CKG)-AI*(1.-CREF)*CDSIN(CKG)
      CRH=(CRHU/CRHD)*AI
1303  WRITE(6,1303) WNE,RG,TAB,TCD, TT ,QA,CRH,RANG,REF,CAZ,CBZ
      FORMAT(1X,F5.3,2X,5(F7.3,2X),2(F8.3,2X),1X,F5.2,2X,F6.3
1     1, 2X,2(F7.3,2X,F7.3,2X))
      RETURN
      END
      SUBROUTINE THCK(GG,QA,CAZ,CBZ,TH,PI,NMD,TAB,TCD)
      IMPLICIT COMPLEX*16(A-E),REAL*8(P-S)
      MDE=NMD+1
      AI=CMPLX(0.,1.)
      CUP=CAZ-CBZ
      CDW=CAZ+CBZ
      CAG=(CUP/CDW)*AI
      WAG=DREAL(CAG)
      TH1=ATAN(WAG)
      WQK=QA/GG
      TH2=ATAN(WQK)
      TH=(TH2-TH1+(MDE-1)*PI)/GG
      ZAB=DREAL(CUP)/DIMAG(CDW)
      ZCD=DIMAG(CUP)/DREAL(CDW)
      TAB=(ATAN(WQK)-ATAN(ZAB))/GG
      TCD=(ATAN(WQK)+ATAN(ZCD))/GG
      RETURN
      END
      SUBROUTINE WFLD(N,WL,T,NE,NA,NG,N3,N2,N1
1     1, T3,T2,T1,CAZ,CBZ,FG,MX,MY,F,NMD)
      IMPLICIT COMPLEX*16(A-C),REAL*8(P-R)

```

```

COMPLEX S23*16,S13*16,S12*16,S3*16,S1*16,S2*16,S21*16,S211*16
REAL NE,NA,N1,N2,NG,NKA,NKAI,NK1, NK2,NK2I,NKG,NKGI,KZ,
U NK1I ,N3,NK3,NK3I
PI=3.1415928
AI=CMPLX(0.,1.)
KD=50
CALL PLOT(5.,0.,-3)
PK=T1+T2+T3
IF(NE-NA) 88,89,89
89 NKA=FNK(NE,NA)
NKA I=0.
96 IF(NG-NE) 90,91,91
91 NKG=FNK(NG,NE)
NKGI=0.
97 IF(N1-NE) 92,93,93
93 NK1=FNK(N1,NE)
NK1 I=0.
98 IF(N2-NE) 94,95,95
95 NK2=FNK(N2,NE)
NK2 I=0.
67 IF(N3-NE) 68,69,69
69 NK3=FNK(N3,NE)
NK3 I=0.
GO TO 99
88 NKA I=FNK(NA,NE)
NKA=0.
GO TO 96
90 NKGI=FNK(NE,NG)
NKG=0.
GO TO 97
92 NK1 I=FNK(NE,N1)
NK1=0.
GO TO 93
94 NK2 I=FNK(NE,N2)
NK2=0.
GO TO 67
68 NK3 I=FNK(NE,N3)
NK3=0.
GO TO 99
99 KZ=2.*PI/WL
BA=CMPLX(NKA,NKAI)
BG=CMPLX(NKG,NKGI)
B1=CMPLX(NK1,NK1I)
B2=CMPLX(NK2,NK2I)
B3=CMPLX(NK3,NK3I)
BKA=BA*KZ
BK1=B1*KZ
BK2=B2*KZ
BK3=B3*KZ
BKG=BG*KZ
B12=B1/B2
B21=B2/B1
B13=B1/B3
B31=B3/B1
B23=B2/B3
B32=B3/B2
A21=(B21+B12)/2.
A23=(B23+B32)/2.
A13=(B13+B31)/2.
S21=(B21-B12)/2.

```

```

S2J=(B2J-B3J)/2.
S1J=(B1J-B3J)/2.
S12=(B12-B21)/2.
A21=A21*A1
S21=S21*A1
BT1=BK1*T1
BT2=BK2*T2
BT3=BK3*T3
S1=COSIN(BT1)
S2=COSIN(BT2)
S3=COSIN(BT3)
C1=CDCOS(BT1)
C2=CDCOS(BT2)
C3=CDCOS(BT3)
AD1=C1*C2*C3
AD2=A23*C1*S3*S2
AD3=A21*S1*C3*S2
AD4=A13*S1*C2*S3
CAD=AD1-AD2-AD3-AD4
RD=RG
GO TO 77
75 WRITE(6,999) NE, RG
999 FORMAT('1', ///, 5X, F10.7, 10X, 2(D12.4, 3X), 10X, 'NC NO ')
GO TO 1S15
77 RDS=DABS(RD)
IF(RDS .LT. 1.) GO TO 75
RR=RTTN(RD)
RKI=QAK(RR)
QK=QAK(RR)/PK
BT11=BT1*A1
EXPKI=CDEXP(BT11)
WRITE(6,993) RK, QK, RKI, T, CAD
993 FORMAT( //, 40X, 'EXP(-JK>)= ', D12.5, 5X, 'KI= ', E12.5
A //, 40X, 'KI*PK= ', D12.5
1 //, 40X, 'THICKNESS OF GUIDE = ', F7.4
2 //, 40X, '(M11+M22)/2=', 2(E12.5, 3X), //)
CALL PLTDT( WL, N, NG, NA, N3, N2, N1, NE, T, T3, T2, T1, RKI, F, NMD)
CALL FLDMK(T1, T2, T, BKA, BKG, BK1, BK2, RR, QK, M,
U N, B12, T3, BK3, B23, KD, CAZ, CBZ, MX, MY, F)
1S15 RETURN
END
FUNCTION RTTN(RD)
IMPLICIT REAL*8(P-S)
SAD=(RD*RD)-1.
RDR=DSQRT(SAD)
IF(RD .LE. 0.) GO TO 82
RTTN=RD+RDR
GO TO 100
82 RTTN=RD-RDP
100 RETURN
END
FUNCTION QAK(RR)
IMPLICIT REAL*8(P-R)
RRS=DABS(RR)
QAK=DLOG(RRS)
RETURN
END
SUBROUTINE PLTDT( W, N, DG, DA, D3, D2, D1, DE, TG, T3, T2, T1, GKI, F
1, NMD)
DIMENSION T(4), D(4), A(4) ,B(2)

```

```

P=T1+T2+T3
MLP=4
TSIX=(TG+1.0)*MLP
TX=(P*MLP*N)+1.5 +TG*MLP
B(1)=NMD
B(2)=N
A(1)=GKI
A(2)=P
A(3)=DE
A(4)=W
T(1)=T1
T(2)=T2
T(3)=T3
T(4)=TG
D(1)=D1
D(2)=D2
D(3)=D3
D(4)=DG
FA=2.
F=F/FA
CALL FACTOR(F)
CALL SYMBOL(0.,0.,0.28,'THICKNESS',90.,9)
CALL SYMBOL(0.,999.,0.28,'(MICRONS)',90.,9)
CALL SYMBOL(0.,5.6,0.28,'REFRACTIVE INDEX',90.,16)
CALL PLOT(0.4,0.56,-3)
CALL SYMBOL(0.,0.,0.28,'TG' NG',90.,23)
CALL PLOT(0.4,0.,-3)
CALL SYMBOL(0.,0.,0.28,'T3' N3',90.,23)
CALL PLOT(0.4,0.,-3)
CALL SYMBOL(0.,0.,0.28,'T2' N2',90.,23)
CALL PLOT(0.4,0.,-3)
CALL SYMBOL(0.,0.,0.28,'T1' N1',90.,23)
CALL PLOT(0.3,1.50,-3)
CALL SYMBOL(0.,0.,0.28,'NUMBER OF PERIOD ',90.,17)
CALL PLOT(0.4,0.,-3)
CALL SYMBOL(0.,0.,0.28,'TE ',90.,4)
CALL PLOT(0.4,0.,-3)
CALL SYMBOL(0.,0.,0.28,'WD(MICRONS) ',90.,12)
CALL PLOT(0.4,0.,-3)
CALL SYMBOL(0.,0.,0.28,'EFFECTIVE INDEX',90.,15)
CALL PLOT(0.4,0.,-3)
CALL SYMBOL(0.,0.,0.28,'PERIOD',90.,6)
CALL SYMBOL(0.,0.,0.28,'PERIOD',90.,6)
CALL PLOT(0.4,0.,-3)
CALL SYMBOL(0.,0.,0.28,'KI',90.,2)
CALL PLOT(0.,5.0,-3)
DO 200 J=1,4
CALL NUMBER(0.,0.,0.28,A(J),90.,3)
CALL PLOT(-0.4,0.,-3)
200 CONTINUE
DO 300 K=1,2
CALL NUMBER(0.,0.,0.28,B(K),90.,-1)
CALL PLOT(-0.4,0.,-3)
300 CONTINUE
CALL PLOT(-0.4,-4.5,-3)
DO 100 I=1,4
CALL NUMBER(0.,0.,0.28,T(I),90.,3)
CALL NUMBER(0.,0.,0.28,D(I),90.,3)
CALL PLOT(-0.4,0.,-3)
100 CONTINUE

```



```

33RK=BK3*RK
BRJ=B3PK*AI
CAG3=(1.+(BK6/BK3))/2.
CSG3=(1.-(BK6/BK3))/2.
EZ=(CAG3*CAZ+CSG3*CBZ)*CDEXP(BR3)
FZ=(CSG3*CAZ+CAG3*CBZ)*CDEXP(-BR3)
BT2=BK2*T2*AI
TZ=T1+T2
BT3Z=BK3*TZ*AI
BT2Z=BK2*TZ*AI
CA32=(1.+(1./B23))/2.
CS32=(1.-(1./B23))/2.
EZE=CDEXP(-BT3Z)
FZE=CDEXP(BT3Z)
CZ=((CA32*EZ+EZE)+(CS32*FZ*FZE))*CDEXP(BT2Z)
DZ=((CS32*EZ*EZE)+(CA32*FZ*FZE))*CDEXP(-BT2Z)
BT1=BK1*T1*AI
BT21=BK2*T1*AI
CA21=(1.+(1./B12))/2.
CS21=(1.-(1./B12))/2.
CZE=CDEXP(-BT21)
DZE=CDEXP(BT21)
AZ=((CA21*CZ*CZE)+(CS21*DZ*DZE))*CDEXP(BT1)
BZ=((CS21*CZ*CZE)+(CA21*DZ*DZE))*CDEXP(-BT1)
PTC=QK*RK
WT3=T3/WN
WT2=T2/WN
WT1=T1/WN
CALL PRARGU(XND,XGD,EFA,EPG,KD)
X= 0.
RTF=1.
DO 103 K=1,N
PLMX=0.
DO 43 LL=1,KD
EF3(K,LL)=FLDRE(X, K,RK,BK3,EZ,FZ,RTF,QK)
X3D(K,LL)=X
X=X+WT3
PF3=DREAL(EF3(K,LL))
RF3=DABS(PF3)
PMF3=DMAX1(RF3,PMAX)
PMAX=PMF3
PLX=DMAX1(PLMX,PF3)
PLMX=PLX
43 CONTINUE
DO 104 L=1,KD
EF2(K,L)=FLDRE(X, K,RK,BK2,CZ,DZ,RTF,QK)
X2D(K,L)=X
X=X+WT2
PF2=DREAL(EF2(K,L))
RF2=DABS(PF2)
PMF2=DMAX1(RF2,PMAX)
PMAX=PMF2
PLX=DMAX1(PLMX,RF2)
PLMX=PLX
104 CONTINUE
DO 105 KK=1,KD
EF1(K,KK)=FLDRE(X, K,RK,BK1,AZ,BZ,RTF,QK)
X1D(K,KK)=X
X=X+WT1
PF1=DREAL(EF1(K,KK))

```

```

RF1=DABS(PF1)
PMF1=DMAX1(PF1,PMAX)
PMAX=PMF1
PLX=DMAX1(PLMX,RF1)
PLMX=PLX
105 CONTINUE
CALL PRLYD(X1D,X2D,X3D,EF1,EF2,EF3,K,KD)
IF(K.EQ.N) GO TO 103
RTF=RTF/RR
103 CONTINUE
PMX=PMAX *WSIGN
DO 301 I=1,KD
BA=EFA(I)
REA(I)=ZNRMZ(PMX,BA)
301 CONTINUE
DO 302 J=1,KD
BG=EFG(J)
REG(J)=ZNRMZ(PMX,BG)
302 CONTINUE
DO 701 K=1,N
DO 303 JJ=1,KD
A3=EF3(K,JJ)
RE3(K,JJ)=ZNRMZ(PMX,A3)
303 CONTINUE
DO 304 L=1,KD
A2=EF2(K,L)
RE2(K,L)=ZNRMZ(PMX,A2)
304 CONTINUE
DO 305 KK=1,KD
A1=EF1(K,KK)
RE1(K,KK)=ZNRMZ(PMX,A1)
305 CONTINUE
701 CONTINUE
TA=XND(1)
CALL GPHH(REA,REG,RE3,RE2,RE1,N,KD,TA,T,T3,T2,T1
1 ,XND,XGD,X3D,X2D,X1D ,MX,MY,F)
RETURN
END
SUBROUTINE PRARGU(X1,X2,Y1,Y2,KD)
IMPLICIT COMPLEX*16(Y-Z)
DIMENSION X1(50),X2(50)
COMPLEX Y1(50),Y2(50)
WRITE(5,903)
908 FORMAT(5X,'E FIELD IN AIR ',30X
1 , 'E FIELD IN GUIDE',////)
DO 100 I=1,KD
WRITE(6,909) X1(I),Y1(I),X2(I),Y2(I)
909 FORMAT( 2(5X, F10.3, 5X, 2( D12.4, 3X) ) )
100 CONTINUE
RETURN
END
FUNCTION FLDR(X, K,RK,BK,UZ,WZ,RTNF,OK)
IMPLICIT COMPLEX*16(A-F),REAL*8(P-R)
COMPLEX UZ*16,#Z*16
AI=CMPLX(0.,1.)
XR=X-K*RK
ARG=BK*XR*AI
FLDR=(UZ*CDEXP(ARG)+(WZ/CDEXP(ARG)))*RTNF
RETURN
END

```

```

SUBROUTINE PFLYD(X1,X2,X3,Y1,Y2,Y3, K,KD)
IMPLICIT COMPLEX*16(Y-Z)
DIMENSION X1(30,50),X2(30,50),X3(30,50)
COMPLEX Y1(30,50),Y2(30,50),Y3(30,50)
WRITE(5,908) K
908 FORMAT('1',15X,12,' TH PERIOD', //,5X,'N1 LAYER'
1 ,35X,'N2 LAYER ', 35X,'N3 LAYER ', //)
DO 100 I=1,KD
WRITE(6,909) X3(K,I),Y3(K,I),X2(K,I),Y2(K,I),X1(K,I),Y1(K,I)
909 FORMAT( 3( 3X, F10.3, 3X, 2(D11.4, 3X)) )
100 CONTINUE
RETURN
END
FUNCTION ZNRMZ(AMX,EE)
REAL AMX*8
COMPLEX EE*16
ZNRMZ=DREAL(EE)/AMX
RETURN
END
SUBROUTINE GRPH(ENA,ENG,EN3,EN2,EN1, N, KD
1 ,TA,T,T3, T2,T1,XND,XGD,X3D,X2D,X1D ,MLA,MLP,F)
IMPLICIT REAL*8(E-G)
DIMENSION ENA(50),ENG(50),EN2(30,50),EN1(30,50),EN3(30,50)
1,XP(50),XGD(50),XND(50),X3D(30,50),X2D(30,50),X1D(30,50)
TSH=T *MLP+3.0
TM=MLA
TXS=( T1+T2+T3)*N*MLP+TSH
CALL PLOT( TSH,0.,-3)
CALL PLTFRM(T1,T2,T3,TA,N,MLP,MLA,F,T)
CALL PLOT(0.,TM,-3)
CALL PLOT(XND(1),0.,3)
CALL PLTEAG(ENA, KD, XND ,MLA,MLP,F)
CALL PLTEAG(ENG, KD, XGD,MLA,MLP,F)
DO 100 K=1,N
CALL PLTE12(EN3, K,KD, X3D,MLA,MLP,F)
CALL PLTE12(EN2, K,KD, X2D,MLA,MLP,F)
CALL PLTE12(EN1, K,KD, X1D ,MLA,MLP,F)
100 CONTINUE
CALL PLOT(0.,0.,-3)
CALL PLOT(TXS,-TM,-3)
RETURN
END
SUBROUTINE PLTFRM(T1,T2,T3,TA,N,MLP,MLA,F,TG)
DIMENSION TP(3)
CALL FACTOR(F)
TK=0.13
TP(1)=T3*MLP
TP(2)=T2*MLP
TP(3)=T1*MLP
TX=(TP(1)+TP(2)+TP(3))*N
TXP=TA*MLP
TYP=MLA*2.
TGM=TG*MLP
CALL PLOT(TXP,0.,2)
CALL PLOT(TXP,TYP,2)
CALL PLOT(0.,TYP,2)
CALL PLOT(0.,0.,2)
CALL PLOT(-TGM,0.,-3)
CALL PLOT(0.,TK,-2)

```

```

CALL PLOT(0.,-TK,-2)
CALL PLCT(TGM,0.,-3)
DO 300 I=1,N
DO 400 J=1,3
CALL PLOT(TP(J),0.,-2)
CALL PLOT(0.,TK,-2)
CALL PLOT(0.,-TK,-2)
400 CONTINUE
CALL PLOT(0.,TYP,-3)
CALL PLOT(0.,-TYP,-2)
300 CONTINUE
CALL PLOT(0.,TYP,-3)
DO 500 K=1,N
DO 500 L=1,3
J=4-L
CALL PLOT(-TP(J),0.,-2)
CALL PLOT(0.,-TK,-2)
CALL PLCT(0.,TK,-2)
500 CONTINUE
TM=MLA
CALL PLCT(0.,-TM,-3)
CALL PLOT(TXP,0.,2)
CALL PLOT(TX,0.,2)
CALL PLOT(0.,0.,-3)
CALL PLCT(0.,-TM,-3)
CALL PLOT(0.,0.,3)
RETURN
END
SUBROUTINE PLTEAG(EF, KD, XD,MLA,MLP,F)
IMPLICIT REAL*8(E-G)
DIMENSIONXP(50),PFP(50),XD(50),EF(50)
CALL FACTOR(F)
DO 90 I=1,KD
XP(I)=XD(I)*MLP
PFP(I)=EF(I)*MLA
CALL PLCT(XP(I),PFP(I),2)
90 CONTINUE
RETURN
END
SUBROUTINE PLTE12(EF, K,KD, XLD,MLA,MLP,F)
IMPLICIT REAL*8(E-G)
DIMENSION EF(30,50),XP(30,50),XLD(30,50),PFP(30,50)
CALL FACTOR(F)
DO 80 I=1,KD
XP(K,I)=XLD(K,I)*MLP
PFP(K,I)=EF(K,I)*MLA
CALL PLCT(XP(K,I),PFP(K,I),2)
80 CONTINUE
RETURN
END

```